Improving the Foundation Layers for Concrete Pavements

TECHNICAL REPORT:

Pavement Foundation Layer Construction – Wisconsin US 10 Field Study

October 2015

Sponsored by
Federal Highway Administration (DTFH 61-06-H-00011 (Work Plan #18))
FHWA TPF-5(183): California, Iowa (lead state), Michigan, Pennsylvania, Wisconsin

National Concrete Pavement Technology Center

Tech Center

CENTER FOR CEER EARTHWORKS ENGINEERING RESEARCH

IOWA STATE UNIVERSITY
Institute for Transportation

About the National CP Tech Center

The mission of the National Concrete Pavement Technology (CP Tech) Center is to unite key transportation stakeholders around the central goal of advancing concrete pavement technology through research, tech transfer, and technology implementation.

About CEER

The mission of the Center for Earthworks Engineering Research (CEER) at Iowa State University is to be the nation's premier institution for developing fundamental knowledge of earth mechanics, and creating innovative technologies, sensors, and systems to enable rapid, high quality, environmentally friendly, and economical construction of roadways, aviation runways, railroad embankments, dams, structural foundations, fortifications constructed from earth materials, and related geotechnical applications.

Disclaimer Notice

The contents of this report reflect the views of the authors, who are responsible for the facts and the accuracy of the information presented herein. The opinions, findings and conclusions expressed in this publication are those of the authors and not necessarily those of the sponsors.

The sponsors assume no liability for the contents or use of the information contained in this document. This report does not constitute a standard, specification, or regulation.

The sponsors do not endorse products or manufacturers. Trademarks or manufacturers' names appear in this report only because they are considered essential to the objective of the document.

Iowa State University Non-Discrimination Statement

Iowa State University does not discriminate on the basis of race, color, age, ethnicity, religion, national origin, pregnancy, sexual orientation, gender identity, genetic information, sex, marital status, disability, or status as a U.S. veteran. Inquiries regarding non-discrimination policies may be directed to Office of Equal Opportunity, Title IX/ADA Coordinator, and Affirmative Action Officer, 3350 Beardshear Hall, Ames, Iowa 50011, 515-294-7612, email eooffice@iastate.edu.

Iowa Department of Transportation Statements

Federal and state laws prohibit employment and/or public accommodation discrimination on the basis of age, color, creed, disability, gender identity, national origin, pregnancy, race, religion, sex, sexual orientation or veteran's status. If you believe you have been discriminated against, please contact the Iowa Civil Rights Commission at 800-457-4416 or the Iowa Department of Transportation affirmative action officer. If you need accommodations because of a disability to access the Iowa Department of Transportation's services, contact the agency's affirmative action officer at 800-262-0003.

The preparation of this report was financed in part through funds provided by the Iowa Department of Transportation through its "Second Revised Agreement for the Management of Research Conducted by Iowa State University for the Iowa Department of Transportation" and its amendments.

The opinions, findings, and conclusions expressed in this publication are those of the authors and not necessarily those of the Iowa Department of Transportation or the U.S. Department of Transportation Federal Highway Administration.

Technical Report Documentation Page

1. Report No.	2. Government Accession No.	3. Recipient's Catalog No.
DTFH 61-06-H-00011 Work Plan 18		

4. Title and Subtitle	5. Report Date
Improving the Foundation Layers for Pavements: Pavement Foundation Layer Construction – Wisconsin US 10 Field Study	October 2015
	6. Performing Organization Code

7. Author(s)	8. Performing Organization Report No.
David J. White, Pavana Vennapusa, Rachel Franz, Heath Gieselman, Alexander J. Wolfe	InTrans Project 09-352

9. Performing Organization Name and Address	10. Work Unit No. (TRAIS)
National Concrete Pavement Technology Center and Center for Earthworks Engineering Research (CEER) Iowa State University 2711 South Loop Drive, Suite 4700 Ames, IA 50010-8664	**11. Contract or Grant No.**

12. Sponsoring Organization Name and Address	13. Type of Report and Period Covered
Federal Highway Administration U.S. Department of Transportation 1200 New Jersey Avenue SE Washington, DC 20590	Technical Report
	14. Sponsoring Agency Code TPF-5(183)

15. Supplementary Notes

Visit www.cptechcenter.org or www.ceer.iastate.edu for color PDF files of this and other research reports.

16. Abstract

This technical project report is one of the field project technical reports developed as part of the TPF-5(183) and FHWA DTFH 61-06-H-00011:WO18 studies.

This report presents results and analysis of field and laboratory tests from a field study conducted on US Highway 10 just north of Junction City, Wisconsin. This project involved new construction on US Highway 10 with portland cement concrete pavement underlain by dense aggregate base, granular subbase, and compacted subgrade. The Iowa State University research team was present on site during construction to conduct field testing on the new pavement and foundation layers. Field and laboratory testing was conducted to determine modulus of subgrade reaction (*k*), elastic modulus (E), California bearing ratio (CBR), resilient modulus (M_r), moisture content, dry unit weight, soil index properties, and frost-heave and thaw-weakening durability of the subgrade and subbase layers.

k values determined from falling weight deflectometer (FWD) and static plate load tests (PLT) were close to the design assumed value. Use of empirical relationships to estimate *k* from CBR and M_r resulted in values that are 3 to 5 times higher than the design value. Field testing conducted in a dense grid pattern showed spatially non-uniform modulus and strength properties on subgrade and subbase layers, while the density measurements were relatively uniform. The high variability in the stiffness/strength properties is attributed to variations in the moisture content and underlying layer properties, which are not reflected in the density measurements.

Laboratory M_r testing on a layered composite sample (i.e., with both subbase and subgrade) showed about 1.4 times lower modulus than a single subbase layer with similar density. The reason for this reduction is attributed to the weaker subgrade layer. Frost-heave test results on subgrade samples indicated that the heave rate was greater for the second freezing cycle than for the first freezing cycle, which indicates that the material is susceptible to increased heave as the number of freeze-thaw (F/T) cycles increases.

17. Key Words	18. Distribution Statement
in situ testing—pavement foundation—portland cement concrete pavements—quality assurance—quality control—resilient modulus	No restrictions.

19. Security Classification (of this report)	20. Security Classification (of this page)	21. No. of Pages	22. Price
Unclassified.	Unclassified.	105	NA

Form DOT F 1700.7 (8-72) **Reproduction of completed page authorized**

IMPROVING THE FOUNDATION LAYERS FOR CONCRETE PAVEMENTS: PAVEMENT FOUNDATION LAYER CONSTRUCTION – WI US 10 FIELD STUDY

Technical Report
October 2015

Research Team Members
Tom Cackler, David J. White, Jeffery R. Roesler, Barry Christopher, Andrew Dawson, Heath Gieselman, Pavana Vennapusa

Report Authors
David J. White, Pavana K. R. Vennapusa,
Rachel Franz, Heath Gieselman, Alexander J. Wolfe
Iowa State University

Sponsored by
the Federal Highway Administration (FHWA)
DTFH61-06-H-00011 Work Plan 18
FHWA Pooled Fund Study TPF-5(183): California, Colorado, Iowa (lead state), Michigan, Pennsylvania, Wisconsin

Preparation of this report was financed in part
through funds provided by the Iowa Department of Transportation
through its Research Management Agreement with the
Institute for Transportation
(InTrans Project 09-352)

National Concrete Pavement Technology Center and
Center for Earthworks Engineering Research (CEER)
Iowa State University
2711 South Loop Drive, Suite 4700
Ames, IA 50010-8664
Phone: 515-294-5798
www.cptechcenter.org and www.ceer.iastate.edu

TABLE OF CONTENTS

ACKNOWLEDGMENTS xi

LIST OF ACRONYMS AND SYMBOLS xiii

EXECUTIVE SUMMARY xv

CHAPTER 1. INTRODUCTION 2

CHAPTER 2. PROJECT INFORMATION 4

- Project Background 4
- Pavement Design Input Parameter Selection and Assumptions 5

CHAPTER 3. EXPERIMENTAL TEST METHODS 7

- Laboratory Testing Methods and Data Analysis 7
  - Particle-Size Analysis and Index Properties 7
  - Resilient Modulus and Shear Strength Testing Sample Preparation 7
  - Resilient Modulus and Shear Strength Triaxial Testing 11
  - Resilient Modulus Data Analysis 13
  - Determination of Dynamic Secant Modulus from Cyclic Stress-Strain Data 13
  - Frost Heave and Thaw Weakening Test 14
- In Situ Testing Methods 19
  - Real-Time Kinematic Global Positioning System 20
  - Zorn Light Weight Deflectometer 20
  - Kuab Falling Weight Deflectometer 21
  - Dynamic Cone Penetrometer 26
  - Nuclear Gauge 26
  - Static Plate Load Test 27
- Determination of *k* Values 28

CHAPTER 4. LABORATORY TEST RESULTS 29

- Particle Size Analysis Results 29
- Moisture-Dry Unit Weight Results 30
- M_r and UU Test Results 33
- Frost Heave and Thaw Weakening Test Results 38

CHAPTER 5. IN SITU TEST RESULTS 42

- Description of Test Sections 42
- Geostatistical Data Analysis 42
- TS1: Subbase Layer Underlain by Subgrade 44
  - Experimental Testing 44
  - In Situ Point Test Results and Discussion 44
- TS2: Subgrade Layer 51
  - Experimental Testing 51
  - In Situ Point Test Results and Statistical Analysis 51
- TS3: PCC Pavement Layer 60
  - Experimental Testing 60

In Situ Point Test Results and Discussion 60
Comparison of Design Values, In Situ Measurements, and Laboratory Measurements 64
CHAPTER 6. SUMMARY AND CONCLUSIONS 66
REFERENCES 69
APPENDIX A: AASHTO 1972, AASHTO (1993), AND PCA (1984) DESIGN CHARTS 73
APPENDIX B: STRESS-STRAIN CURVES FROM RESILIENT MODULUS TESTS 79

LIST OF FIGURES

Figure 1. Approximate project start and end locations and ISU test section locations 5
Figure 2. Split mold, steel platen (4 in. diameter), and vibratory hammer for compaction of subbase material samples 8
Figure 3. Compaction of a subbase material sample in the split mold (left) and verification of the thickness of each lift using calipers (right) 9
Figure 4. Aluminum spacers (4 in. diameter) used during static compaction 10
Figure 5. Photos showing the static compaction procedure (left) and sample extrusion procedure (right) of a compacted cohesive soil sample 10
Figure 6. Triaxial chamber, load frame, and computer equipment for resilient modulus tests 11
Figure 7. Graphical representation of one load cycle in M_r testing 12
Figure 8. Comparison of resilient ($M_{r(T-307)}$), cyclic secant ($E^*_{s(T-307)}$), and dynamic secant ($E_{s(T-307)}$) modulus values 14
Figure 9. Schematic drawing of frost-heave and thaw-weakening test assembly 16
Figure 10. Three dimensional illustration of frost-heave and thaw-weakening test assembly 17
Figure 11. Inside view of the frost-heave and thaw-weakening test compaction mold with six rings 17
Figure 12. Frost-heave and thaw-weakening test compaction mold setup with collar 18
Figure 13. Temperature control water baths used to freeze and thaw samples 18
Figure 14. Target top and bottom temperatures with time per ASTM D5918-06 during F/T cycles 19
Figure 15. Example of measured top and bottom temperatures during F/T cycles and determination of heave rate for 1st and 2nd freezing cycles 19
Figure 16. Trimble SPS-881 hand-held GPS receiver, Kuab falling weight deflectometer, and Zorn light weight deflectometer (top row left to right); dynamic cone penetrometer, nuclear gauge; and static plate load test (bottom row left to right) 21
Figure 17. FWD deflection sensor setup used for this study and an example deflection basin with SCI, BDI, and BCI calculation procedure 22
Figure 18. Void detection using load-deflection data from FWD test 23
Figure 19. Static k_{PLT} values versus Dynamic k_{FWD} measurements reported in literature 26
Figure 20. E_{V1} and E_{V2} determination procedure from static PLT for subgrade and base materials 27
Figure 21. TS1 and TS2: Particle size distribution curves of subgrade and subbase materials 30
Figure 22. TS1 and TS2: Moisture-dry unit weight relationships of subgrade material from Proctor tests, moisture-dry unit weight of M_r samples, and in situ moisture-dry unit weight measurements 31
Figure 23. TS1: Moisture-dry unit weight relationships of subbase material from Proctor tests, moisture-dry unit weight of M_r samples, and in situ moisture-dry unit weight measurements 32
Figure 24. TS1: Moisture-dry unit weight relationships of subbase material from vibratory compaction tests, moisture-dry unit weight of M_r samples, and in situ moisture-dry unit weight measurements 32
Figure 25. Summary of σ_d versus M_r for laboratory compacted subgrade samples at different dry unit weights and moisture contents 35

Figure 26. Summary of σ_B versus M_r for sand subbase samples at different dry unit weights and moisture contents 36
Figure 27. Summary of σ_B versus M_r for subbase, subgrade, and composite samples 37
Figure 28. Sand + subgrade layered composite sample during M_r testing (left) and after shearing (right)....37
Figure 29. Sand + subgrade layered composite sample extruded sample after shearing....38
Figure 30. TS2: Frost heave and temperature versus time plots for the lean clay subgrade sample 39
Figure 31. TS2: Moisture content profiles of subgrade samples immediately after F/T testing....40
Figure 32. Description of a typical experimental and spherical semivariogram and its parameters (Isaaks and Srivastava 1989)....43
Figure 33. TS1-1: Plan view (top) and a photo (bottom) of in situ test locations on TS1-1 45
Figure 34. TS1-2: Photo of in situ testing locations 46
Figure 35. TS1-2: Excavation through the thin sand subgrade layer for tests on the subbase 46
Figure 36. TS1-1: NG, LWD, and DCP test results....47
Figure 37. TS1-2: In situ NG, LWD, and DCP test results 48
Figure 38. TS1-1: DCP-CBR profiles at each test location....48
Figure 39. TS1-2: DCP-CBR profiles at each test location....49
Figure 40. TS1-1: Histograms of in situ test measurements....50
Figure 41. TS2: Photograph of the compacted subgrade....52
Figure 42. TS2: Plan view of test locations....53
Figure 43. TS2: In situ NG, LWD, and DCP test results....54
Figure 44. TS2: In situ PLT results....55
Figure 45. TS2: DCP-CBR profiles from each test location 56
Figure 46. TS2: Histograms of in situ test measurements 57
Figure 47. TS2: Kriged spatial contour maps (top) and semivariograms of γ_d and *w* measurements (bottom)....58
Figure 48. TS2: Kriged spatial contour maps and semivariograms of LWD and DCP measurements....59
Figure 49. TS3: FWD test locations 61
Figure 50. TS3: Collecting DCP data 61
Figure 51. TS3: In situ FWD test results 62
Figure 52. TS3: Pavement temperature profiles during FWD testing 63
Figure 53. TS3: DCP-CBR profiles at each test location 63
Figure 54. TS1, TS2, and TS3: Bar chart comparing the design target *k* value with measured and estimated *k* values from field and laboratory measurements....64
Figure 55. Chart for estimating $k_{comp\text{-}AASHTO(1972)}$ (reproduced from AASHTO 1972)....73
Figure 56. Chart to estimate modulus of subbase layer (E_{SB}) from CBR (from AASHTO 1993 based on results from van Til et al. 1972)....74
Figure 57. Chart to estimate M_r of subgrade from CBR (from AASHTO 1993 Appendix FF)....75
Figure 58. Chart for estimating composite modulus of subgrade reaction ($k_{comp\text{-}AASHTO(1993)}$) assuming a semi-infinite subgrade depth (from AASHTO 1993) 76
Figure 59. Chart for estimating modulus of subgrade reaction (*k*) from CBR (from PCA 1984) 77

Figure 60. Cyclic stress-strain curves for subgrade sample # 1.....79
Figure 61. Cyclic stress-strain curves for subgrade sample # 2.....80
Figure 62. Cyclic stress-strain curves for subgrade sample # 3.....81
Figure 63. Cyclic stress-strain curves for subgrade sample # 4.....82
Figure 64. Cyclic stress-strain curves for subbase sample # 1 83
Figure 65. Cyclic stress-strain curves for subbase sample # 2 84
Figure 66. Cyclic stress-strain curves for subbase sample # 3 85
Figure 67. Cyclic stress-strain curves for subbase sample # 4 86
Figure 68. Cyclic stress-strain curves for subbase sample # 5 87
Figure 69. Cyclic stress-strain curves for subbase + subgrade composite sample 88

LIST OF TABLES

Table 1. Summary of pavement thickness design input parameters/assumptions (AASHTO 1972 Interim Guide Actual Method).....6
Table 2. Resilient modulus test sequences and stress values for base/subbase and subgrade materials (AASHTO T-307).....12
Table 3. Frost susceptibility classifications (ASTM D5918-06).....15
Table 4. Summary of material index properties.....29
Table 5. Summary of M_r and UU test results.....34
Table 6. Summary of frost-heave and thaw-weakening test results on TS2 subgrade samples.....41
Table 7. Test sections, test dates, material properties, in situ tests, and comments.....42
Table 8. TS1, TS2, and TS3: Summary statistics of in situ test results.....65

ACKNOWLEDGMENTS

This research was conducted under Federal Highway Administration (FHWA) DTFH61-06-H-00011 Work Plan 18 and the FHWA Pooled Fund Study TPF-5(183), involving the following state departments of transportation:

- California
- Iowa (lead state)
- Michigan
- Pennsylvania
- Wisconsin

The authors would like to express their gratitude to the National Concrete Pavement Technology (CP Tech) Center, the FHWA, the Iowa Department of Transportation (DOT), and the other pooled fund state partners for their financial support and technical assistance.

Jeffrey Horsfall and many others from the Wisconsin Department of Transportation (WisDOT) provided assistance in identifying the project, providing access to the project site, and obtaining project design information. We greatly appreciate their help.

We also thank Michael Eidem and Andrew Wilcuts of Iowa State University for their help with laboratory and field testing.

LIST OF ACRONYMS AND SYMBOLS

a, b, c	Regression coefficients
AASHTO	American Association of State Highway and Transportation Officials
$AREA_4$	Parameter determined from FWD deflection basin using data from 4 sensors
CBR	California bearing ratio
COV	Coefficient of variation
C_d	Coefficient of drainage
DCP	Dynamic cone penetrometer
$DCP\text{-}CBR_{Subgrade}$	CBR of subgrade determined from DCP test
$DCP\text{-}CBR_{Subbase}$	CBR of subbase determined from DCP test
DPI	Dynamic penetration index
D_0	Deflection measured under the plate
D_0^*	Non-dimensional deflection coefficient
D_1 to D_7	Deflections measured away from the plate at various set distances
D_{10}	Grain size diameter corresponding to 10% passing by mass
D_{60}	Grain size diameter corresponding to 60% passing by mass
E	Elastic modulus
E_s or $E_{s(T\text{-}307)}$	Dynamic secant modulus
$E_{LWD\text{-}Z3}$	Elastic modulus determined from 300 mm diameter plate Zorn light weight deflectometer
F	Shape factor
FWD	Falling weight deflectometer
G_s	Specific gravity
H_{SB}	Thickness of subbase
I	Intercept
k	Modulus of subgrade reaction
$k_{AASHTO(1972)}$	Modulus of subgrade reaction determined following AASHTO (1972) procedure
$k_{AASHTO(1993)}$	Modulus of subgrade reaction determined following AASHTO (1993) procedure
k_{comp}	Composite modulus of subgrade reaction
$k_{comp\text{-}AASHTO(1972)}$	Composite modulus of subgrade reaction determined following AASHTO (1972) procedure
$k_{comp\text{-}AASHTO(1993)}$	Composite modulus of subgrade reaction determined following AASHTO (1993) procedure
$k_{comp\text{-}ACPA\ (2012)}$	Composite modulus of subgrade reaction determined following ACPA (2012) online estimator
k_{PCA}	Modulus of subgrade reaction estimated from CBR following PCA (1984) procedure
$k_{FWD\text{-}Dynamic}$	Dynamic modulus of subgrade reaction from FWD test
$k_{FWD\text{-}Dynamic\text{-}Corr}$	Dynamic modulus of subgrade reaction from FWD test and corrected for slab size
$k_{FWD\text{-}Static}$	Static modulus of subgrade reaction from FWD test
$k_{FWD\text{-}Static\text{-}Corr}$	Static modulus of subgrade reaction from FWD test and corrected for slab size
k_1, k_2, k_3	Regression coefficients in “universal” model

L	Radius of relative stiffness
L′	Slab size (smaller dimension of a rectangular slab, length of width)
LL	Liquid limit
LTE	Load transfer efficiency
M_r	Resilient modulus
n	Number of measurements
P	Applied load by FWD
p	Number of parameters
PCC	Portland cement concrete
PI	Plasticity index
PL	Plastic limit
PLT	Plate load test
P_a	Atmospheric pressure
RMV	Resonant meter value
R^2	Coefficient of determination
r	Plate radius
s_u	Undrained shear strength
w	Moisture content
w_{opt}	Optimum moisture content
ε	Axial strain
ε_p	Permanent strain
ε_r	Resilient strain
γ_d	Dry unit weight
γ_{dmin}	Minimum dry unit weight
γ_{dmax}	Maximum dry unit weight
μ	Statistical mean or average
η	Poisson's ratio
σ	Statistical standard deviation
σ_B	Bulk stress
σ_d	Deviator stress
σ_0	Applied axial stress
$\sigma_1, \sigma_2, \sigma_3$	Principal stresses
τ_{oct}	Octahedral shear stress

EXECUTIVE SUMMARY

Quality foundation layers (i.e., the natural subgrade, subbase, and embankment) are essential to achieving excellent pavement performance. Unfortunately, many pavements in the United States still fail due to inadequate foundation layers. To address this problem, a three-year research project, Improving the Foundation Layers for Pavements (FHWA DTFH 61-06-H-00011 WO #18; FHWA TPF-5(183)), was undertaken by Iowa State University (ISU) to identify, and provide guidance for implementing, best practices regarding foundation layer construction methods, material selection, in situ testing and evaluation, and performance-related designs and specifications. As part of the project, field studies were conducted of several in-service concrete pavements across the country that represented either premature failures or successful long-term pavements. A key aspect of each field study was to tie performance of the foundation layers to key engineering properties and pavement performance. In situ foundation layer performance data, as well as original construction data and maintenance/rehabilitation history data, were collected and geospatially and statistically analyzed to determine the effects of site-specific foundation layer construction methods, site evaluation, materials selection, design, treatments, and maintenance procedures on the performance of the foundation layers and of the related pavements. A technical report was prepared for each field study.

This report presents results and analysis from a field study conducted on US Highway 10 just north of Junction City, Wisconsin. The project involved new construction of 5.44 miles of US Highway 10 in Portage County, Wisconsin. The ISU research team was present at the project site during the construction process from May 23 to May 26, 2010, to conduct a field study on the pavement foundation layers constructed for the new pavement. Field testing was conducted on three test sections (TS). TS1 involved testing the sand subbase and subgrade layers, TS2 involved testing the subgrade layer, and TS3 involved testing an existing portland concrete cement (PCC) layer paved in 2009.

The following field tests were conducted:

- Kuab falling weight deflectometer (FWD) to determine deflection basin parameters and modulus of subgrade reaction;
- Zorn light weight deflectometer (LWD) to determine elastic modulus;
- dynamic cone penetrometer (DCP) to estimate California bearing ratio, resilient modulus, and modulus of subgrade reaction;
- Humboldt nuclear gauge (NG) to determine moisture and dry unit weight; and
- static plate load test (PLT) to obtain elastic modulus and modulus of subgrade reaction.

The modulus of subgrade reaction *k* values were determined from FWD, PLT, and DCP tests to compare with the design *k* values. CBR in a thawed state and M_r tests were conducted in the laboratory to estimate *k* values and compare with the design *k* values. Some key findings from these comparisons are as follows:

- The average *k* value determined from the FWD ($k_{FWD\text{-}Static\text{-}Corr}$) was close to the design

k value, while the static PLT (k_{PLT*}) was about 1.3 times lower than the design value. On the other hand, the estimated *k* values following empirical relationships from AASHTO (1993) and PCA (1984) based on in situ DCP-CBR measurements, were about 4.1 and 1.6 times higher than the design *k* value, respectively.

- The *k* values calculated from laboratory-determined subgrade M_r values were also about 4 times higher than the design *k* value.
- The composite *k* values (accounting for the subbase layer modulus and thickness) determined following AASHTO (1972), AASHTO (1993), and ACPA (2012) procedures based on in situ DCP-CBR measurements were also about 4.0 to 4.6 times higher than the design *k* value. The composite *k* values that were determined based on thawed subgrade CBR measurements following AASHTO (1993) procedures were about 3 times higher than the design *k* value.

These findings indicate that the estimated *k* values vary significantly depending on the test method and the procedure followed. The *k* values determined from FWD and PLT tests are somewhat direct measurements although some empirical corrections were made. On the other hand, all other methods (i.e., laboratory tests and in situ DCP tests) are indirect and rely solely on empirical relationships to determine *k* values. The difference in *k* values from direct versus indirect measurements is significant and calls into question the various methods listed in the new *Mechanistic-Empirical Pavement Design Guide* (MEPDG) that are solely based on empirical relationships between laboratory tests (e.g., soil classification and CBR) and in situ DCP tests.

LWD, NG, and DCP tests were conducted on subbase and subgrade layers by spacing the test measurements about 3 m apart to capture the variability along the road alignment and also in a dense grid pattern (spaced at about 1 to 3 m) to capture spatial variability over a small area. Geostatistical semivariogram analysis was performed to analyze the point test data from dense grid pattern testing to characterize and quantify spatial non-uniformity of the foundation layer properties. Some key findings from field test results and analysis are as follows:

- The coefficient of variation in NG dry unit weight measurements of subbase and subgrade layers was about 2%, while the DCP-CBR, LWD modulus, and *k* values were in the range of 17% to 74%. The high variability in the stiffness/strength properties is attributed to variations in the moisture content and the influence of underlying layer properties, which are not reflected in the surface layer dry unit weight measurements.
- Geostatistical analysis of data obtained in a dense grid pattern on a subgrade test section showed that a spherical semivariogram model fit well for all the measurements. DCP-CBR and LWD modulus kriged contour maps showed similar spatial variations of soft and stiff areas, but they did not match with the spatial variability observed with dry unit weight measurements.

Laboratory testing was conducted on foundation layer materials obtained from the field to determine index properties, moisture-dry unit weight relationships from compaction tests, and M_r, and frost-heave and thaw-weakening susceptibility ratings. M_r tests were conducted on homogeneous samples and layered composite samples (i.e., subbase over subgrade) to assess the influence of composite layers on M_r values. Frost-heave tests were conducted on subgrade samples by exposing the samples to two freeze/thaw (F/T) cycles. Thaw-weakening

susceptibility ratings were determined by conducting CBR tests on compacted samples before and after two thawing cycles. Some key findings from laboratory M_r and frost-heave/thaw-weakening susceptibility rating tests are as follows:

- Comparing the M_r values of a homogenous sample and a layered composite sample (with subbase over subgrade) indicated that on average, the layered composite sample had about 1.4 times lower M_r than the single layer subbase sample at a similar density. This reduction in M_r in the layered composite sample is attributed to the weaker subgrade layer. This is an important finding and must be further studied with adequate testing of other layered composite sample configurations. Some of this work has been carried out on other studies that are part of the larger research project to further investigate the influence of composite soil layer configurations on M_r properties.
- Frost-heave tests on subgrade samples indicated that the heave rate was greater for the second freezing cycle than for the first freezing cycle, which indicates that the material is susceptible to increased heave with greater F/T cycles. Based on the frost-heave rate measurements, the subgrade soil is classified to have *medium* potential to frost-heave.
- After completing the two F/T cycles, a moisture content profile in the sample was obtained by taking samples at different depths. Results showed that the moisture content was higher at all depths in the samples compared to the initial moisture content, as expected. The moisture content at the top of the sample was closer to the initial moisture content and increased with depth.
- The CBR test on the post F/T samples decreased to an average CBR = 7 on the four samples from about 26 on a pre-freeze/thaw sample in unthawed state. Based on the thawed CBR values, the subgrade soil is classified to have *medium* potential to thaw-weakening.

The findings from the field studies under the Improving the Foundation Layers for Pavements research project will be of significant interest to researchers, practitioners, and agencies dealing with design, construction, and maintenance of PCC pavements. The technical reports are included in Volume II (Appendices) of the *Final Report: Improving the Foundation Layers for Pavements*. Data from the field studies are used in analyses of performance parameters for pavement foundation layers in the *Mechanistic-Empirical Pavement Design Guide* (M-E PDG) program. New knowledge gained from this project will be incorporated into the *Manual of Professional Practice for Design, Construction, Testing and Evaluation of Concrete Pavement Foundations*, to be published in 2015.

CHAPTER 1. INTRODUCTION

This report presents results and analysis from a field study conducted on US Highway 10 just north of Junction City, Wisconsin. This project involved new construction of 5.44 miles of the highway in Portage County, Wisconsin. The new pavement structure consisted of 254 mm (10 in.) thick jointed portland cement concrete (PCC) pavement with dowels, 152 mm (6 in.) thick dense aggregate base, 610 mm (24 in.) select borrow granular fill subbase, and clay subgrade.

The Iowa State University (ISU) research team was present at the project site from May 23 to May 26, 2010, during the construction process, to conduct field testing on the foundation layers constructed for the new pavement. The spatial northing and easting of all test measurement locations were obtained using a real-time kinematic (RTK) global positioning system (GPS). Other in situ tests used these devices:

- Kuab falling weight deflectometer (FWD) to determine deflection basin parameters and modulus of subgrade reaction;
- Zorn light weight deflectometer (LWD) to determine elastic modulus;
- dynamic cone penetrometer (DCP) to estimate California bearing ratio, resilient modulus, and modulus of subgrade reaction;
- Humboldt nuclear gauge (NG) to determine moisture and dry unit weight; and
- static plate load test (PLT) to determine elastic modulus and modulus of subgrade reaction.

Field testing was conducted on three test sections (TS). TS1 involved testing the sand subbase and subgrade layers, TS2 involved testing the subgrade layer, and TS3 involved testing an existing PCC layer paved in 2009. Field point testing was conducted on TS1 and TS2 by spacing the test measurements about 3 m apart to capture the variability along the road alignment. Testing was also conducted in a dense grid pattern (spaced at about 1 to 3 m) to capture spatial variability over a small area on TS1. Geostatistical semivariogram analysis was performed to analyze the point test data from dense grid pattern testing to characterize and quantify spatial non-uniformity of the foundation layer properties.

Bag samples of subgrade and subbase materials were obtained for laboratory testing which involved characterizing their index properties, moisture-dry unit weight relationships from compaction tests, resilient modulus (M_r) tests, and frost-heave and thaw-weakening susceptibility tests. The M_r tests were conducted on single samples as well as well as composite samples (i.e., subbase over subgrade) to assess its influence on the M_r values. Frost-heave tests were conducted on subgrade material using a setup specially fabricated at ISU for this research project to assess the foundation materials susceptibility to frost-heave, by exposing the samples to two F/T cycles. Thaw-weakening susceptibility rating of the foundation materials was determined by conducting California bearing ratio (CBR) tests on compacted samples before and after two thawing cycles.

This report contains six chapters. Chapter 2 provides background information of the project, and the pavement design input parameters. Chapter 3 presents an overview of the laboratory and in

situ testing methods used in this project. Chapter 4 presents results from laboratory testing. Chapter 5 presents results from in situ testing and analysis with discussion on comparison between the laboratory and in situ measured values and the design assumed values. Chapter 6 presents key findings and conclusions from this study.

The findings from this report should be of significant interest to researchers, practitioners, and agencies who deal with design, construction, and maintenance of PCC pavements. This project report was developed as part of the TPF-5(183) and FHWA DTFH 61-06-H-00011:WO18 studies.

CHAPTER 2. PROJECT INFORMATION

This chapter presents brief background information on the project, pavement thickness design parameter selection and assumptions during the design phase of the project, and the new pavement foundation layer construction details.

Project Background

This project involved new construction of 5.44 miles of US Highway 10 from Sta. 285+50 (Northing – 235272.34 ft and Easting – 935272.34 ft) to Sta. 580+50 (Northing – 230175.79 ft and Easting – 123601.69 ft) in Portage County, Wisconsin. ISU testing was conducted on three test sections (TS) located on the east side of County Highway O (TS1), west side of County Highway G (TS2), and west side of US Highway 34 and US Highway 10 interchange (TS3). TS3 was on PCC pavement constructed in 2009 with grading performed in 2008. A Google Earth view of the location of ISU test sections is provided in Figure 1.

The following pavement and foundation layer structure was used on the project:

- 254 mm (10 in.) Plain PCC with dowels
- 152 mm (6 in.) Dense aggregate base
- 610 mm (24 in.) Grade 1 select borrow granular fill

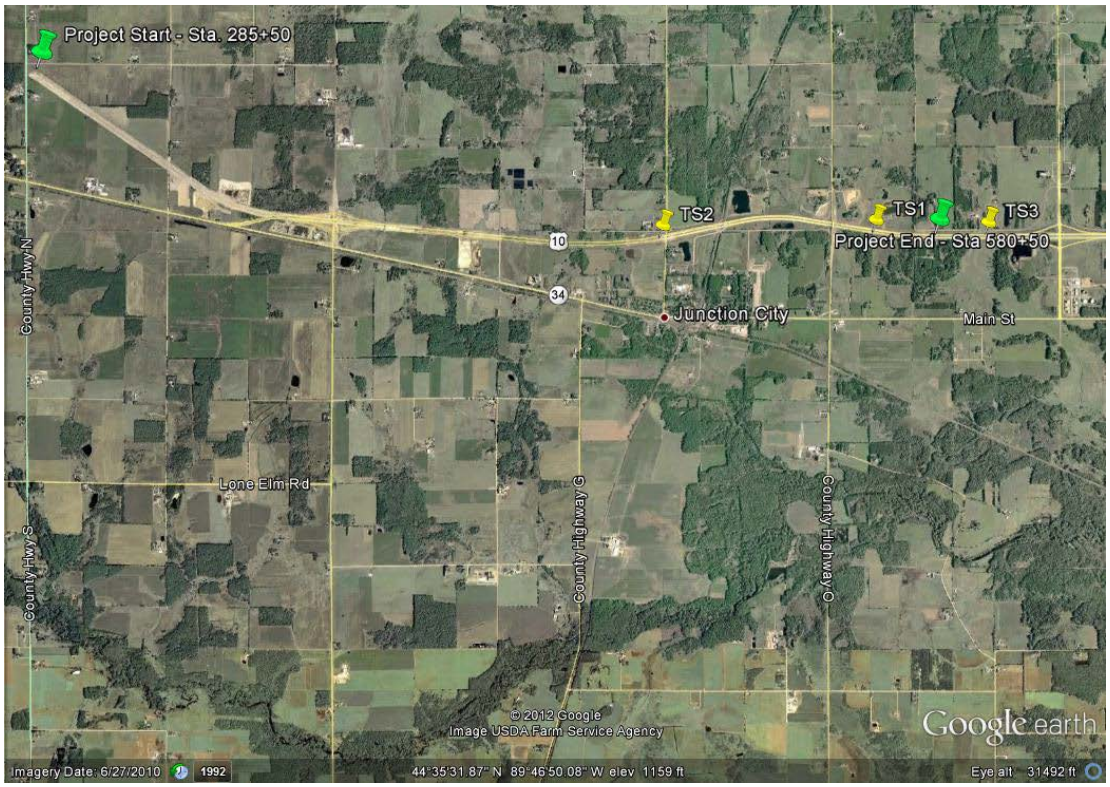

Figure 1. Approximate project start and end locations and ISU test section locations

Pavement Design Input Parameter Selection and Assumptions

A summary of pavement thickness design input parameters used by Wisconsin Department of Transportation (WisDOT) is provided in Table 1. The AASHTO 1972 interim guide method was followed for pavement design. A modulus of subgrade reaction, k = 41 kPa/mm (150 pci), was used in the design. According to the WisDOT pavement engineer, selection of this k value was based on a database of relationships between subgrade soil type and k values. These design assumptions are compared with the actual field measurements in Chapter 6.

Table 1. Summary of pavement thickness design input parameters/assumptions (AASHTO 1972 Interim Guide Actual Method)

Parameter	Value
General Assumptions	
Total equivalent 18-kip single axle load applications (in thousands)	9,884,200
Design period	20 years
Surface Layer Design Assumptions	
Pavement Type	Plain PCC with Dowels
Terminal serviceability	2.5
Working stress in concrete, ft	3,378 kPa (490 psi)
28-day mean PCC modulus of rupture, S_c	4,482 kPa (650 psi)
Foundation Layer Design Assumptions	
Subbase layer	152 mm (6 in.) Dense aggregate, 610 mm (24 in.) Grade 1 granular subbase
Modulus of subgrade reaction, *k*	41 kPa/mm (150 pci)
Pavement Thickness Design	
Calculated design thickness	254 mm (10 in.)

CHAPTER 3. EXPERIMENTAL TEST METHODS

This chapter summarizes the laboratory and in situ testing methods used in this study.

Laboratory Testing Methods and Data Analysis

Particle-Size Analysis and Index Properties

Samples from granular subbase and subgrade layers were collected from the field and were carefully sealed and transported to the laboratory for testing. Particle-size analysis tests on the OGDC material samples were performed in accordance with ASTM C136-06 *Standard test method for sieve analysis of fine and coarse aggregates.* Particle-size analysis tests on the sand subbase and subgrade materials were conducted in accordance with ASTM D422-63 *Standard Test Method for Particle-Size Analysis of Soils.*

Atterberg limit tests (i.e., liquid limit—LL, plastic limit—PL, and plasticity index—PI) were performed in accordance with ASTM D4318-10 *Standard test methods for liquid limit, plastic limit, and plasticity index of soils* using the dry preparation method. Using the results from particle-size analysis and Atterberg limits tests, the samples were classified using the unified soil classification system (USCS) in accordance with ASTM D2487-10 *Standard Practice for Classification of Soils for Engineering Purposes (Unified Soil Classification System)* and AASHTO classification system in accordance with ASTM D3282-09 *Standard Practice for Classification of Soils and Soil-Aggregate Mixtures for Highway Construction Purposes.*

Two laboratory compaction tests were used to determine the relationship between dry density and moisture content for the soils obtained from the field. Subgrade soil compaction characteristics were determined using standard and modified Proctor compaction methods in accordance with ASTM D698-07 *Standard test methods for laboratory compaction characteristics of soil using standard effort* and ASTM D1557-07 *Standard test methods for laboratory compaction characteristics of soil using modified effort*, respectively. Maximum and minimum index density tests were performed using a vibratory table on subbase material in accordance with ASTM D4253-00 *Standard test methods for maximum index density and unit weight of soil using a vibratory table* and D4254-00 *Standard test methods for minimum index density and unit weight of soils and calculation of relative density.* Moisture-unit weight relationships of the subbase material were determined by performing maximum index density tests by incrementally increasing the moisture content by approximately 1.5% for each test.

Resilient Modulus and Shear Strength Testing Sample Preparation

Subgrade and subbase materials were tested for resilient modulus (M_r) and unconsolidated undrained (UU) shear strength generally following the procedure from AASHTO T-307, Standard method of test for determining the resilient modulus of soils and aggregate materials, granular base/subbase and cohesive subgrade. Composite soil samples (i.e., those with both

subbase and subgrade) were also tested. The following sections describe the methods used to prepare the samples.

Subbase Material

Subbase material samples were prepared using the vibratory compaction method as described in AASHTO T-307 for preparation of granular base/subbase materials. Prior to compaction, materials were moisture-conditioned and allowed to mellow for at least 3 to 6 hours. A 101.6 mm (4 in.) diameter split mold was used to compact the sample (Figure 2) in five lifts of equal mass and thickness using an electric rotary hammer drill and a circular steel platen placed against the material (Figure 3). Calipers were used to verify consistent compaction layer thicknesses (Figure 3).

Figure 2. Split mold, steel platen (4 in. diameter), and vibratory hammer for compaction of subbase material samples

Figure 3. Compaction of a subbase material sample in the split mold (left) and verification of the thickness of each lift using calipers (right)

Subgrade Material

Disturbed bag samples were used to prepare samples for testing using static compaction method as described in AASHTO T-307. Before compaction, the materials were moisture-conditioned and allowed to mellow for at least 16 hours. Static compaction involved a hydraulic press, steel mold, and six steel spacers (Figure 4) to form the soil into a 101.6 mm diameter by 203.2 mm tall (4 in. diameter by 8 in. tall) cylinder. It must be noted that AASHTO T-307 describes compaction procedure to prepare a 71 mm diameter by 142 mm tall (2.8 in. diameter by 5.6 in. tall) samples. Figure 5 shows the static compaction process. When making the samples, the soil was compacted in five lifts of equal mass and thickness. Each lift of soil was pressed between the steel spacers to a uniform thickness. After compaction, the soil samples were extruded (Figure 5).

Figure 4. Aluminum spacers (4 in. diameter) used during static compaction

Figure 5. Photos showing the static compaction procedure (left) and sample extrusion procedure (right) of a compacted cohesive soil sample

Composite Subbase and Subgrade Samples

AASHTO T-307 does not describe a procedure for fabricating composite samples. Layered composite samples tested in this study included 101.6 mm (4 in.) thick subbase over 101.6 mm (4 in.) thick subgrade. For each composite sample, the bottom subgrade layer was compacted first using the static compaction technique described above, in three lifts. The first two lifts were about 40.6 mm (1.6 in.) thick, and the third lift was about 20.3 mm (0.8 in.) thick. A pre-determined amount of material was placed in each lift to keep the unit weight constant in each lift. After compacting the subgrade, the sample was extruded and placed on the triaxial chamber base. The split mold used for granular materials was then placed around the sample, and the base

layer was compacted in three equal lifts of 33.9 mm (1.3 in.) using the vibratory compaction procedure described in AASHTO T-307.

Resilient Modulus and Shear Strength Triaxial Testing

M_r and UU tests were performed using the Geocomp automated M_r test setup (Figure 6) in accordance with AASHTO T-307. The setup consists of a Load Trac-II load frame, an electrically controlled servo valve, an external signal conditioning unit, and a computer with a network card for data acquisition. The system uses a real-time adjustment of proportional-integral-derivative (PID) controller to adjust the system control parameters as the stiffness of the sample changes to apply the target loads during the test. Figure 6 shows the triaxial test chamber used in this study. The chamber is set up for both 71 mm (2.8 in.) and 101.6 mm (4 in.) diameter samples. Two linear voltage displacement transducers (LVDTs) are mounted to the piston rod to measurement resilient strains in the sample during the test.

M_r tests were performed following the AASHTO T-307 conditioning and loading sequences suggested for base and subgrade materials (Table 2). Each load cycle consisted of a 0.1 second haversine-shaped load pulse followed by a 0.9 second rest period. M_r is calculated as the ratio of the applied cyclic deviator stress (σ_d) and resilient strain (ε_r). The σ_d and ε_r values from a typical stress-strain cycle during the test are shown in Table 2. The average σ_d and ε_r of the last five cycles of a loading sequence are used in M_r calculations. After M_r testing, UU shear strength testing was performed on each sample by applying a confining pressure of 34.5 kPa (5 psi) to the base and subbase samples and 27.6 kPa (4 psi) to the subgrade samples. The raw test data for all M_r tests are provided in Appendix B.

Figure 6. Triaxial chamber, load frame, and computer equipment for resilient modulus tests

Table 2. Resilient modulus test sequences and stress values for base/subbase and subgrade materials (AASHTO T-307)

Base/Subbase Materials						Subgrade Materials					
	Confining Pressure		Max. Axial Stress				Confining Pressure		Max. Axial Stress		
Sequence No.	kPa	psi	kPa	psi	No. of cycles	Sequence No.	kPa	psi	kPa	psi	No. of cycles
0	103.4	15	103.4	15	500-1000	0	41.4	6	27.6	4	500-1000
1	20.7	3	20.7	3	100	1	41.4	6	13.8	2	100
2	20.7	3	41.4	6	100	2	41.4	6	27.6	4	100
3	20.7	3	62.1	9	100	3	41.4	6	41.4	6	100
4	34.5	5	34.5	5	100	4	41.4	6	55.2	8	100
5	34.5	5	68.9	10	100	5	41.4	6	68.9	10	100
6	34.5	5	103.4	15	100	6	27.6	4	13.8	2	100
7	68.9	10	68.9	10	100	7	27.6	4	27.6	4	100
8	68.9	10	137.9	20	100	8	27.6	4	41.4	6	100
9	68.9	10	206.8	30	100	9	27.6	4	55.2	8	100
10	103.4	15	68.9	10	100	10	27.6	4	68.9	10	100
11	103.4	15	103.4	15	100	11	13.8	2	13.8	2	100
12	103.4	15	206.8	30	100	12	13.8	2	27.6	4	100
13	137.9	20	103.4	15	100	13	13.8	2	41.4	6	100
14	137.9	20	137.9	20	100	14	13.8	2	55.2	8	100
15	137.9	20	275.8	40	100	15	13.8	2	68.9	10	100

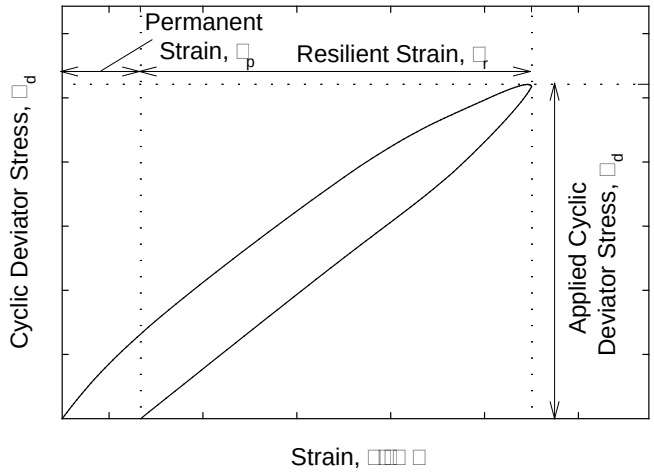

Figure 7. Graphical representation of one load cycle in M_r testing

Resilient Modulus Data Analysis

M_r values are used in pavement design as a measure of stiffness of unbound materials in the pavement structure. The M_r parameter is a highly stress-dependent parameter. Many non-linear constitutive models have been proposed that incorporate the effects of stress levels and predict M_r values. Most soils exhibit the effects of increasing stiffness with increasing bulk stress and decreasing stiffness with increasing shear stress (Andrei et al. 2004). A non-linear constitutive model (also called the universal model) proposed by Witczak and Uzan (1988) (Equation 1) was used in this study

$$M_r = k_1 P_a \left(\frac{\sigma_B}{P_a}\right)^{k_2} \left(\frac{\tau_{oct}}{P_a} + 1\right)^{k_3} \quad (1)$$

where P_a = atmospheric pressure (MPa); σ_B = bulk stress (MPa) = $\sigma_1 + \sigma_2 + \sigma_3$; τ_{oct} = octahedral shear stress (MPa) = $\{[(\sigma_1-\sigma_2)^2+(\sigma_2-\sigma_3)^2+(\sigma_3-\sigma_1)^2]^{1/2}\} / 3$; σ_1, σ_2, σ_3 = principal stresses; and k_1, k_2, k_3 = regression coefficients. The k_1 coefficient is proportional to M_r and therefore is always > 0. The k_2 coefficient explains the behavior of the material with changes in the volumetric stresses. Increasing volumetric stresses increases the M_r value and therefore the k_2 coefficient should be ≥ 0. The k_3 coefficient explains the behavior of the material with changes in shear stresses. Increasing shear stress softens the material and yields a lower M_r value; therefore, the k_3 coefficient should be ≤ 0.

The R^2 values determined for this model were adjusted for the number of regression parameters using Equation 2

$$R^2(\text{Adjusted}) = 1 - \left[\frac{(1-R^2)(n-1)}{n-p-1}\right] \quad (2)$$

where *n* = the number of data points and *p* = the number of regression parameters.

Determination of Dynamic Secant Modulus from Cyclic Stress-Strain Data

The cyclic stress-strain data obtained from the resilient modulus test was used to estimate dynamic secant modulus (E_s) to compare with dynamic elastic modulus measurements from the field. Secant modulus was determined from the slope of the line connecting the origin to a selected point on the stress-strain curve of a material, as illustrated in Figure 8. The difference between secant moduli and resilient moduli is the use of permanent strain instead of resilient strain in the calculations.

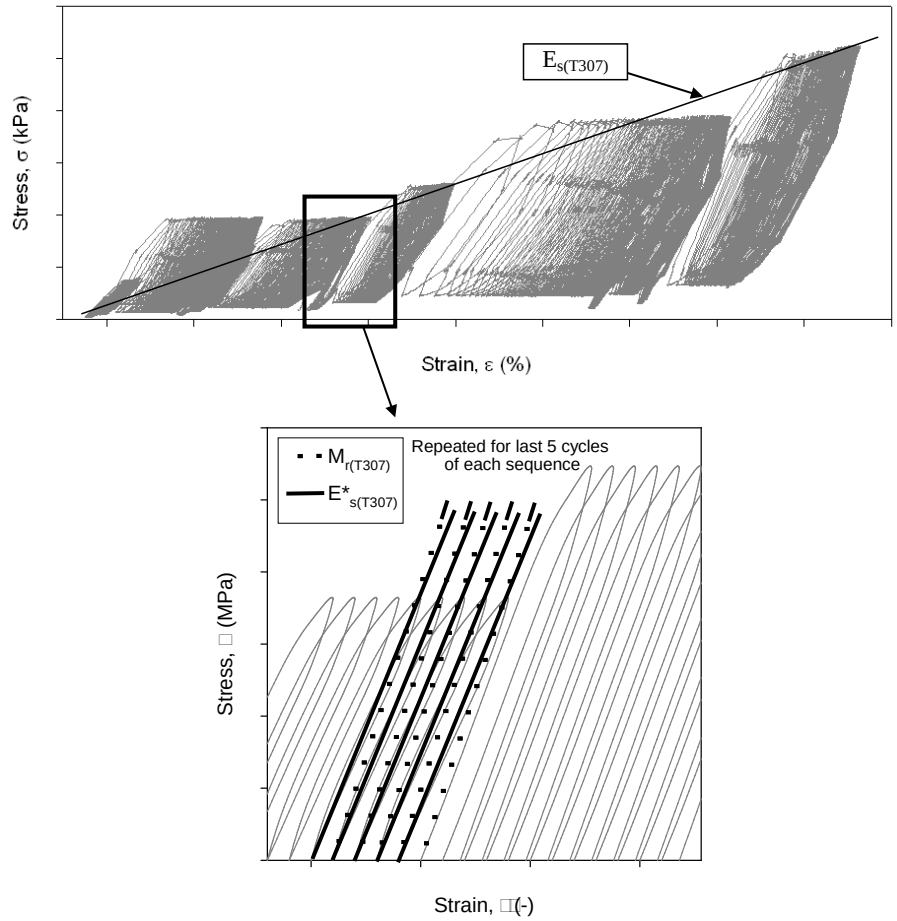

Figure 8. Comparison of resilient ($M_{r(T-307)}$), cyclic secant ($E^*_{s(T-307)}$), and dynamic secant ($E_{s(T-307)}$) modulus values

Frost Heave and Thaw Weakening Test

The frost heave and thaw weakening test was performed in general accordance with ASTM D5918-06 *Standard test methods for frost heave and thaw weakening susceptibility of soils*. The test is used to classify the frost heave and thaw weakening susceptibility of soils based on the heave rate and the thawed CBR values determined from the test. The heave rate and post-test F/T CBR values are compared with a classification system provided in the standard to determine the susceptibility ratings Table 3. It must be noted that the test results can only be used to compare the relative frost heave and thaw weakening susceptibility between material types and cannot be used to directly determine the amount of frost heave or thaw weakening in situ in a pavement system.

Table 3. Frost susceptibility classifications (ASTM D5918-06)

Frost Susceptibility Classification	Heave Rate (mm/day)	Thawed CBR (%)
Negligible	<1	>20
Very low	1 to 2	20 to 15
Low	2 to 4	15 to 10
Medium	4 to 8	10 to 5
High	8 to 16	5 to 2
Very High	>16	<2

A cross-sectional view and a three-dimensional view of the custom made test setup fabricated at Iowa State University are shown in Figure 9 and Figure 10, respectively. The samples were 146 mm (5.75 in.) in diameter and 152 mm (6 in.) in height and were compacted inside six rings with a rubber membrane between the soil and the rings. The compaction mold setup is shown in Figure 11 and Figure 12. A water supply was made available at a level of 13 mm (0.5 in.) above the bottom of the sample using a Mariotte tube as illustrated in Figure 9, to saturate the sample. A surcharge weight was applied to the sample to simulate the loading of a typical pavement section. During the test, laser transducers installed on a ring stand and a bracket above the sample were used to obtain heave and consolidation measurements, and thermocouples installed in the sample obtained the temperature profile (Figure 9). The laser transducers used in this study had a measurement range of 50 mm and a resolution of 0.75 μm. The lasers and thermocouples were connected to a data acquisition system that recorded the temperature in one-minute intervals.

The test was carried out by exposing four soil samples to two F/T cycles over a five day period. The samples were placed in a temperature controlled chest freezer (Figure 10) and then frozen and thawed by changing the temperature at the top and bottom of the samples using temperature controlled water baths (Figure 13). The programmable water baths used in this study had an operating range of -30°C to +200°C; were adjustable to ±0.01°C; and were filled with a 50% ethylene glycol-water solution. Insulating tape was wrapped around the flexible tubing between the water baths and the temperature control end plates to help reduce temperature variations in the solution. The target top and bottom of the sample temperatures (Figure 14) were programmed into the water baths and the actual temperatures were measured during the test. An example of the measured temperatures at the top and bottom of the sample is shown in Figure 15. Results indicated that the measured temperatures were higher during freezing and lower during thawing than the target values. This discrepancy likely occurred because of temperature losses in the glycol solution when transported from the temperature control baths to the temperature control end plates (although care was taken to reduce these variations as indicated above). Once the test sequence was completed, CBR test was performed on the thawed samples in accordance with ASTM D1883-07 and a moisture content profile of the sample was determined by carefully trimming the thawed sample to desired depths.

The heave rate of the sample was determined from the slope of the heave versus time plot as illustrated in Figure 15 for a period of about 24 hours for both 1st and 2nd freezing cycles.

ASTM D5918 specifies determining heave rate during the first eight hours of each freezing cycle. However, a few samples that were obtained from other research project sites did not heave during the first eight hours, and the samples that did heave during the first eight hours showed similar heave rates over the 8 hour and the 24 hour periods. To be consistent in comparing measurements from different project sites, the research team decided to present the heave rate over the 24 hour period.

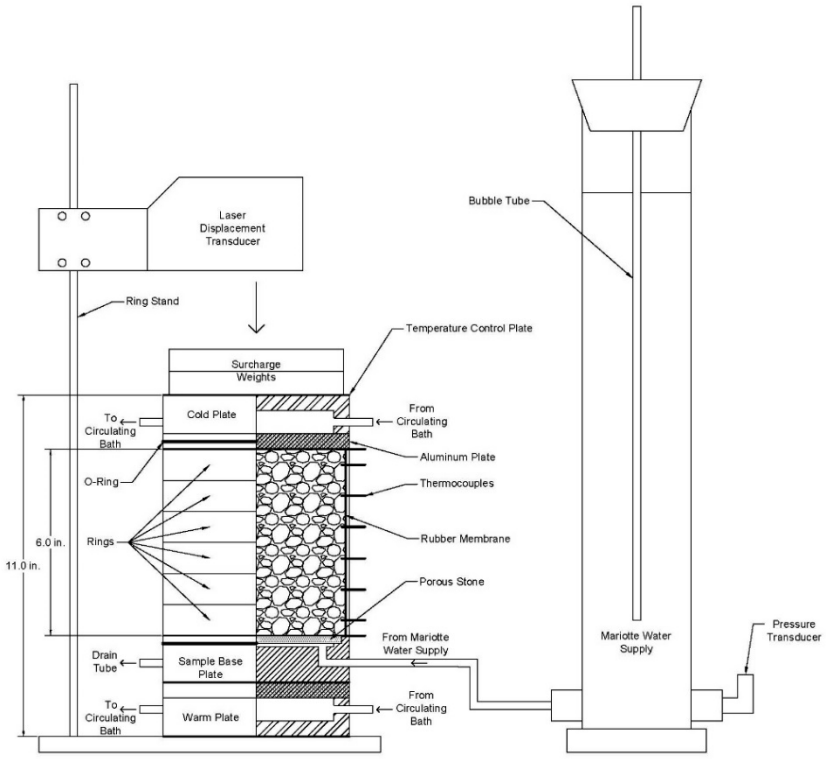

Figure 9. Schematic drawing of frost-heave and thaw-weakening test assembly

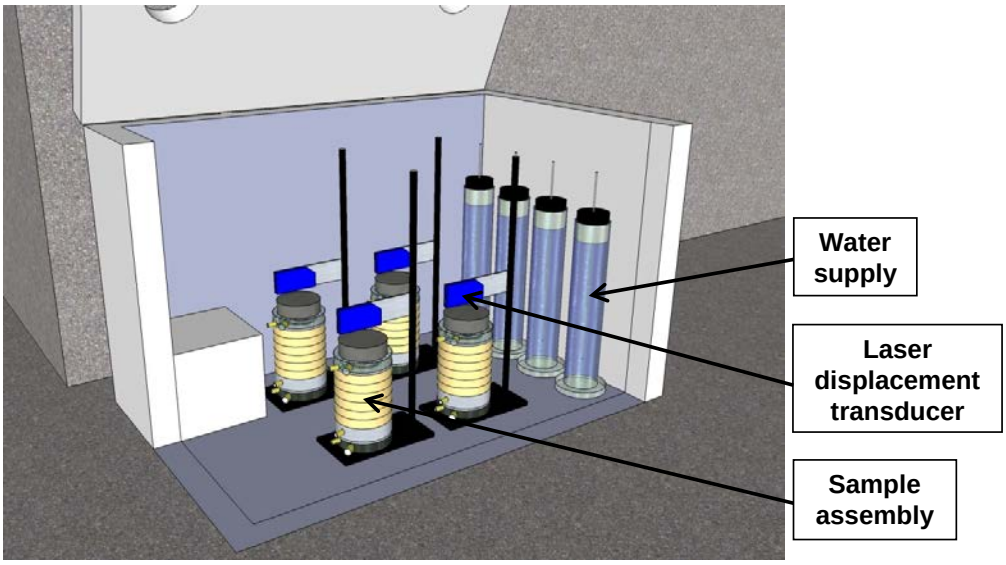

Figure 10. Three dimensional illustration of frost-heave and thaw-weakening test assembly

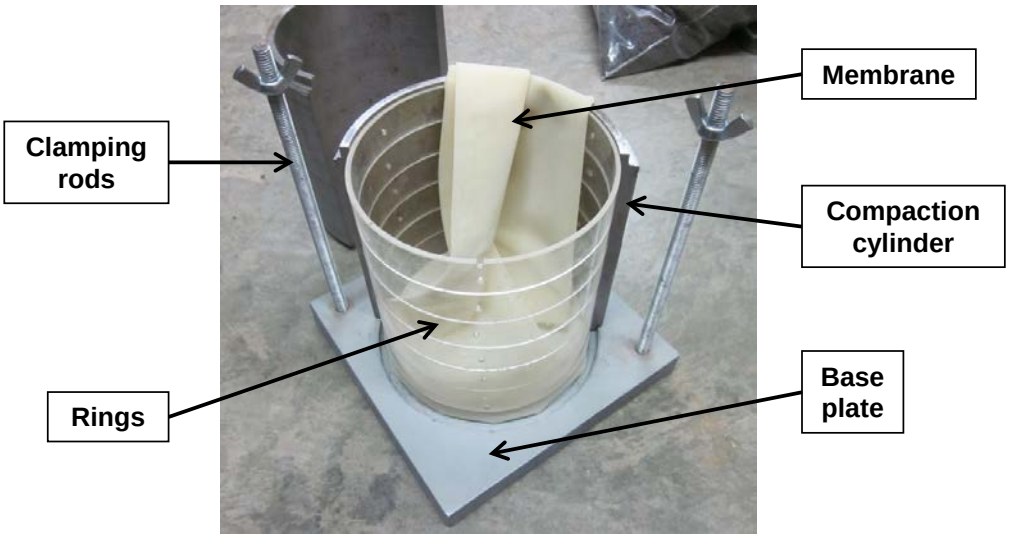

Figure 11. Inside view of the frost-heave and thaw-weakening test compaction mold with six rings

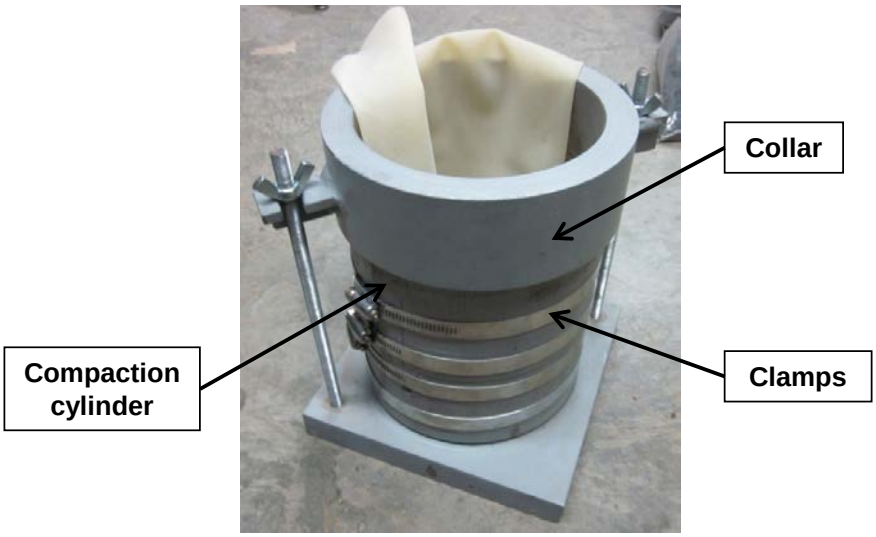

Figure 12. Frost-heave and thaw-weakening test compaction mold setup with collar

Figure 13. Temperature control water baths used to freeze and thaw samples

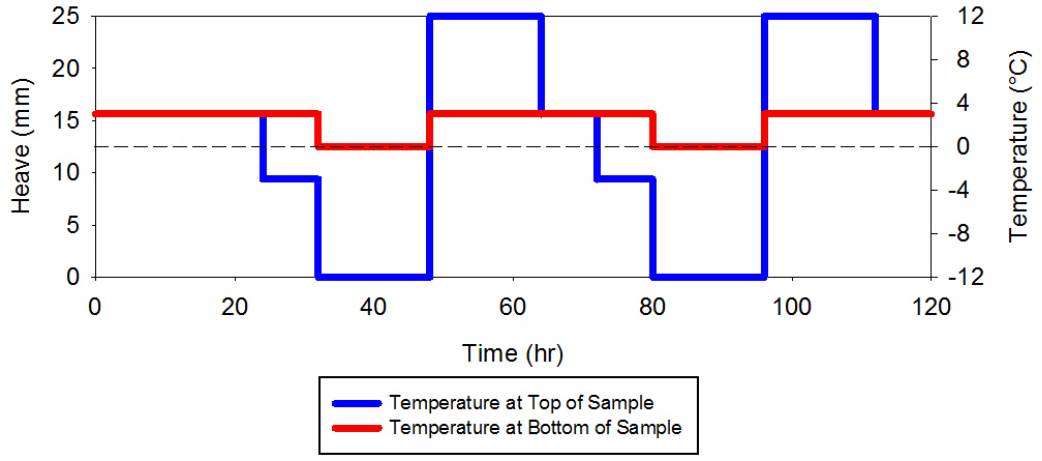

Figure 14. Target top and bottom temperatures with time per ASTM D5918-06 during F/T cycles

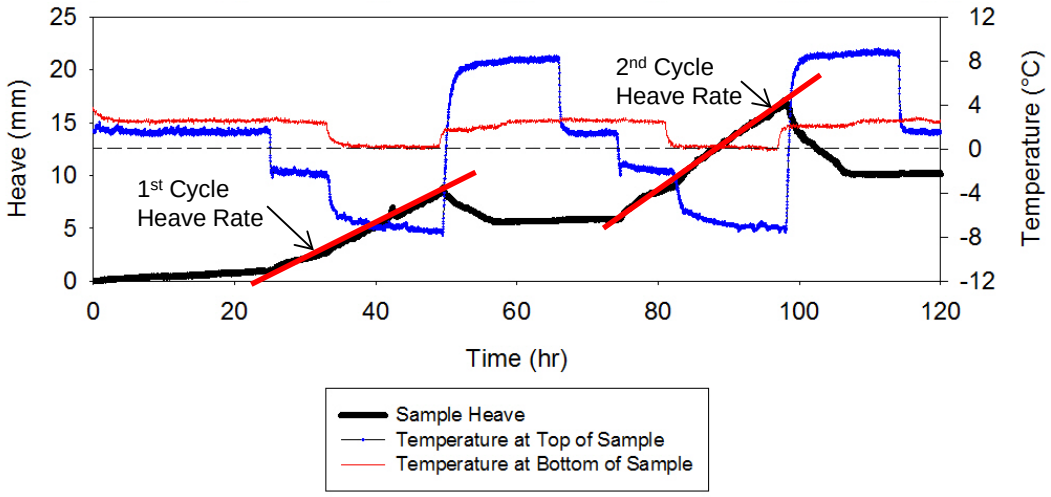

Figure 15. Example of measured top and bottom temperatures during F/T cycles and determination of heave rate for 1st and 2nd freezing cycles

In Situ Testing Methods

The following in situ testing methods and procedures were used in this study: (a) real-time kinematic (RTK) global positioning system (GPS); (b) Kuab falling weight deflectometer (FWD) setup with 300 mm diameter plate; (c) Zorn light weight deflectometer (LWD) setup with 300 mm diameter plate; (d) dynamic cone penetrometer (DCP); (e) calibrated Humboldt nuclear gauge (NG); and (g) static plate load test (PLT) setup with 300 mm diameter plate. Pictures of these test devices are shown in Figure 16. Drive core samples were obtained at two locations to compare with NG test measurements. Brief descriptions of these test procedures follow.

Real-Time Kinematic Global Positioning System

RTK-GPS system was used to obtain spatial coordinates (x, y, and z) of in situ test locations and tested pavement slabs. A Trimble SPS 881 receiver was used with base station correction provided from a Trimble SPS851 established on site. According to the manufacturer, this survey system is capable of horizontal accuracies of < 10 mm and vertical accuracies < 20 mm.

Zorn Light Weight Deflectometer

Zorn LWD tests were performed on subbase and subgrade layers to determine elastic modulus. The LWD was set up with 300 mm diameter plate and 71 cm drop height. The tests were performed following manufacturer recommendations (Zorn 2003) and the elastic modulus values were determined using Equation 3:

$$E = \frac{(1-\eta^2)\sigma_0 r}{D_0} \times F \tag{3}$$

where E = elastic modulus (MPa); D_0 = measured deflection under the plate (mm); η = Poisson's ratio (0.4); σ_0 = applied stress (MPa); r = radius of the plate (mm); and F = shape factor depending on stress distribution (assumed as 8/3) (see Vennapusa and White 2009). The results are reported as $E_{LWD\text{-}Z3}$ (where Z represents Zorn LWD and 3 represents 300 mm diameter plate).

Figure 16. Trimble SPS-881 hand-held GPS receiver, Kuab falling weight deflectometer, and Zorn light weight deflectometer (top row left to right); dynamic cone penetrometer, nuclear gauge; and static plate load test (bottom row left to right)

Kuab Falling Weight Deflectometer

Falling weight deflectometer (FWD) tests were conducted using a Kuab FWD setup with a 11.81 in. diameter loading plate by applying one seating drop and three loading drops. The applied loads varied from about 27 kN (6,000 lb) to 54 kN (12,000 lb) in the three loading drops. The actual applied loads were recorded using a load cell, and deflections were recorded using seismometers mounted on the device, per ASTM D4694-09 *Standard Test Method for Deflections with a Falling-Weight-Type Impulse Load Device.* The FWD plate and deflection sensor setup and a typical deflection basin are shown in Figure 17. To compare deflection values from different test locations at the same applied contact stress, the values at each test location were normalized to a 40 kN (9,000 lb) applied force.

FWD tests were conducted at the center of the PCC slab panels and at the joints. Tests conducted at the joints were used to determine joint load transfer efficiency (LTE) and voids beneath the

pavement based on "zero" load intercept values. Tests conducted at the center were used to determine modulus of subgrade reaction (*k*) values and the intercept values. The procedure used to calculate these parameters are described below.

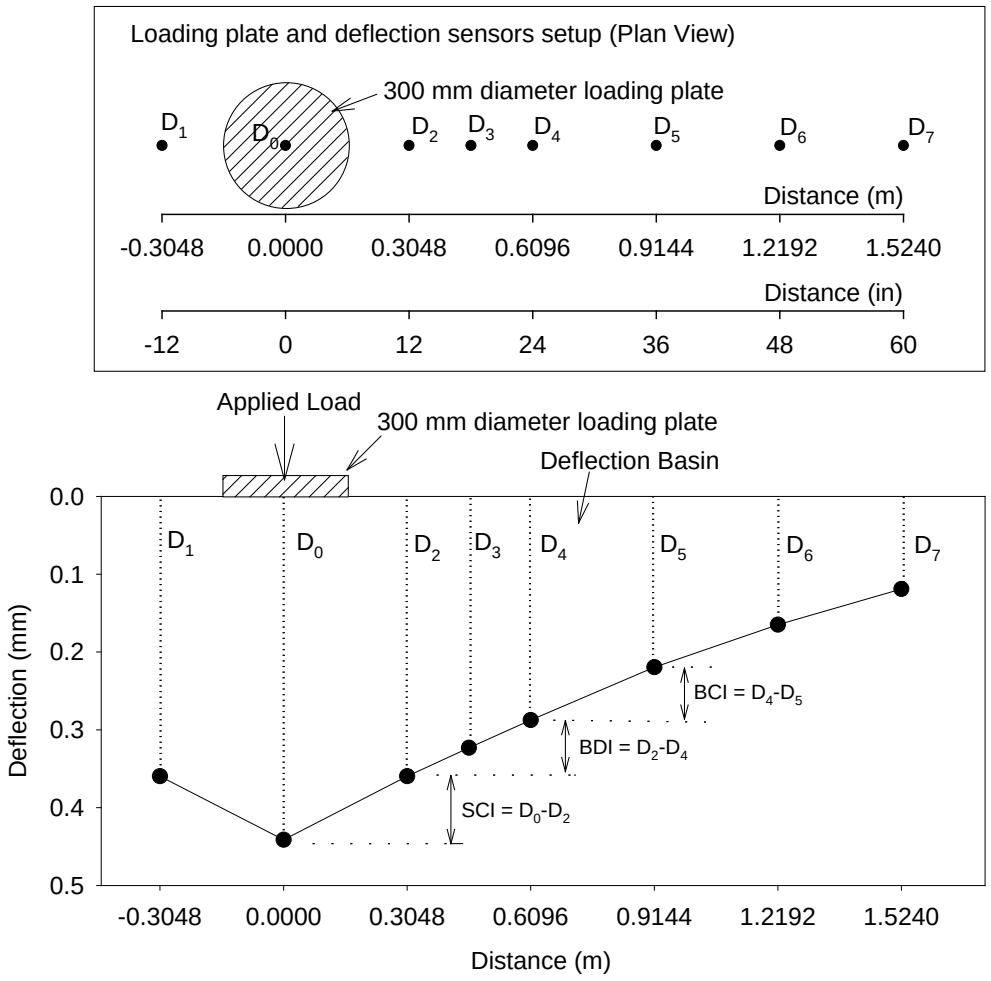

Figure 17. FWD deflection sensor setup used for this study and an example deflection basin with SCI, BDI, and BCI calculation procedure

LTE was determined by obtaining deflections under the plate on the loaded slab (D_0) and deflections of the unloaded slab (D_1) using a sensor positioned about 305 mm (12 in.) away from the center of the plate (Figure 17). The LTE was calculated using Equation 4.

$$LTE(\%) = \frac{D_1}{D_0} \times 100 \tag{4}$$

Voids underneath pavements can be detected by plotting the applied load measurements on the x-axis and the corresponding deflection measurements on the y-axis, and plotting a best fit linear regression line as illustrated in Figure 18, to determine the "zero" load intercept (I) values.

AASHTO (1993) suggests I = 0.05 mm (2 mils) as a critical value for void detection. According to Quintus and Simpson (2002), if I = -0.01 and +0.01 mm, then the response would be considered elastic. If I > 0.01 then the response would be considered deflection hardening, and if I < -0.01 then the response would be considered deflection softening.

Pavement layer temperatures at different depths were obtained during FWD testing, in accordance with the guidelines from Schmalzer (2006). The temperature measurements were used to determine equivalent linear temperature gradients (T_L) following the temperature-moment concept suggested by Jannsen and Snyder (2000). According to Vandenbossche (2005), the I-values are sensitive to temperature induced curling and warping affects. Large positive temperature gradients (i.e., when surface is warmer than bottom) that cause the panel corners to curl down result in false negative I-values. Conversely, large negative gradients (i.e., when surface is cooler than bottom) that cause the panel corners to curl upward result in false positive I-values. Interpretation of I-values therefore should consider the temperature gradient. Concerning LTE measurements for doweled joints, the temperature gradient is reportedly not a critical factor Vandenbossche (2005).

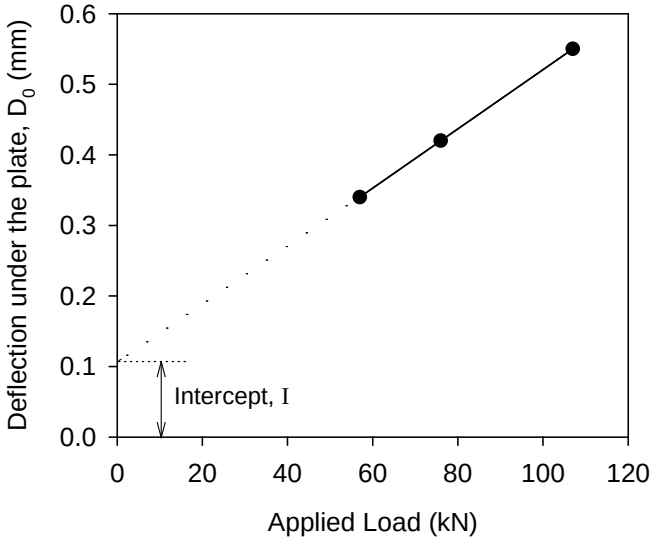

Figure 18. Void detection using load-deflection data from FWD test

The *k* values were determined using the $AREA_4$ method described in AASHTO (1993). The AREA method was first proposed by Hoffman and Thompson (1981) for flexible pavements and has since been applied extensively for concrete pavements (Darter et al. 1995). Since the *k* value determined from FWD test represents a dynamic value, it is referred to here as $k_{FWD\text{-}Dynamic}$. Deflections obtained from four sensors, i.e., D_0, D_2, D_4, and D_5 (see Figure 17) are used in the $AREA_4$ calculation. $AREA_4$ is calculated using Equation 5 and has dimensions of length (in.), as it is normalized with deflections under the center of the plate (D_0):

$$AREA_4 = 6 + 12 \times \left(\frac{D_2}{D_0}\right) + 12 \times \left(\frac{D_4}{D_0}\right) + 6 \times \left(\frac{D_5}{D_0}\right) \quad (4)$$

where D_0 = deflections measured directly under the plate (in.); D_2 = deflections measured at 305 mm (12 in.) away from the plate center (in.); D_4= deflections measured at 610 mm (24 in.) away from the plate center (in.); and D_5 = deflections measured at 914 mm (36 in.) away from the plate center (in.). AREA method can also be calculated using different sensor configurations and setups, i.e., using deflection data from 3, 5, or 7 sensors and those methods are described in detail in the literature (Stubstad et al. 2006, Smith et al. 2007)

In the early research conducted using the AREA method, the ILLI-SLAB finite element program was used to compute a matrix of maximum deflections at the plate center and the AREA values by varying the subgrade *k*, the modulus of the PCC layer, and the thickness of the slab (ERES Consultants, Inc. 1982). Measurements obtained from FWD tests were then compared with the ILLI-SLAB program results to determine the *k* values through back calculation. Later, in the 1990s to replace the back calculation procedure, Barenberg and Petros (1991) and Ioannides (1990) proposed a forward solution procedure based on Westergaard's solution for loading on an infinite plate. This forward solution presented a unique relationship between AREA value (for a given load and sensor arrangement) and the dense liquid radius of relative stiffness (L) in which subgrade is characterized by the *k* value. The radius of relative stiffness (L) is estimated using Equation 5:

$$L = \left[\frac{\ln\left(\frac{x_1 - AREA_4}{x_2} \right)}{x_3} \right]^{x_4} \tag{5}$$

where $x_1 = 36$; $x_2 = 1812.279$; $x_3 = -2.559$; $x_4 = 4.387$. It must be noted that the x1 to x4 values vary with the sensor arrangement and these values are only valid for the AREA4 sensor setup. Once the L value is known, the $k_{FWD\text{-}Dynamic}$ value can be estimated using Equation 6:

$$k_{FWD-Dynamic}(pci) = \frac{PD_0^*}{D_0 L^2} \tag{6}$$

where P = applied load (lb); D_0 = deflection measured at plate center (inches); and D_0* = non-dimensional deflection coefficient calculated using Equation 7:

$$D_0^* = a \cdot e^{-be^{-cL}} \tag{7}$$

where a = 0.12450; b = 0.14707; and c = 0.07565. It must be noted that these equations and coefficients are valid for an FWD setup with an 11.81 in. diameter plate.

The advantages of the AREA method are the ease of use without any back calculations and its use of multiple sensor data. The disadvantages are that the process assumes the slab and the

subgrade are horizontally infinite. This assumption leads to an underestimation of the *k* value. Crovetti (1993) developed the following slab size corrections for a square slab based on finite element analysis conducted using the ILLI-SLAB program, for use in the $k_{\text{FWD-Dynamic}}$ (Eq. 6):

$$Adjusted\ D_0 = D_0\left(1 - 1.15085e^{-0.71878\left(\frac{L'}{L}\right)^{0.80151}}\right) \quad (8)$$

$$Adjusted\ L = L\left(1 - 0.89434e^{-0.61662\left(\frac{L'}{L}\right)^{1.04831}}\right) \quad (9)$$

where L′ = slab size (smaller dimension of a rectangular slab, length or width). This procedure also has limitations: (1) it considers only a single slab with no load transfer to adjacent slabs, and (2) it assumes a square slab. The square lab assumption is considered to produce sufficiently accurate results when the smaller dimension of a rectangular slab is assumed as L′ (Darter et al. 1995). Darter et al. 1995 suggested using $L' = \sqrt{Length \times Width}$ to further refine the slab size corrections. There are no established procedures reported to date on correcting for load transfer to adjacent slabs, which remains as a limitation of this method. In this project, $k_{\text{FWD-Dynamic}}$ values corrected for slab size are reported as $k_{\text{FWD-Dynamic-Corr}}$.

AASHTO (1993) suggests dividing the $k_{\text{FWD-Dynamic}}$ value by a factor of 2 to determine the equivalent $k_{\text{FWD-Static}}$ value. The origin of this factor 2 dates back to Foxworthy's work in the 1980s. Foxworthy (1985) reported comparisons between the $k_{\text{FWD-Dynamic}}$ values obtained using Dynatest model 8000 FWD and the Static *k* values (Static k_{PLT}) obtained from 30 in. diameter plate load tests (Foxworthy did not report the exact procedure followed to calculate the Static k_{PLT}). Foxworthy used the AREA-based back calculation procedure using the ILLI-SLAB finite element program. Results obtained from Foxworthy's study are shown in Figure 19, and are based on 7 FWD tests conducted on PCC pavements with slab thicknesses varying from about 10 in. to 25.5 in. and plate load tests conducted on the foundation layer immediately beneath the pavement over a 4 ft x 5 ft test area. A few of these sections consisted of a 5 to 12 in. thick base course layer and some did not. The subgrade layer material consisted of CL soil from Sheppard Air Force Base in Texas, SM soil from Seymour-Johnson Air Force Base in North Carolina, and from McDill Air Force base in Florida (soil type was unspecified). No slab size correction was performed on this dataset.

Data from Foxworthy (1985) yielded a logarithmic relationship between the dynamic and the static *k* values. On average, the $k_{\text{FWD-Dynamic}}$ values were about 2.4 times greater than the Static k_{PLT} values. Darter et al. (1995) indicated that the factor 2 is reasonable based on results from other test sites (Figure 19). Darter et al. (1995) also compared FWD test data from eight long term pavement performance (LTPP) test sections with the Static k_{PLT} values and reported factors ranging from 1.78 to 2.16, with an average of about 1.91. The $k_{\text{FWD-Dynamic}}$ values used in that comparison were corrected for slab size.

For the analysis conducted in this research project, the $k_{FWD\text{-}Dynamic\text{-}Corr}$ values were divided by 2 and are reported as $k_{FWD\text{-}Static\text{-}Corr}$ values.

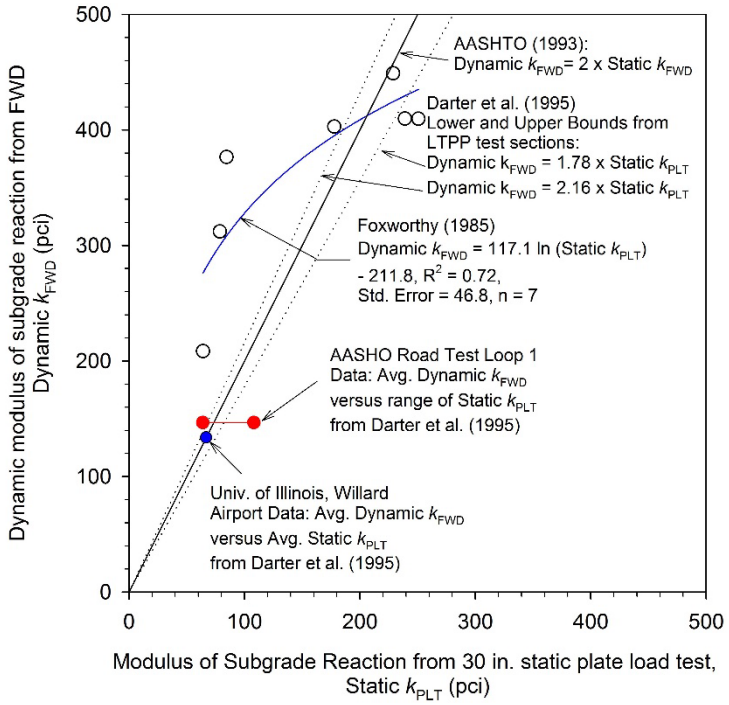

Figure 19. Static k_{PLT} values versus Dynamic k_{FWD} measurements reported in literature

Dynamic Cone Penetrometer

DCP tests were performed in accordance with ASTM D6951-03 *Standard Test Method for Use of the Dynamic Cone Penetrometer in Shallow Pavement Applications* to determine dynamic penetration index (DPI) and estimate California bearing ratio (CBR) using Equation 10.

$$CBR = \frac{292}{DPI^{1.12}} \tag{10}$$

DCP test results are presented in this report as CBR with depth profiles at a test location and as point values of $DCP\text{-}CBR_{Subbase}$ or $DCP\text{-}CBR_{Subgrade}$. The point data values represent the weighted average CBR within each layer. The depths of each layer were identified using the DCP-CBR profiles.

Nuclear Gauge

A calibrated nuclear moisture-density gauge (NG) device was used to provide rapid measurements of soil dry unit weight (γ_d) and moisture content (w) in the base materials. Tests

were performed following ASTM D6938-10 *Standard Test Method for In-Place Density and Water Content of Soil and Soil-Aggregate by Nuclear Methods (Shallow Depth).* Measurements of *w* and γ_d were obtained at each test location and the average value was reported.

Static Plate Load Test

Static plate load tests (PLT) were conducted on the subgrade layer by applying a static load on 300 mm diameter plate against a 62 kN capacity reaction force. The applied load was measured using a 90 kN load cell and deformations were measured using three 50-mm linear voltage displacement transducers (LVDT). The load and deformation readings were continuously recorded during the test using a data logger. E_{V1} and E_{V2} values were determined from Equation 4 using deflection values at 0.1 and 0.2 MPa contact stresses, as illustrated in Figure 20. Modulus of subgrade reaction were also determined from the PLT results using Equation 11,

$$k_{PLT} = \frac{\sigma_0}{D_0} \tag{11}$$

where k_{PLT} = modulus of subgrade reaction from 300 mm diameter plate load test (kPa/mm); D_0 = measured deflection under the plate (mm) for 200 kPa to 400 kPa applied stress range; and σ_0 = applied stress (kPa).

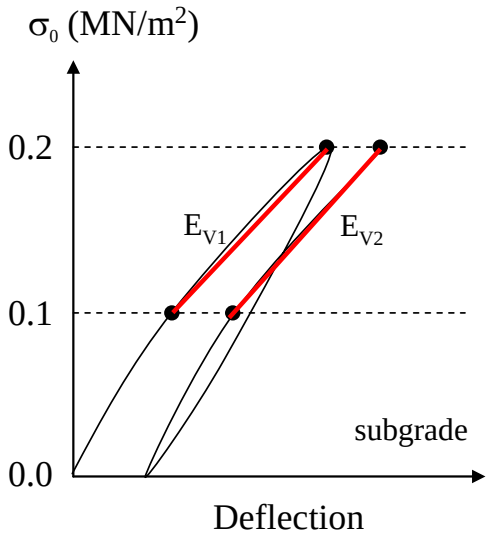

Figure 20. E_{V1} and E_{V2} determination procedure from static PLT for subgrade and base materials

PLTs were performed using a 300 mm (11.8 in.) diameter plate, but the *k* value used in the pavement design guides is based on a 762 mm (30 in.) diameter plate. Therefore, the measured k_{PLT} values were corrected for plate size using a theoretical relationship (Equation 12) proposed by Terzaghi and Peck (1967) for cohesive soils.

$$k_{PLT^*} = k_{PLT}\left[\frac{B_1}{B}\right] \quad (12)$$

where k_{PLT^*} = modulus of subgrade reaction using a 762 mm (30 in.) diameter plate; B_1 = 300 mm; and B = 762 mm.

Determination of *k* Values

Subgrade k values were determined directly from field measurements using PLT and FWD testing, empirical relationships from DCP test measurements, and empirical relationships from laboratory measurements. All of these values are compared in this report with reference to the design assumed value. The k values determined using different procedures and the notations are listed below:

- k_{PLT^*} – determined from the static plate load test (and corrected for plate size).
- $k_{FWD\text{-}Static\text{-}Corr}$ – determined from the FWD test and corrected for slab size.
- $k_{AASHTO(1993)}$ – determined using Equation 8, where M_r is determined from DCP-$CBR_{Subgrade}$ using charts provided in AASHTO (1993) (see Appendix A) or directly from laboratory measurements.

$$k_{AASHTO(1993)} = \frac{M_r}{19.4} \quad (8)$$

Note: as shown in Eq. 8, units for M_r are [psi] and k are [psi/in]; multiply the right side of the equation by 39.6 for units of M_r in [MPa] and k in [kPa/mm]

- $k_{PCA(1984)}$ – determined from CBR using charts provided in PCA (1984) (see Appendix A).
- $k_{comp\text{-}AASHTO(1972)}$ – determined using subgrade M_r determined from DCP-$CBR_{Subgrade}$ and modulus of subbase layer (E_{SB}) using charts provided in AASHTO (1972) (see Appendix A). E_{SB} is determined from DCP-CBR using charts provided in AASHTO (1993) (see Appendix A).
- $k_{comp\text{-}AASHTO(1993)}$ – determined using subgrade M_r determined from DCP-$CBR_{Subgrade}$, E_{SB}, and thickness of subbase/base layer (H_{SB}) using charts provided in AASHTO (1993) (see Appendix A). H_{SB} is determined from DCP profiles, and E_{SB} is determind as described for $k_{comp\text{-}AASHTO(1972)}$.
- $k_{comp\text{-}ACPA(2012)}$ – determined using subgrade M_r determined from DCP-$CBR_{Subgrade}$, modulus E_{SB} from DCP-$CBR_{Subbase}$, and H_{SB} using ACPA (2012) online estimator. M_r and E_{SB} values were estimated using AASHTO (1993) charts (see Appendix A).

CHAPTER 4. LABORATORY TEST RESULTS

Laboratory test results of subgrade and subbase layer samples collected from the field are presented in this chapter. A summary of the material index properties (i.e., laboratory compaction test, grain-size analysis, Atterberg limits test, soil classification, and specific gravity results) is provided in Table 4.

Table 4. Summary of material index properties

Parameter	Sand Subbase (TS1)	Subgrade (TS1)	Subgrade (TS2)
Standard Proctor Test Results (ASTM D698-07)			
γ_{dmax} (kN/m^3)	17.37	17.41	18.67
w_{opt}	11.8	18.3	12.0
Modified Proctor Test Results (ASTM D1557-07)			
γ_{dmax} (kN/m^3)	17.67	*	20.27
w_{opt}	11.6	*	10.4
Maximum and Minimum Relative Density Test Results (ASTM D4253-00 and D4254-00)			
γ_{dmax} (kN/m^3)	18.19	*	*
γ_{dmin} (kN/m^3)	15.07		
Particle-Size Analysis Results (ASTM D 422-63 and ASTM C136-06)			
Gravel Content (%) (> 4.75mm)	3	11	13
Sand Content (%) (4.75mm–75μm)	97	26	28
Silt Content (%) (75μm–2μm)	0	40	46
Clay Content (%) (< 2μm)		23	13
D_{10} (mm)	0.2149	**	**
D_{30} (mm)	0.2905	0.0053	0.0030
D_{60} (mm)	0.4035	0.0629	0.0812
Coefficient of Uniformity, c_u	1.88	**	**
Coefficient of Curvature, c_c	0.97	**	**
Atterberg Limits Test Results (ASTM D4318-05)			
Liquid Limit, LL (%)	Non Plastic	45	38
Plastic Limit, PL (%)		18	20
Plasticity Index, PI (%)		18	27
AASHTO Classification (ASTM D3282-09)	A-3	A-7-6(14)	A-6(8)
USCS Classification (ASTM D2487-00)	SP	CL	CL

*Test not performed; **Cannot be determined

Particle Size Analysis Results

Grain-size distribution curves from particle-size analysis tests for subbase and subgrade layer materials are provided in Figure 21. The subgrade materials from TS1 and TS2 showed parallel grain size distribution curves except that the fines passing the No. 200 sieve and clay content in the TS1 subgrade material was higher than in the TS2 subgrade material.

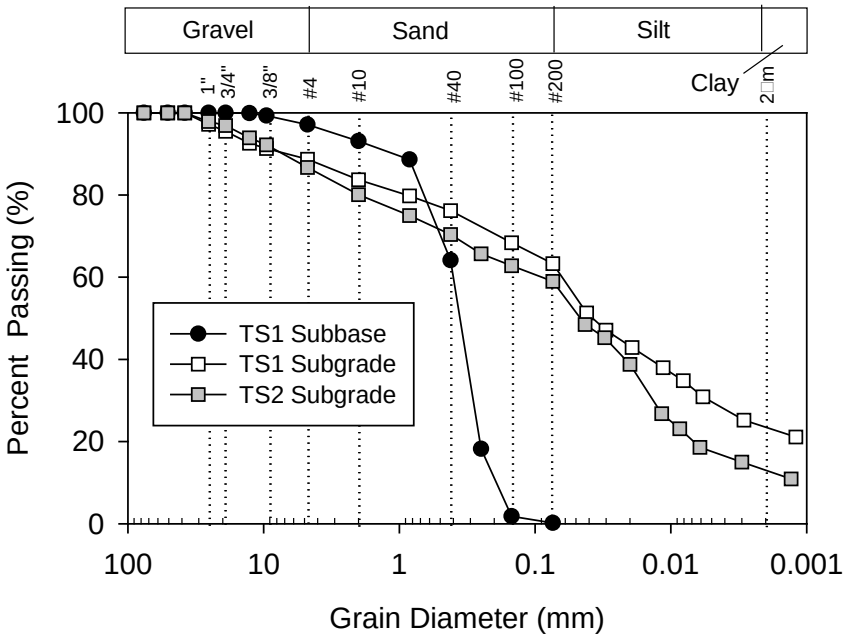

Figure 21. TS1 and TS2: Particle size distribution curves of subgrade and subbase materials

Moisture-Dry Unit Weight Results

Moisture-dry unit weight relationships from standard and modified Proctor tests of subgrade and subbase materials are shown in Figure 22 and Figure 23, respectively. Both materials showed a maximum dry unit weight and optimum moisture content at standard and modified Proctor energies, as summarized in Table 3. Vibratory compaction tests were also conducted at different moisture contents varying from 0 to 10%, and the results are shown in Figure 24. Vibratory compaction test results indicate a bulking moisture content of about 2.0% for the subbase material. Minimum and maximum dry unit weight from vibration compaction tests at oven-dry moisture content are summarized in Table 3. Figure 22 through Figure 24 also include the moisture and dry unit weight of M_r samples prepared in the laboratory and in situ moisture and dry unit weight measurements for reference.

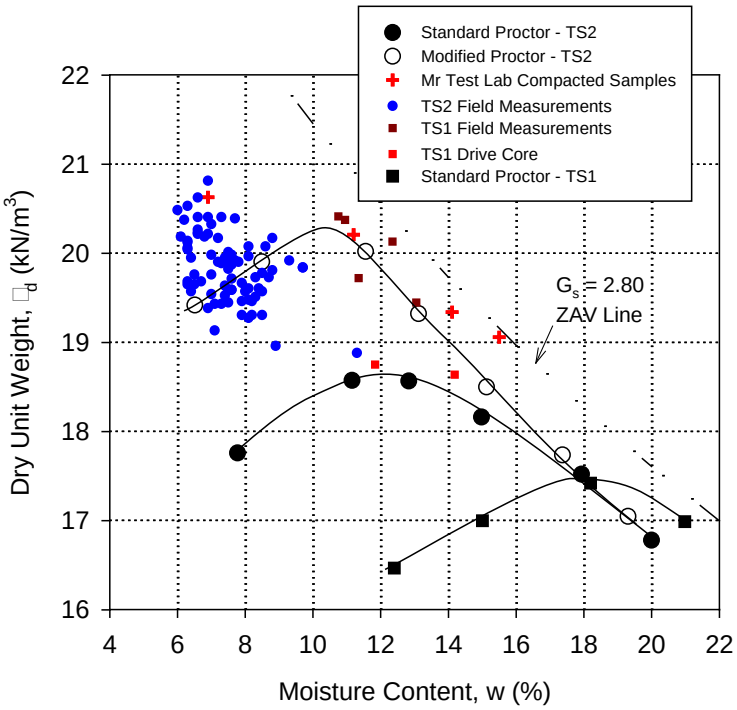

Figure 22. TS1 and TS2: Moisture-dry unit weight relationships of subgrade material from Proctor tests, moisture-dry unit weight of M_r samples, and in situ moisture-dry unit weight measurements

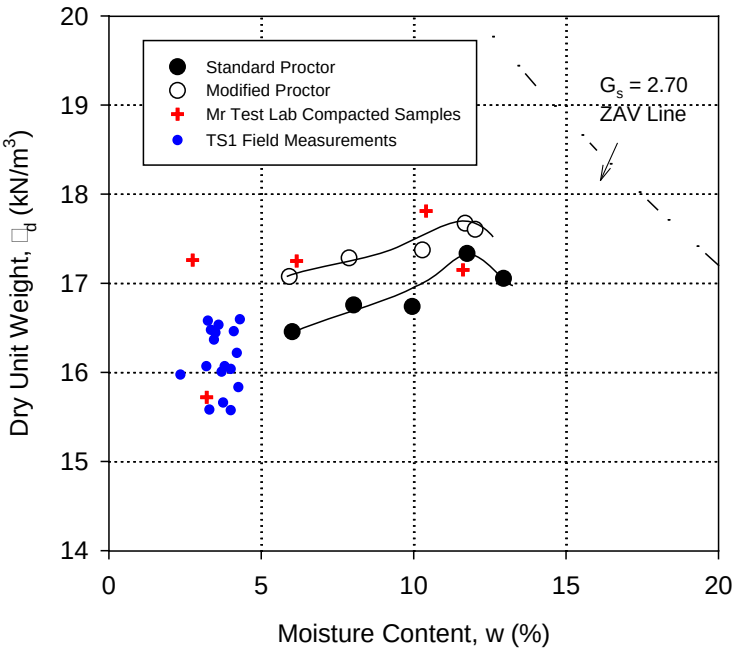

Figure 23. TS1: Moisture-dry unit weight relationships of subbase material from Proctor tests, moisture-dry unit weight of M_r samples, and in situ moisture-dry unit weight measurements

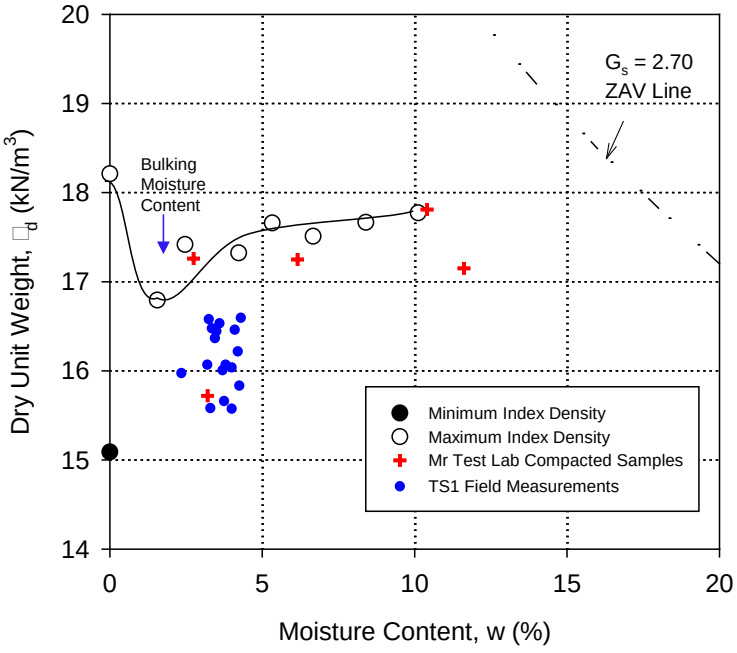

Figure 24. TS1: Moisture-dry unit weight relationships of subbase material from vibratory compaction tests, moisture-dry unit weight of M_r samples, and in situ moisture-dry unit weight measurements

M_r and UU Test Results

The test results for the three materials showing the γ_d, *w*, average M_r of the 15 AASHTO T-307 loading sequences; M_r at specific stress states; dynamic secant modulus (E_s); permanent strain (ε_p) at the end of the M_r test; universal model regression coefficients; undrained shear strength (s_u) at failure or at 5% axial strain; and s_u at 1% strain are summarized in Table 5. Stress states for granular and cohesive materials were recommended in NCHRP 1-28A report (NCHRP 2004) as σ_3 = 35 kPa (5 psi) and σ_{cyclic} = 103 kPa (15 psi) for base or subbase materials, and as σ_3 = 14 kPa (2 psi) and σ_{cyclic} = 41 kPa (6 psi) for subgrade materials. Equation 1 and the k_1, k_2, and k_3 regression coefficients were used to calculate the M_r at those stress states.

Deviator stress (σ_d) versus M_r for laboratory compacted subgrade samples, along with the universal model prediction curves, are presented in Figure 25. As expected for subgrade materials, these figures illustrate that the M_r generally decreases with increasing σ_d. Bulk stress (σ_B) versus M_r for sand subbase samples along with the corresponding universal model prediction curves are presented in Figure 26. Results indicated that the M_r of subbase material increase with increasing bulk stresses, as expected. Increasing moisture content decreased M_r and increasing dry unit weight increased M_r for both subbase and subgrade materials.

Figure 27 shows σ_B versus M_r measurements for a layered composite sample and single-material subbase and subgrade samples and corresponding universal model prediction curves. Pictures of a layered composite sample (i.e., subbase over subgrade) during and after testing are shown in Figure 28 and Figure 29. Comparing the M_r values of the layered composite and homogeneous samples reveals that the average M_r of layered composite sample is about 1.4 times lower than the average M_r of a single layer subbase sample at a similar density. This reduction in M_r in the layered composite sample is attributed to the weaker subgrade layer. This is an important finding and must be further studied with adequate testing in various combinations of layered composite sample configurations. Efforts are underway in at other sites in the larger research project to further investigate the influence of layered composite soil layer configurations on M_r properties.

Table 5. Summary of M_r and UU test results

			M_r Test								UU Test	
Sample	γ_d (kN/m^3)	*w* (%)	Ave. M_r (MPa)	M_r at selected Stress States (MPa)[#]	E_s (MPa)	ε_p (%)	k_1	k_2	k_3	R^2 (adj.)	s_u (kPa)[§]	s_u @ ε = 1% (kPa)
Subgrade*	19.34	14.1	55.8	52.6	55.8	0.5	769.5	0.15	-2.09	0.75	117.3	64.6
Subgrade*	20.63	6.9	150.8	126.9	150.5	0.1	1835.5	0.49	-1.63	0.49	546.1	370.7
Subgrade*	19.06	15.5	56.8	48.8	56.8	0.5	1069.0	0.17	-4.35	0.75	102.7	60.6
Subgrade*	20.21	11.2	115.5	107.6	115.4	0.1	1400.8	0.19	-1.37	0.11	311.6	163.5
Subbase*	15.72	3.2	139.0	102.2	137.5	3.8	655.5	0.79	-0.35	0.94	—	—
Subbase*	17.15	11.6	172.7	117.9	172.7	0.4	686.1	0.92	-0.34	0.99	75.1	75.1
Subbase*	17.26	2.8	171.1	131.0	164.6	0.4	797.3	0.52	0.28	0.88	77.0	77.2
Subbase*	17.25	6.2	183.3	146.6	183.3	0.3	1057.4	0.61	-0.32	0.92	74.1	74.4
Subbase*	17.81	10.4	198.3	152.9	197.9	0.4	1083.6	0.70	-0.44	0.93	83.7	83.5
Composite subbase* + subgrade*	17.04 19.60	8.2 11.3	119.8	99.9	119.7	0.6	873.14	0.54	-0.68	0.96	96.25	94.2

* = laboratory compacted sample, [#] subgrade: σ_3 = 14 kPa (2 psi) and σ_{cyclic} = 41 kPa (6 psi), and for subbase σ_3 = 35 kPa (5 psi), σ_{cyclic} = 103 kPa (15 psi); [§]at axial strain ε = 5% or at failure

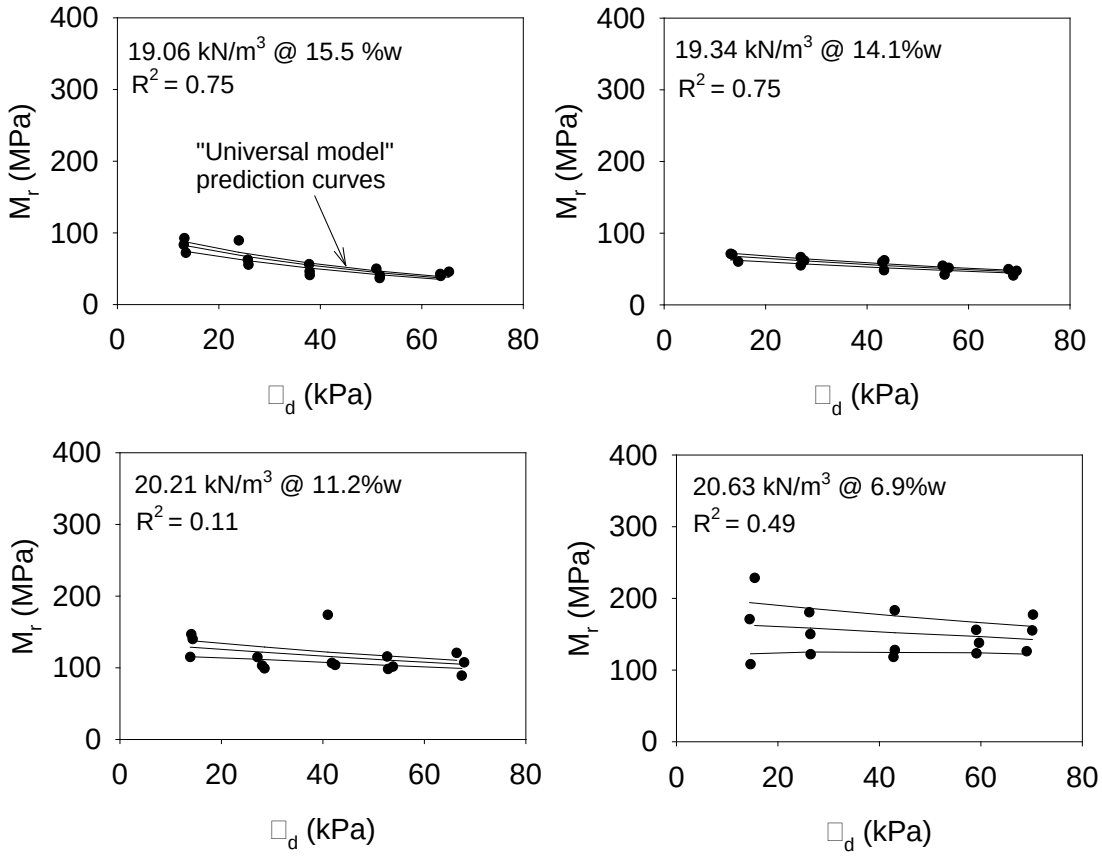

Figure 25. Summary of σ_d versus M_r for laboratory compacted subgrade samples at different dry unit weights and moisture contents

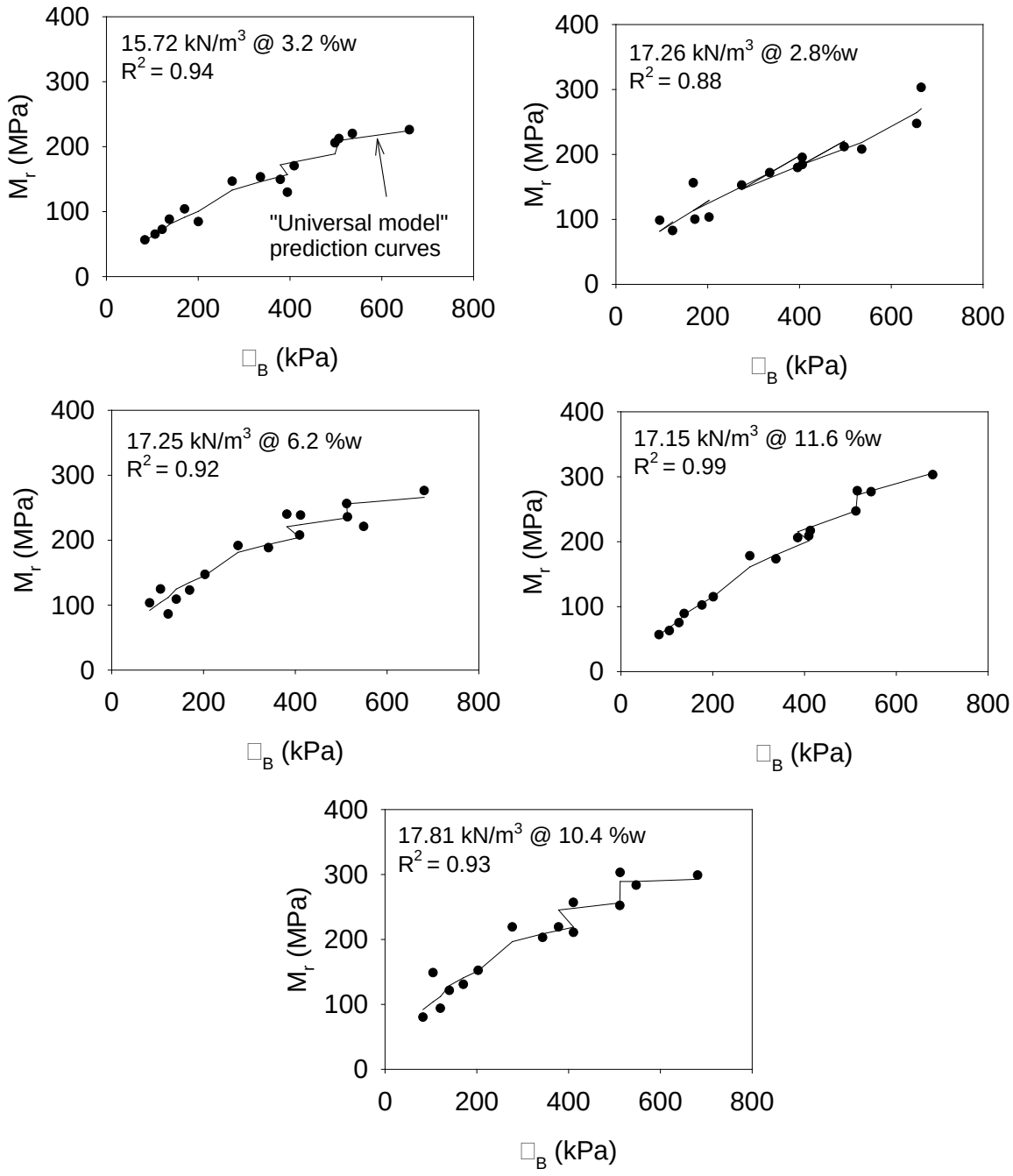

Figure 26. Summary of σ_B versus M_r for sand subbase samples at different dry unit weights and moisture contents

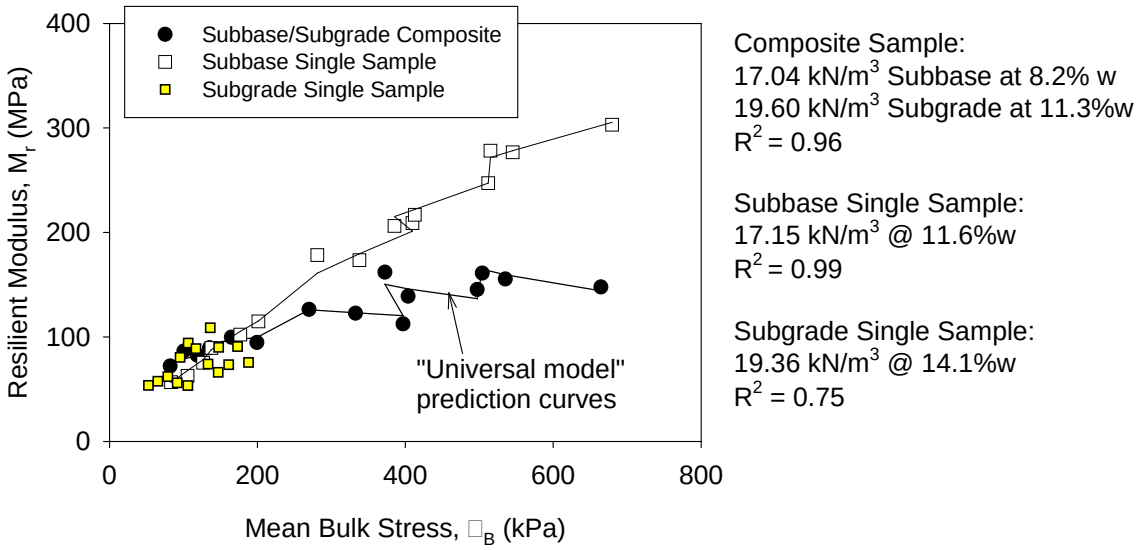

Figure 27. Summary of σ_B versus M_r for subbase, subgrade, and composite samples

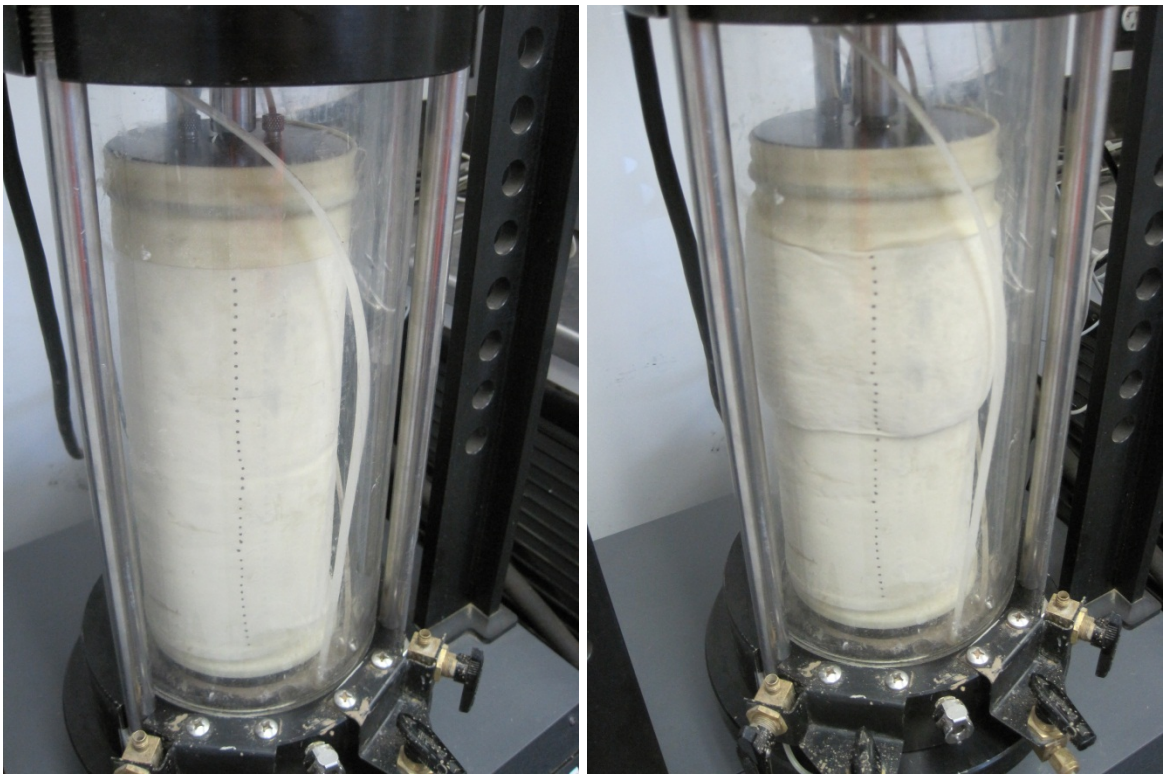

Figure 28. Sand + subgrade layered composite sample during M_r testing (left) and after shearing (right)

Figure 29. Sand + subgrade layered composite sample extruded sample after shearing

Frost Heave and Thaw Weakening Test Results

Frost-heave and thaw-weakening tests were conducted on four compacted subgrade samples from TS2. The samples were compacted to a target w = 12.4% and γ_d = 18.69 kN/m^3. The actual w of the samples varied between 12.0% and 13.9% and the actual γ_d varied between 18.10 kN/m^3 and 18.39 kN/m^3, with a degree of saturation at about 65% to 77%. The CBR of the compacted sample before saturation was determined as about 26%.

The frost-heave and temperature versus time results are shown in Figure 30. Results indicated that the heave rate was greater for the second freezing cycle than for the first freeze cycle, which indicates that the material is susceptible to increased heave with greater F/T cycles. The average heave rates for the 1st and 2nd freezing cycles are summarized in Table 6. Based on the frost-heave rate measurements, the TS2 soil is classified to have medium potential to frost-heave according to ASTM D5918.

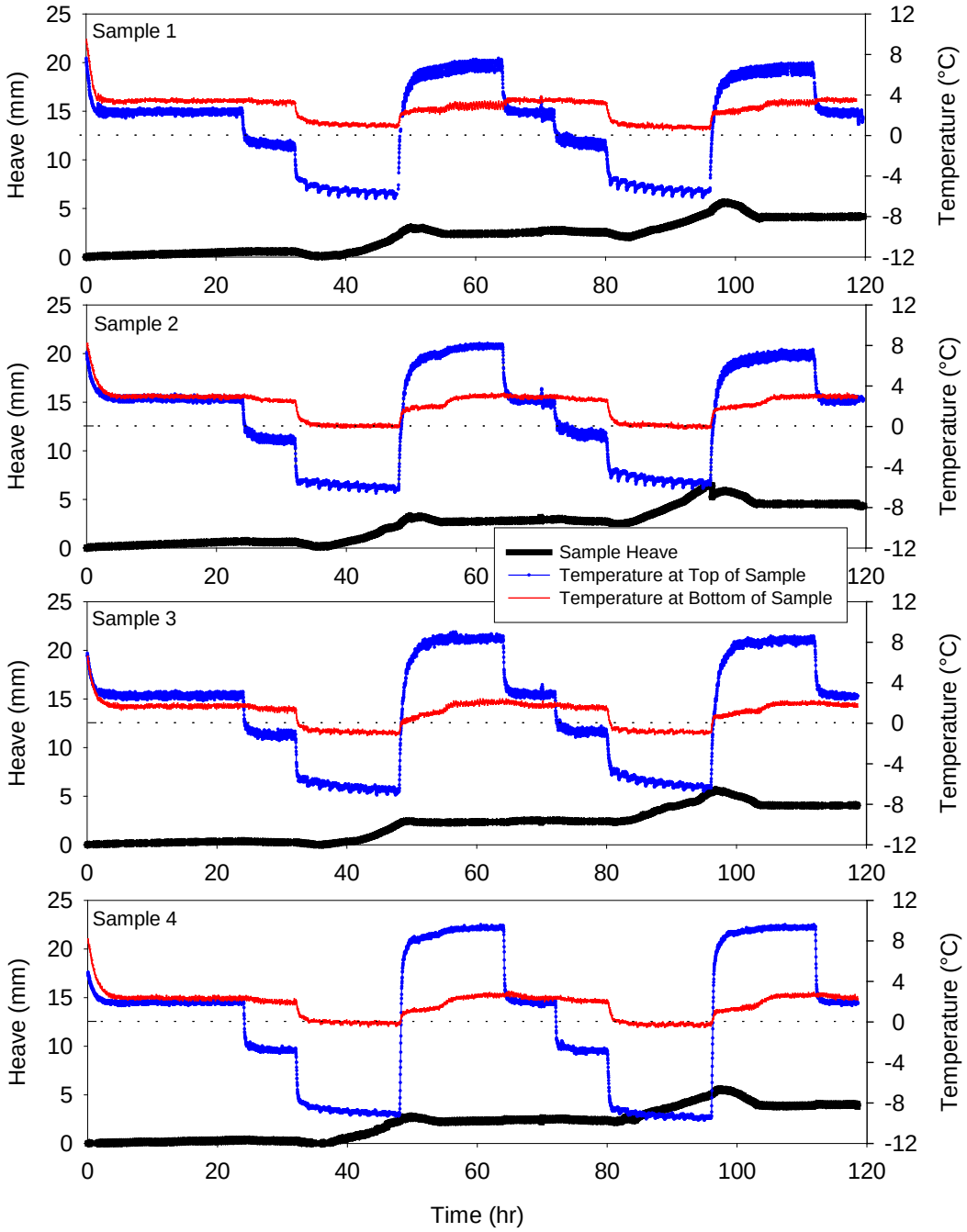

Figure 30. TS2: Frost heave and temperature versus time plots for the lean clay subgrade sample

The height of the samples increased by about 13 to 21 mm (8% to 14%) after the two cycles, and the mass of the sample increased by about 232 to 298 gm (4% to 6%). This indicates that the moisture drawn into the sample during the freezing period by capillary action did not completely drain from the soil during the thawing period. Moisture contents at different depths were determined for each sample immediately after the test are presented in Figure 31. The moisture content at 100% saturation (assuming the initial γ_d of each sample) and the initial moisture

content of the sample during compaction are also shown on Figure 31 for reference. Results indicated that the moisture content is higher at all depths in the samples compared to the initial moisture content. The moisture content at the top of the sample was closer to the initial moisture content and the moisture content increased with depth.

The CBR test on the thawed samples decreased to an average CBR = 7 on the four samples (Table 6). Based on the thawed CBR values, the soil is classified to have medium potential to thaw-weakening according to ASTM D5918.

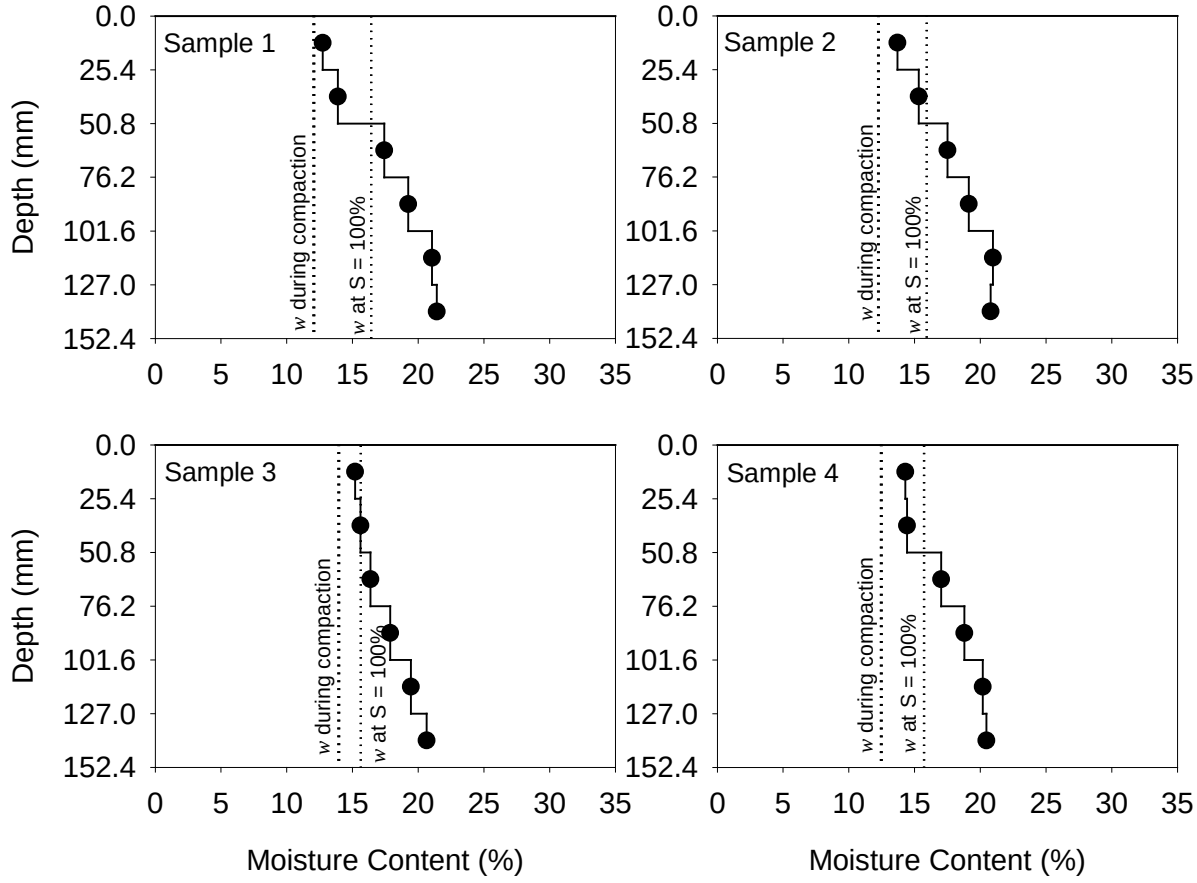

Figure 31. TS2: Moisture content profiles of subgrade samples immediately after F/T testing

Table 6. Summary of frost-heave and thaw-weakening test results on TS2 subgrade samples

Parameter	μ	σ	COV (%)	Number of samples
CBR (%) (standard test)	25.9	—	—	1
CBR (%) (after frost-susceptibility test)	7.2	4	5.5	
1st Frost-heave rate (mm/day)	4.6	0.2	4.2	
2nd Frost-heave rate (mm/day)	5.5	0.9	17.2	4
1st Frost-heave susceptibility rating	Medium	—	—	
2nd Frost-heave susceptibility rating	Medium	—	—	
Thaw-weakening susceptibility rating	Medium	—	—	

CHAPTER 5. IN SITU TEST RESULTS

Description of Test Sections

In situ tests were conducted on three test sections (TS). TS1 consisted of a sand subbase layer (with variable thickness) underlain by subgrade; TS2 consisted of a subgrade layer; and TS3 consisted of a PCC surface paved in 2009. Table 7 summarizes the in situ testing methods that were used to characterize the foundation layer properties.

Table 7. Test sections, test dates, material properties, in situ tests, and comments

TS	Date	Location	Material	In Situ Tests	Comments
1	5/25/10	US10WB lane at two locations: TS1-1: Between Sta. 555+00 and 565+00 TS1-2: Near Sta. 575+50	Sandy subbase (loose) underlain by subgrade. Note: Thick sand subbase (~ 600 mm) at location 1 and very thin (~50 to 100 mm) sand subbase at location 2	NG, DCP, LWD	TS1-1: Tests performed every 3 m along the centerline of US 10WB lane. In addition, seven tests across pavement width near Sta. 560+00. TS1-2: Tests performed at five test locations by excavating the sand subbase layer down to subgrade
2	5/24 to 5/25/10	US10 WB lane West of Co Rd G near Sta. 495+00	Subgrade	NG, DCP, LWD, PLT	8 m x 28 m dense spatial grid section and tests every 3 m along the centerline of US 10WB
3	5/26/10	Between Sta. 615+00 and Sta. 580+50 (started 12 panels west of 615+00) along US10 WB right lane	PCC pavement (paved in 2009), underlain by crushed rock base, sand subbase, and subgrade (graded in 2008)	DCP, FWD	FWD at mid panel and joints, and DCP at three select locations to a depth of about 1.8 m below pavement surface

Note: TS – test section; NG – nuclear gauge; DCP – dynamic cone penetrometer (DCP) test; LWD – Zorn light weight deflectometer with a 300 mm plate; FWD – Kuab falling weight deflectometer; PLT –static plate load test.

Geostatistical Data Analysis

Spatially referenced in situ point measurements in a dense grid pattern were obtained for TS2. This dataset provides an opportunity to quantify the non-uniformity of compacted fill materials. Non-uniformity can be assessed using conventional univariate statistical methods (i.e., by statistical standard deviation (σ) and coefficient of variation (COV)), but these methods do not address the spatial aspect of non-uniformity. Vennapusa et al. (2010) demonstrated the use of semivariogram analysis in combination with conventional statistical analysis to evaluate non-uniformity in QC/QA during earthwork construction. A semivariogram is a plot of the average

squared differences between data values as a function of separation distance and is a common tool used in geostatistical studies to describe spatial variation. A typical semivariogram plot is presented in Figure 32. The semivariogram function ($\gamma(h)$), is defined as one-half of the average squared differences between data values that are separated at a distance *h* (Isaaks and Srivastava 1989). When this calculation is repeated for many different values of *h* (as the sample data will support), the result can be graphically presented as an experimental semivariogram, shown as circles in Figure 32. More details on experimental semivariogram calculation procedure are available elsewhere (e.g., Clark and Harper 2002, Isaaks and Srivastava 1989).

To obtain an algebraic expression for the relationship between separation distance and experimental semivariogram, a theoretical model is fit to the data. Some commonly used models are linear, spherical, exponential, and Gaussian models. A spherical model was used for data analysis in this report. Arithmetic expression of the spherical model and a spherical semivariogram are shown in Figure 32. Three parameters are used to construct a theoretical semivariogram: sill ($C+C_0$); range (R); and nugget (C_0). These parameters are briefly described in Figure 32. More discussion on the theoretical models can be found elsewhere (e.g., Clark and Harper 2002, Isaaks and Srivastava 1989). For the results presented in this report, the sill, range, and nugget values during theoretical model fitting were determined by checking the models for goodness using the modified Cressie goodness fit method (see Clark and Harper 2002) and cross-validation process (see Isaaks and Srivastava 1989). From a theoretical semivariogram model, a low "sill" and longer "range of influence" represent best conditions for uniformity, while the opposite represents an increasingly non-uniform condition.

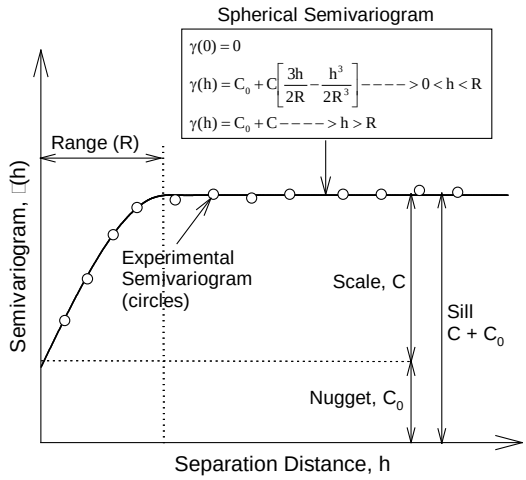

Range, R: As the separation distance between pairs increase, the corresponding semivariogram value will also generally increase. Eventually, however, an increase in the distance no longer causes a corresponding increase in the semivariogram, i.e., where the semivariogram reaches a plateau. The distance at which the semivariogram reaches this plateau is called as range. Longer range values suggest greater spatial continuity or relatively larger (more spatially coherent) "hot spots".

Sill, $C+C_0$: The plateau that the semivariogram reaches at the range is called the sill. A semivariogram generally has a sill that is approximately equal to the variance of the data.

Nugget, C_0: Though the value of the semivariogram at h = 0 is strictly zero, several factors, such as sampling error and very short scale variability, may cause sample values separated by extremely short distances to be quite dissimilar. This causes a discontinuity at the origin of the semivariogram and is described as nugget effect. (Isaaks and Srivastava, 1989)

Figure 32. Description of a typical experimental and spherical semivariogram and its parameters (Isaaks and Srivastava 1989)

TS1: Subbase Layer Underlain by Subgrade

Experimental Testing

TS1 consisted of a relatively loose sand subbase layer placed over the subgrade along US 10WB lane between Sta. 555+00 and 575+00. NG, LWD, and DCP tests were conducted at two locations: TS1-1 between Sta. 555+00 and 565+00 at every 3 m along the centerline and seven tests across the pavement width near Sta. 560+00 (Figure 33) and TS1-2 near Sta. 575+00 at five test locations by excavating the sand subbase layer down to subgrade (Figure 35). Tests on TS1-1 were conducted on top of the nominal 600 mm thick sand subbase layer. Because the sand subbase layer at TS1-2 was only 50 to 100 mm thick, the sand was excavated prior to testing.

In Situ Point Test Results and Discussion

In situ test results from TS1-1 and TS1-2 are presented in Figure 36 and Figure 37, respectively. DCP-CBR profiles from each test location are provided in Figure 38 and Figure 39. Histograms of all measurements from TS1-1 are provided in Figure 40. The average dry unit weight of the subbase layer was about 16.15 kN/m^3, which was about 93% of standard Proctor γ_{dmax}. The average moisture content of the subbase layer was about 3.7%, which was about 8.1% dry of standard Proctor w_{opt}. The average dry unit weight of the subgrade layer was about 20.02 kN/m^3, which was about 115% of standard Proctor γ_{dmax}. The average moisture content of the subbase layer was about 11.7%, which was about 0.1% dry of standard Proctor w_{opt}. Comparisons of in situ moisture-dry unit weight measurements with laboratory Proctor test results are presented in the laboratory test results chapter of this report (see Figure 22 and Figure 23).

Based on DCP profiles, the subbase layer thickness on TS1-1 varied from about 375 to 556 mm. On average, the subbase layer thickness was about 150 mm lower than the target 610 mm thickness. DOT field engineers on the site indicated that the subbase layer would be graded to target thickness prior to paving.

The average DCP-CBR$_{Subgrade}$ on TS1-1 and TS1-2 was 17.4 (note that the DCP-CBR$_{Subgrade}$ was determined from the top 300 mm of subgrade). Using the AASHTO (1993) approach, the $k_{Estimated}$ value from this CBR is about 197 kPa/mm (721 pci), which is significantly higher than the 41 kPa/mm (150 pci) target k value in the pavement design.

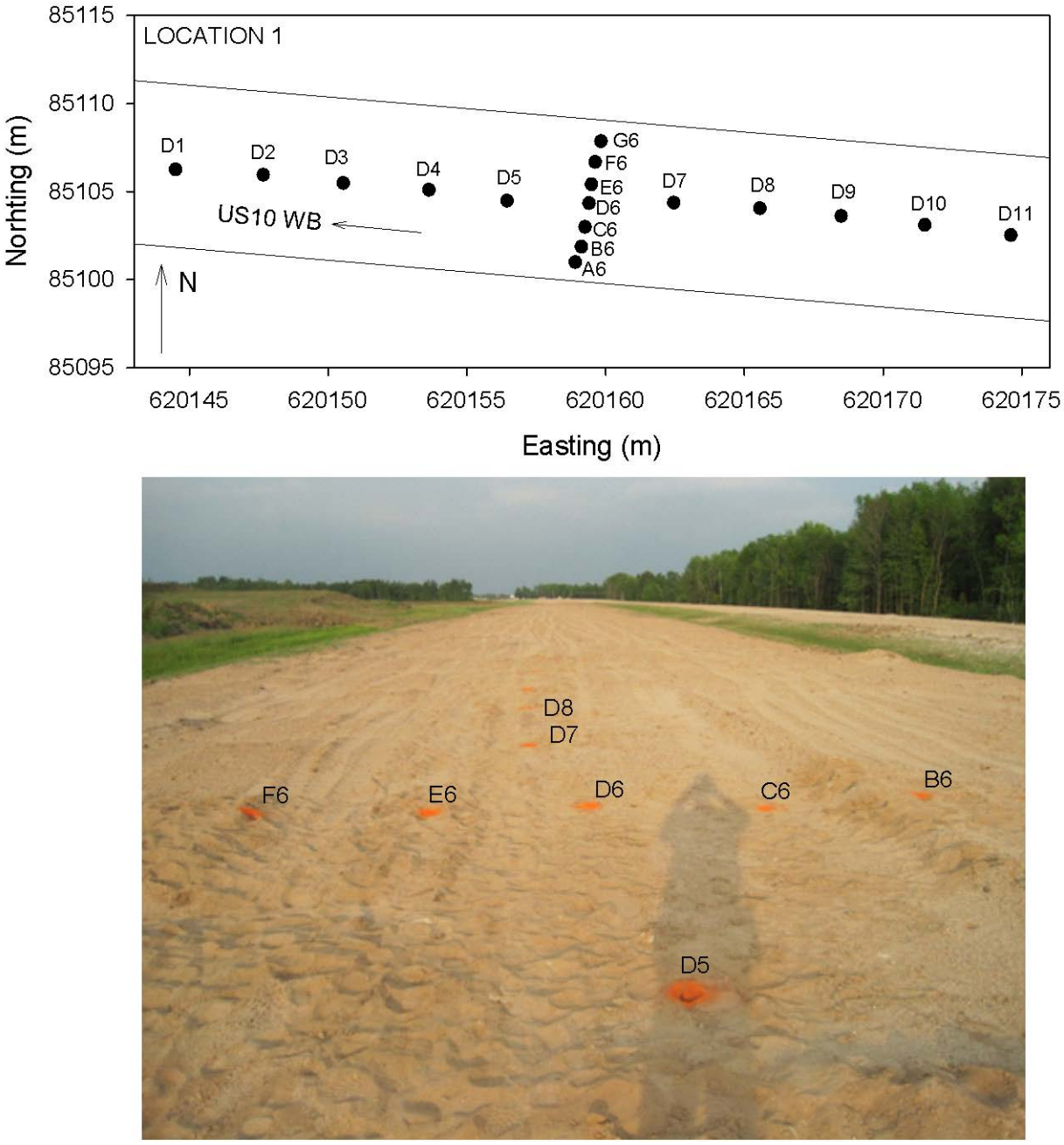

Figure 33. TS1-1: Plan view (top) and a photo (bottom) of in situ test locations on TS1-1

Figure 34. TS1-2: Photo of in situ testing locations

Figure 35. TS1-2: Excavation through the thin sand subgrade layer for tests on the subbase

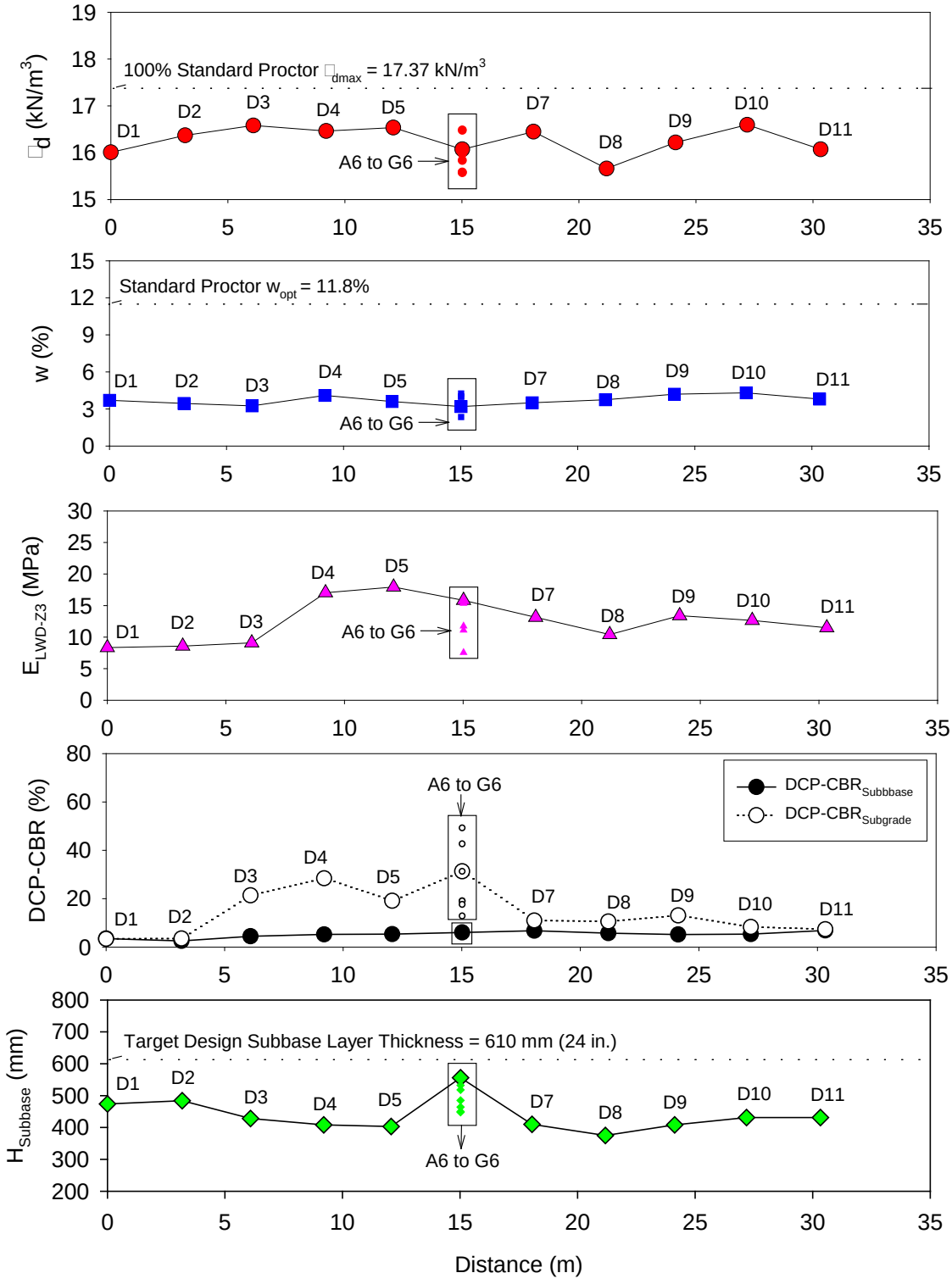

Figure 36. TS1-1: NG, LWD, and DCP test results

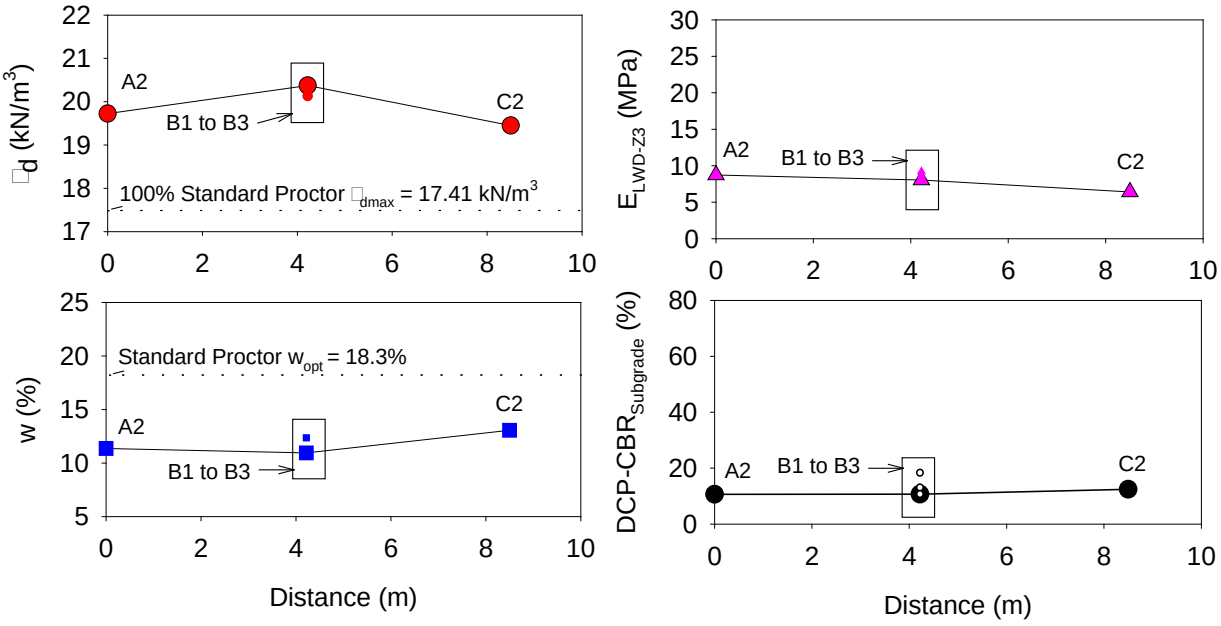

Figure 37. TS1-2: In situ NG, LWD, and DCP test results

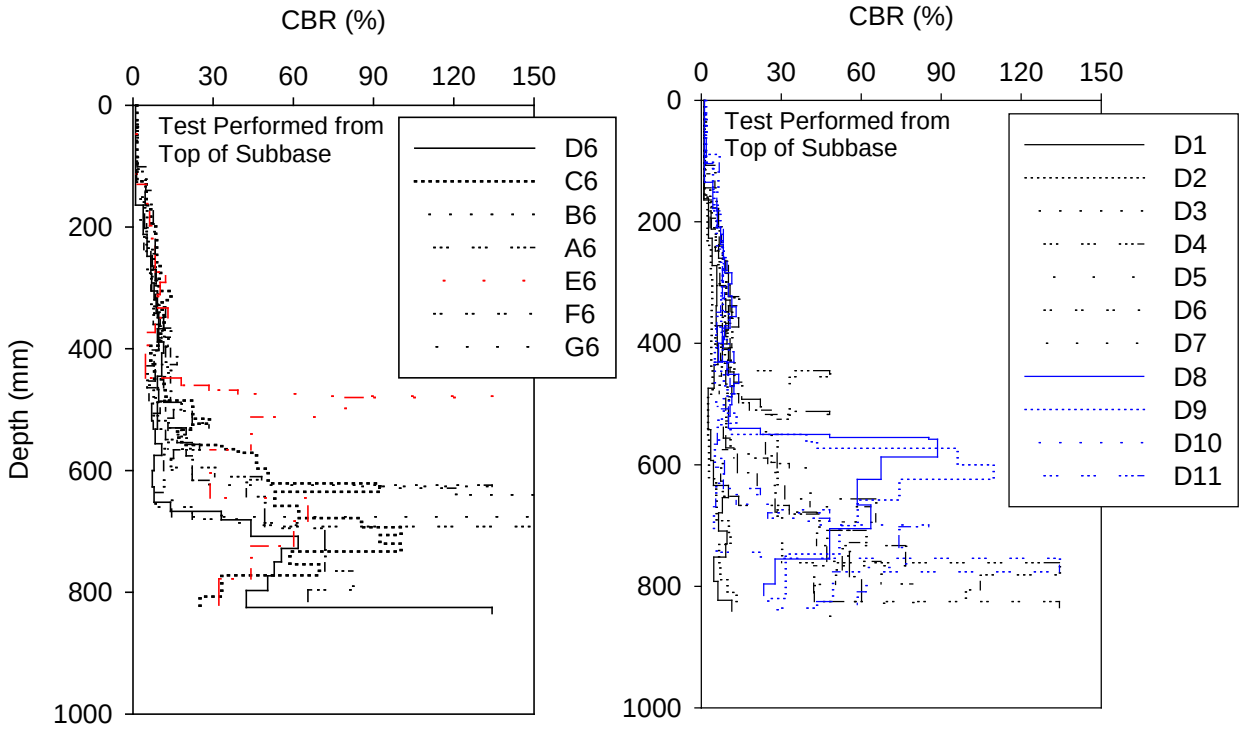

Figure 38. TS1-1: DCP-CBR profiles at each test location

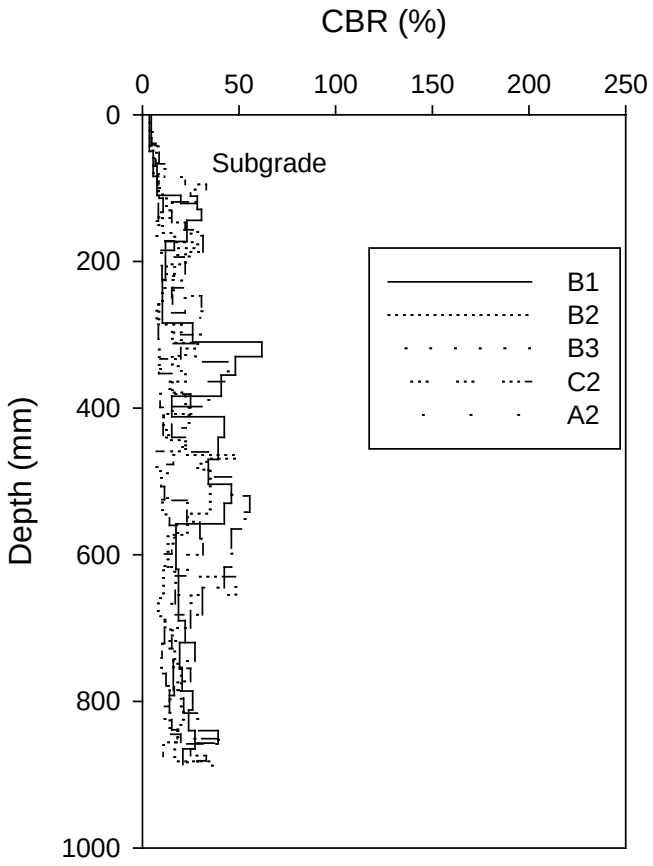

Figure 39. TS1-2: DCP-CBR profiles at each test location

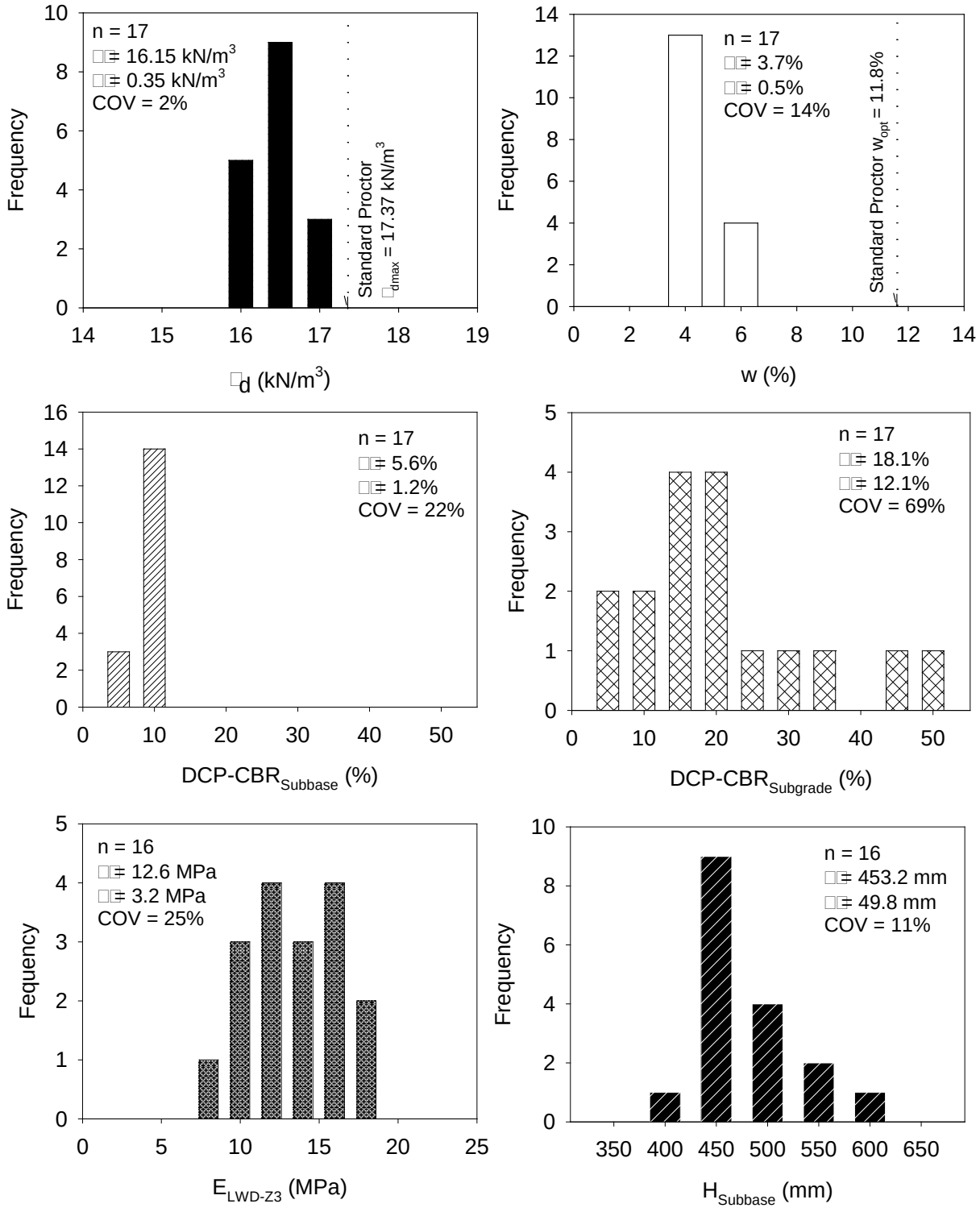

Figure 40. TS1-1: Histograms of in situ test measurements

TS2: Subgrade Layer

Experimental Testing

TS2 consisted of testing the final compacted subgrade layer along US10WB lane near Sta. 495+00. A plan area of about 8 m x 28 m was selected for dense grid testing with about 70 test locations. In addition, tests were conducted every 3 m along the centerline of the alignment over 65 m long stretch of the road. A plan view of the TS with GPS measurements of the test locations is provided in Figure 42. In situ tests on this TS involved PLT, LWD, NG, and DCP tests.

In Situ Point Test Results and Statistical Analysis

In situ NG, LWD, and DCP test results along the 65 m long stretch of the roadway are presented in Figure 43. E_{V1}, E_{V2}, and k_{PLT*} results from PLT are presented in Figure 44. Also included in Figure 44 is the design *k* value for reference. DCP-CBR profiles from TS2 are presented in Figure 45. Histogram plots of all in situ measurements are shown in Figure 46.

The average $DCP\text{-}CBR_{Subgrade}$ on TS2 was 15.5 (note that the $DCP\text{-}CBR_{Subgrade}$ was determined from the top 300 mm of subgrade). Using the AASHTO (1993) approach, the $k_{Estimated}$ value from this CBR is about 179 kPa/mm (655 pci), which is significantly higher than the target *k* value used in design (41 kPa/mm (150 pci)). However, the average actual *k* value measured directly from PLT (k_{PLT*}) on this TS was about 30.5 kPa/mm (112 pci), which is about 1.3 times lower than the target *k* value.

Test measurements obtained in a dense grid pattern with 70 tests over a plan area of about 8 m by 28 m provided a robust dataset to characterize the spatial characteristics of the measurements using geostatistical analysis. Kriged spatial contour maps, semivariograms, and histograms of each in situ point measurement are presented in Figure 47 and Figure 48. The spatial statistical parameters (i.e., sill, range, and nugget) are provided in the semivariogram plots. A spherical semivariogram model showed best fit for all the measurements. $DCP\text{-}CBR_{Subgrade}$ and $E_{LWD\text{-}Z3}$ kriged contour maps showed similar spatial variation of soft and stiff areas. Spatial variability on dry unit weight measurements did not match with $E_{LWD\text{-}Z3}$ and $DCP\text{-}CBR_{Subgrade}$ measurements.

Figure 41. TS2: Photograph of the compacted subgrade

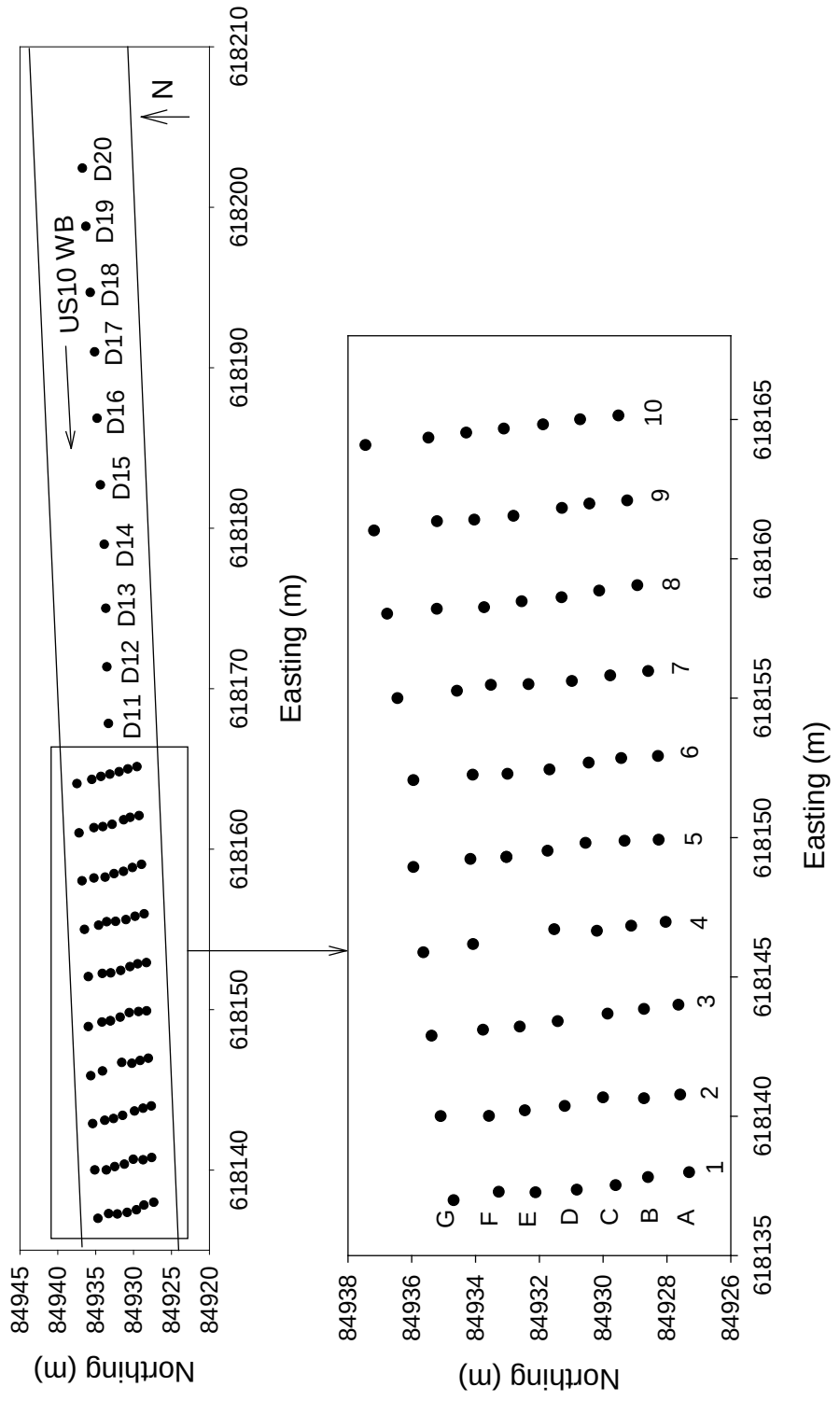

Figure 42. TS2: Plan view of test locations

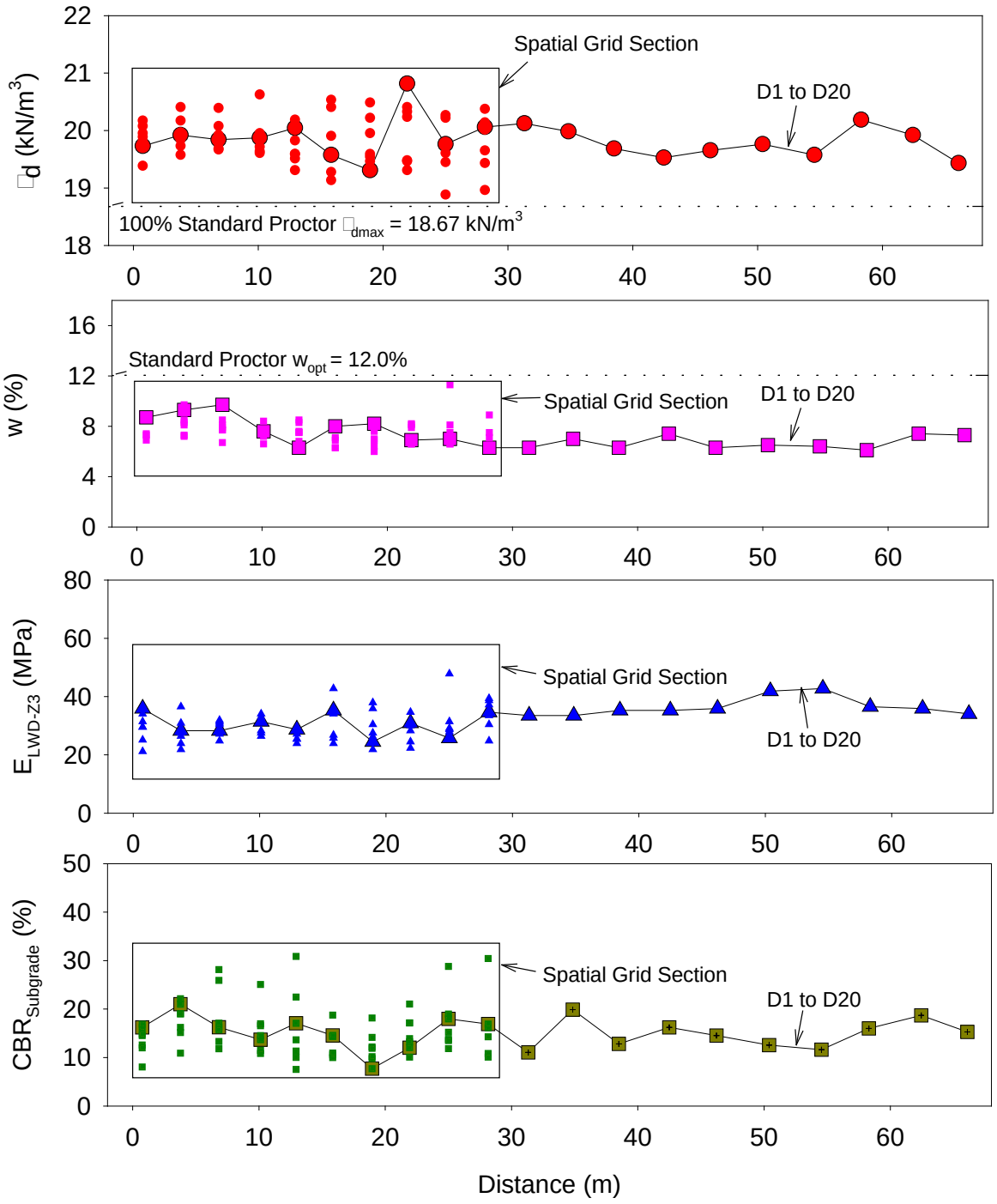

Figure 43. TS2: In situ NG, LWD, and DCP test results

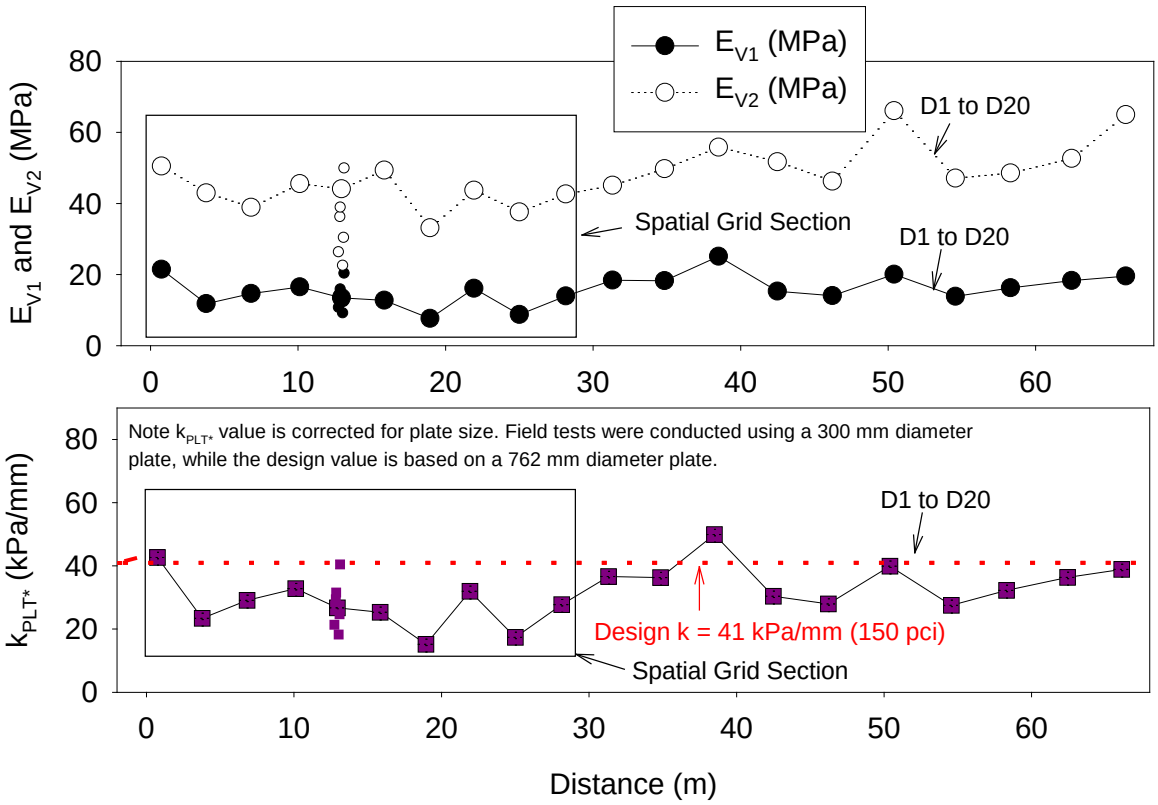

Figure 44. TS2: In situ PLT results

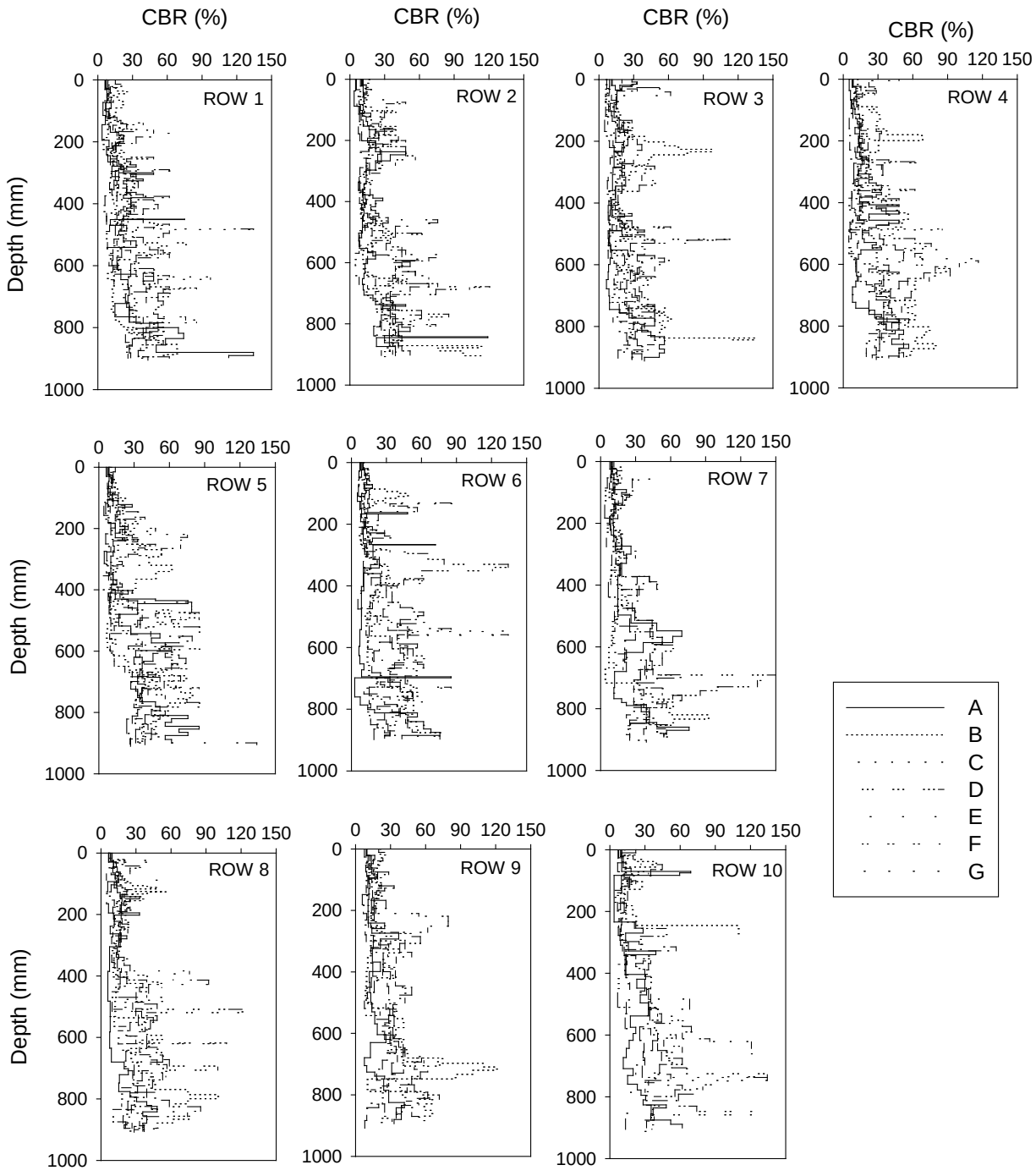

Figure 45. TS2: DCP-CBR profiles from each test location

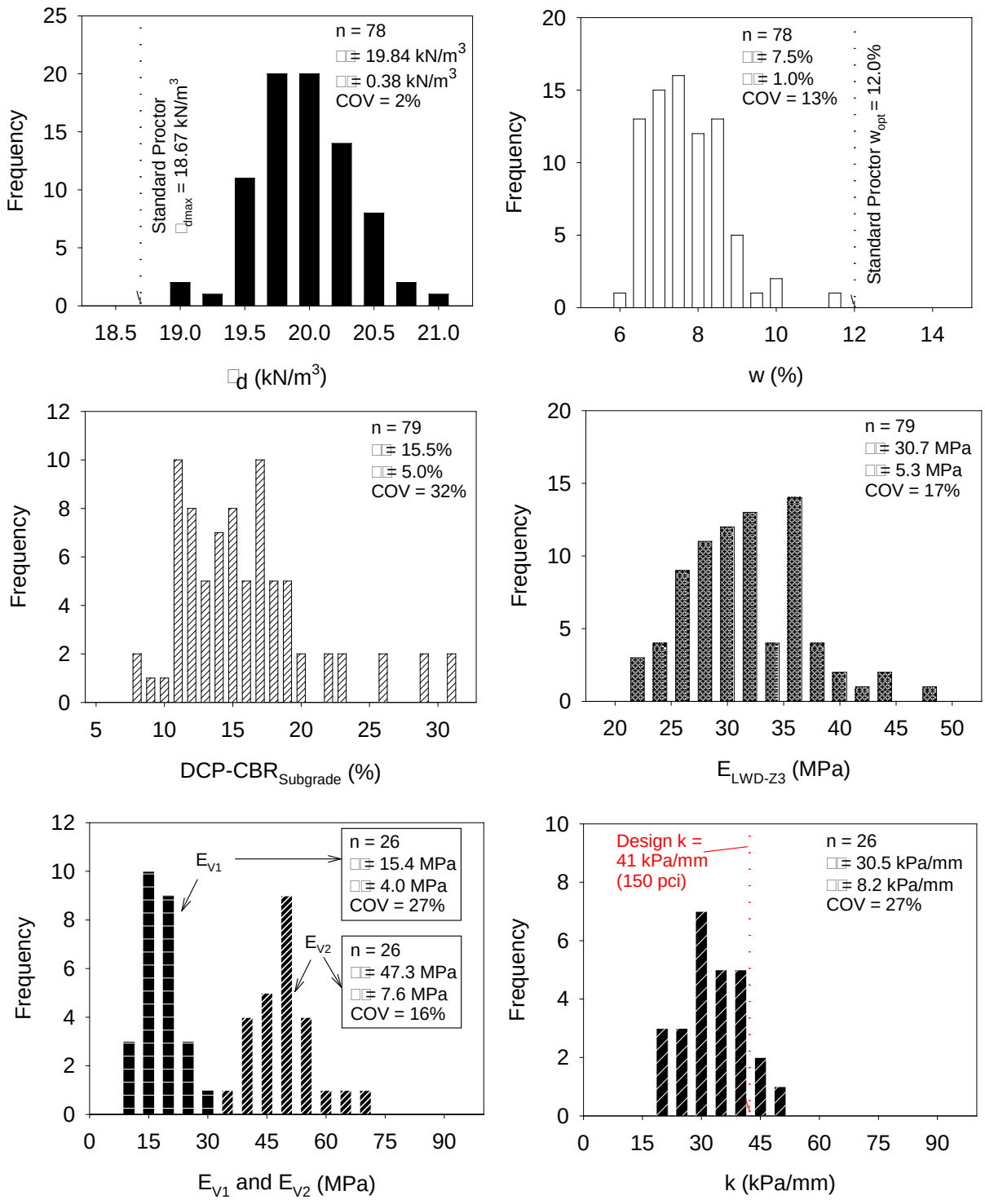

Figure 46. TS2: Histograms of in situ test measurements

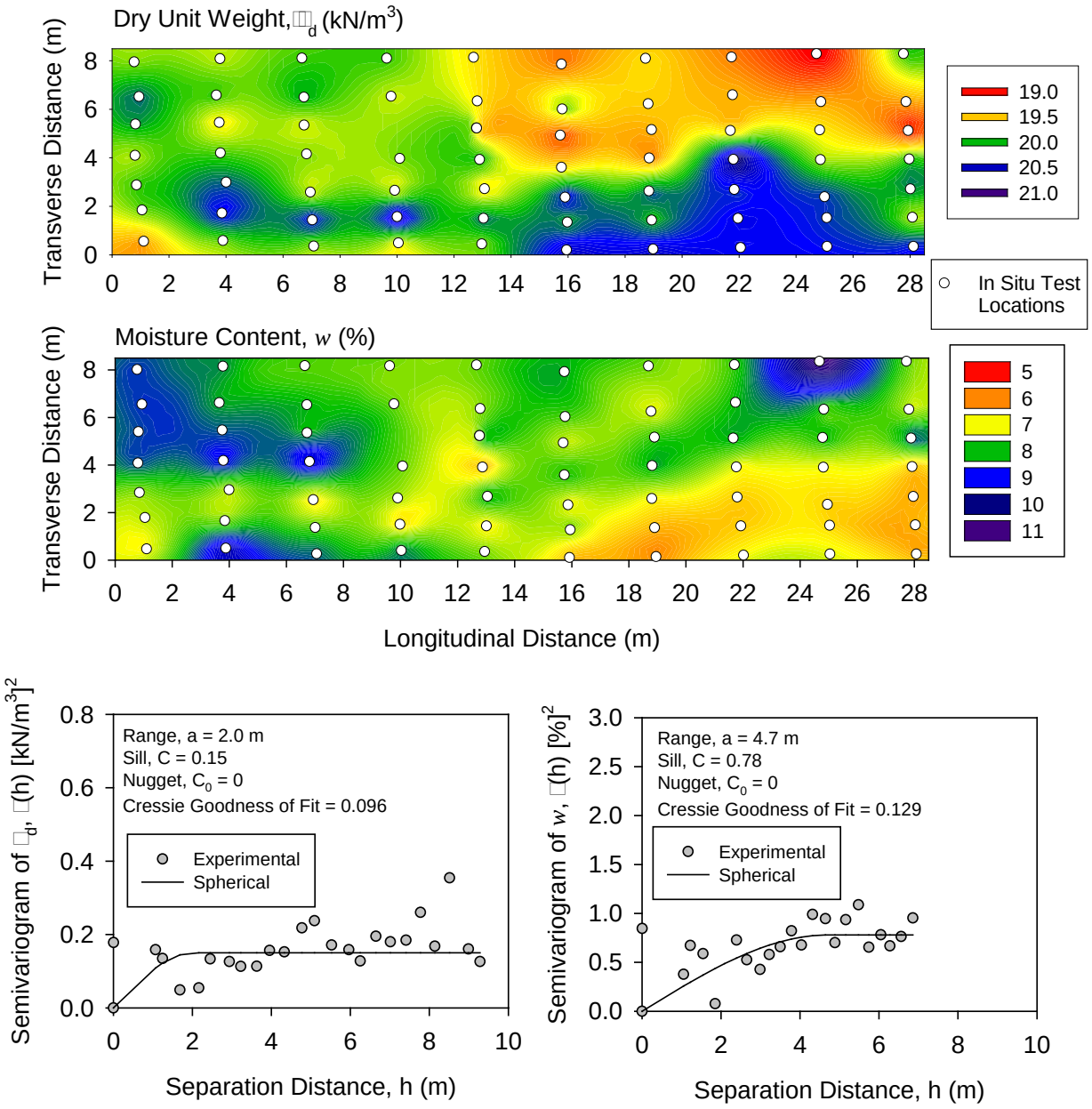

Figure 47. TS2: Kriged spatial contour maps (top) and semivariograms of γ_d and *w* measurements (bottom)

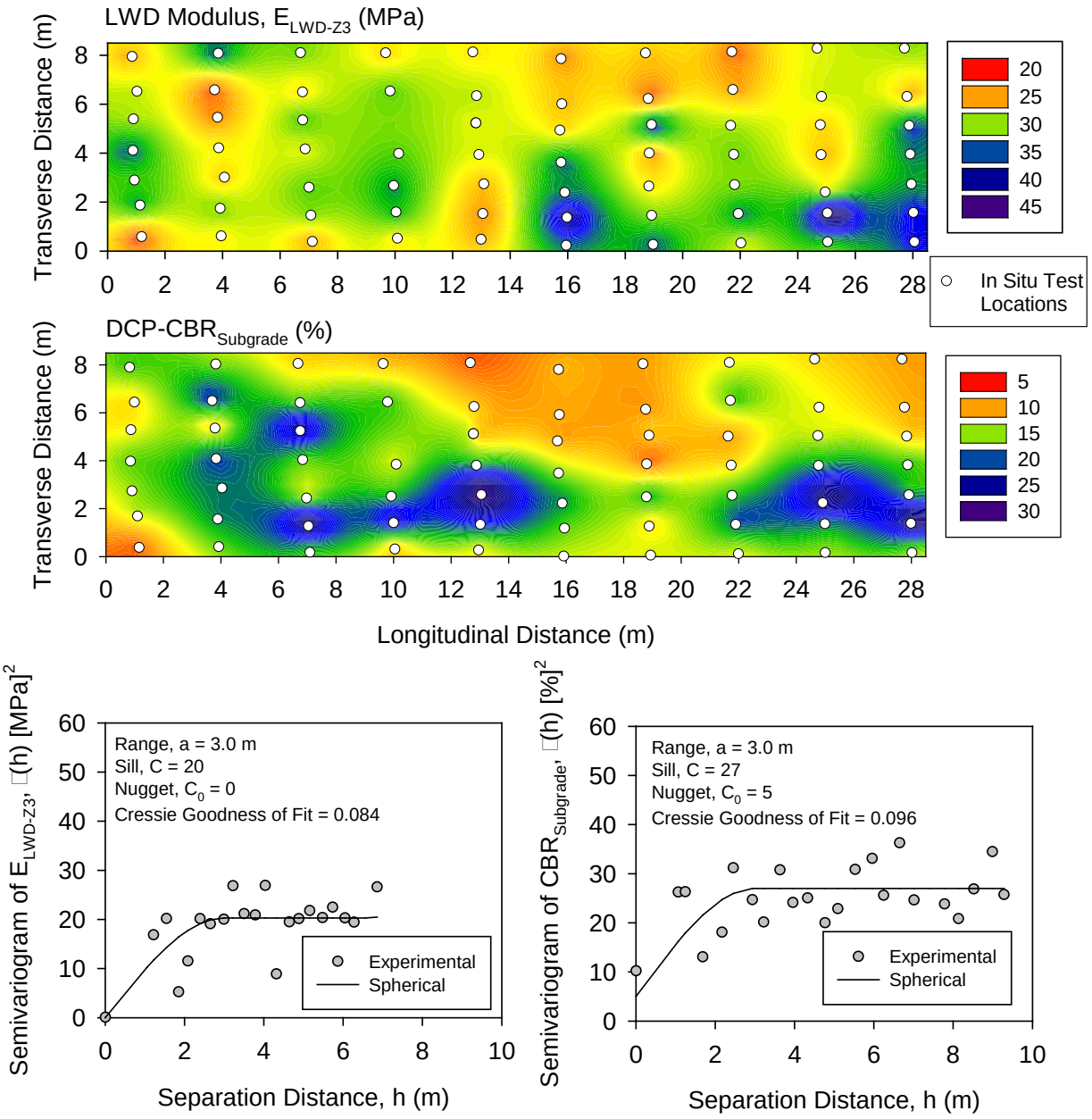

Figure 48. TS2: Kriged spatial contour maps and semivariograms of LWD and DCP measurements

TS3: PCC Pavement Layer

Experimental Testing

TS3 consisted of testing the PCC surface layer along US 10WB (right) lane with FWD at mid panel and at joints and the foundation layers with DCP. DCP tests were conducted at three selected FWD test locations by drilling a hole in the pavement. FWD tests were conducted on 36 panels between Sta. 615+00 and Sta. 585+00. The PCC pavement was constructed in 2009 and reportedly, grading for the pavement foundation layers were completed in this area in summer 2008. Temperature profiles in the pavement were also obtained during FWD testing to aid in interpretation of FWD test results. Temperature measurements were obtained from the surface, and at 51 mm, 102 mm, 152 mm, and 241 mm below the surface.

In Situ Point Test Results and Discussion

Results from FWD tests including the maximum deflections under plate at mid panel at 40 kN applied force (9,000 lb) D_0, LTE at joints, zero load intercept, and back-calculated $k_{FWD\text{-}Static}$ values along the 900 m long stretch of the roadway is presented in Figure 51. Pavement temperature profiles indicate positive temperature gradients (i.e., surface warmer than bottom) varying from about 0.04 to 0.12°C/m (Figure 52). All intercept measurements were close to zero or slightly below zero, indicating no apparent voids beneath the pavement. On average, LTE was about 96% (ranging from about 94 to 97%) indicating good joint conditions. $k_{FWD\text{-}Static\text{-}Corr}$ values varied from about 33.7 to 60.3 kPa/mm (123 to 221 pci) with an average of about 45.9 kPa/mm (168 pci), which is higher than the target *k* value assumed in the design (41 kPa/mm (150 pci)).

The DCP test results from three test locations indicated about 780 mm thick subbase layer (dense aggregate + sand) over subgrade layer. The average DCP-$CBR_{Subbase}$ was about 47% and the average DCP-$CBR_{Subgrade}$ (in the top 300 mm of subgrade) was about 15%. Using the AASHTO (1993) approach, the $k_{Estimated}$ value from this CBR is about 179 kPa/mm (655 pci), which is significantly higher than the *k* value used in the design (41 kPa/mm (150 pci)) and the average $k_{FWD\text{-}Static\text{-}Corr}$ value (45.9 kPa/mm (168 pci)).

Figure 49. TS3: FWD test locations

Figure 50. TS3: Collecting DCP data

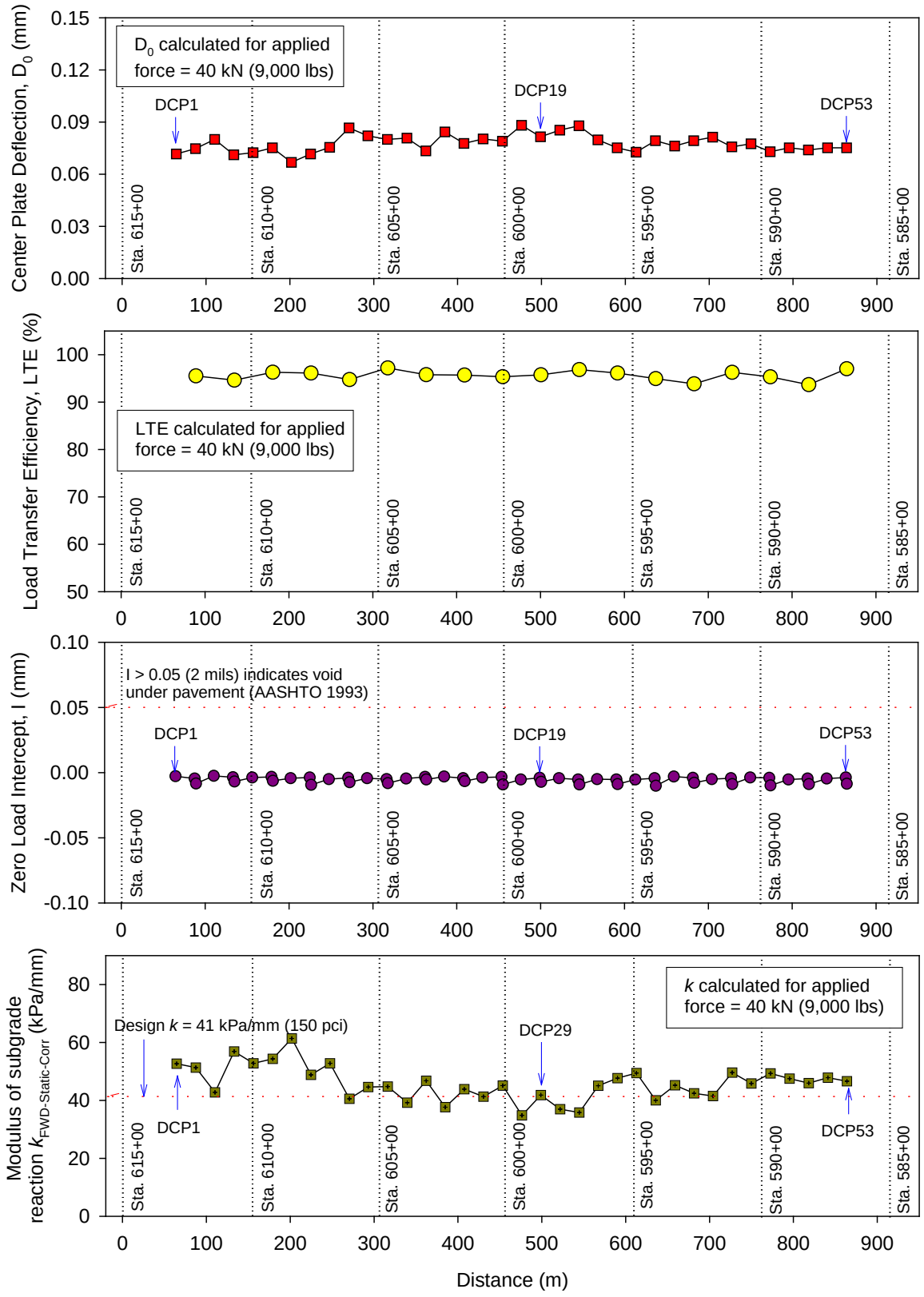

Figure 51. TS3: In situ FWD test results

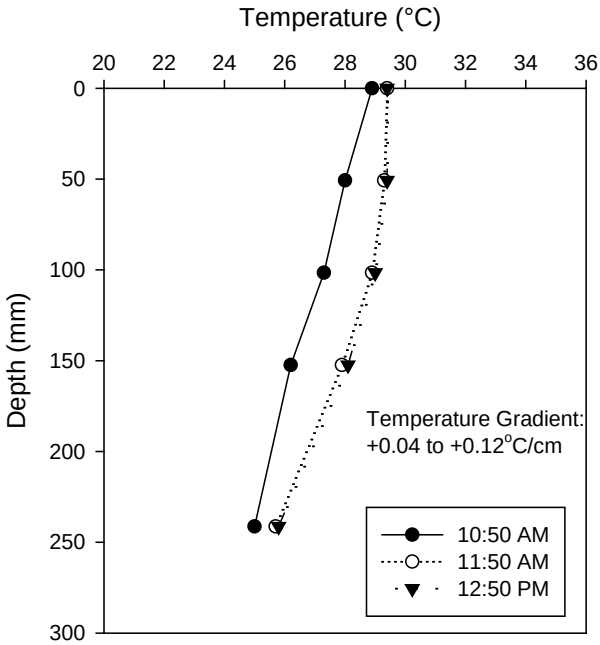

Figure 52. TS3: Pavement temperature profiles during FWD testing

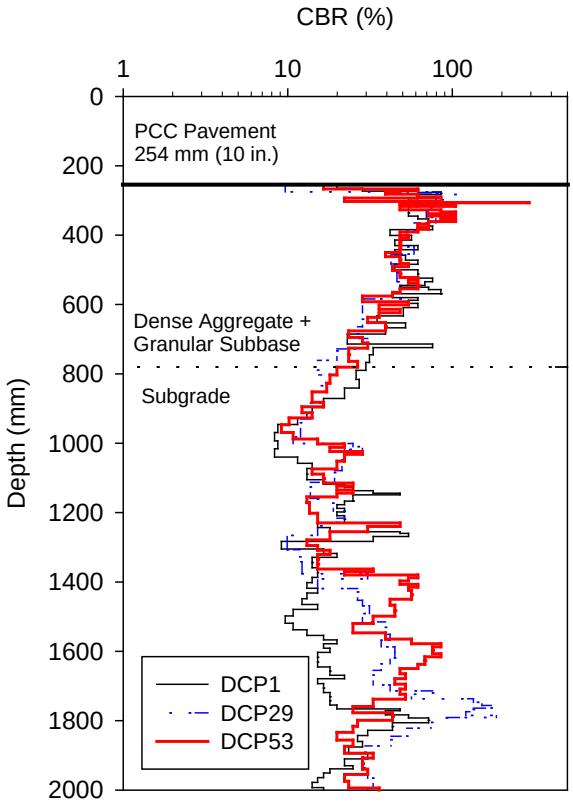

Figure 53. TS3: DCP-CBR profiles at each test location

Comparison of Design Values, In Situ Measurements, and Laboratory Measurements

A summary of the in situ measurement value statistics (i.e., μ, σ, and COV) from each TS is provided in Table 8. A bar chart of the average *k* values determined using AASHTO, PCA, and ACPA procedures from PLT, FWD, DCP, and laboratory M_r measurements is shown in Figure 54 in comparison with the design target *k* = 41 kPa/mm (150 pci). *k* value from laboratory M_r is determined by calculating M_r at σ_3 = 14 kPa (2 psi) and σ_{cyclic} = 41 kPa (6 psi) (from Table 4) for different dry unit weight and moisture contents, averaging them, and using in Equation 1. Using the averge thawed CBR = 7.2% from thaw weakening test results on the subgrade material, the thawed M_r is calculated as 52 MPa using relationships presented in AASHTO (1993). Use this M_r value, and the average E_{SB} and H_{SB} values from TS3, $k_{comp\text{-}AASHTO(1993)}$ = 139 kPa/mm (510 pci). This value is also shown in Figure 54.

The average $k_{FWD\text{-}Static\text{-}Corr}$ determined from FWD test was close to the design *k* value, while average k_{PLT*} was about 1.3 times lower than the design *k* value. All other *k* values estimated following AASHTO, PCA, and ACPA procedures (from in situ DCP-CBR values or laboratory M_r and thawed CBR values) were about 1.5 to 4.6 times higher than the design *k* value.

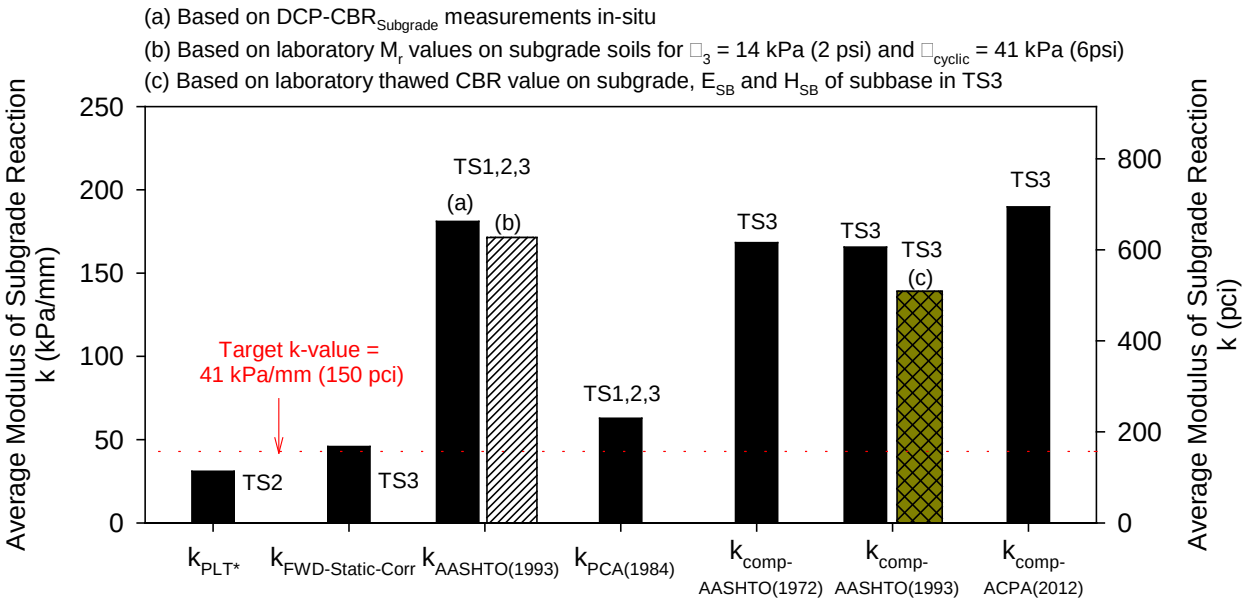

Figure 54. TS1, TS2, and TS3: Bar chart comparing the design target *k* value with measured and estimated *k* values from field and laboratory measurements

The results presented in Figure 54 indicate that the estimated *k* values vary significantly depending on the test method and procedure followed. The *k* values determined from FWD and PLT tests are somewhat direct measurements although some empirical corrections are made. On the other hand, all other methods (from laboratory tests and in situ DCP tests) are indirect and rely solely on empirical relationships to determine *k* values. The difference in *k* values from direct versus indirect measurements is significant as show in Figure 1 and calls into question the

various methods listed in the new mechanistic-empirical pavement design guide (MEPDG) that are based solely on empirical relationships between soil classifications, CBR, etc.

Table 8. TS1, TS2, and TS3: Summary statistics of in situ test results

Measurement	n	μ	σ	COV (%)
TS1 Sand Subbase/Subgrade				
Subbase γ_d (kN/m^3)	17	16.15	0.35	2
Subbase w (%)	17	3.7	0.5	14
Subgrade γ_d (kN/m^3)	5	20.02	0.4	2
Subgrade w (%)	5	11.7	1.0	8
DCP-CBR$_{Subbase}$ (%)[1]	17	5.6	1.2	22
DCP-CBR$_{Subgrade}$(%)	22	17.4	12.9	74
Subbase $E_{LWD\text{-}Z3}$ (MPa) [1]	17	12.6	3.2	26
Subgrade $E_{LWD\text{-}Z3}$ (MPa)	5	8.2	1.1	13
$k_{AASHTO(1993)}$ (kPa/mm)	22	196.8	95.4	48
$k_{PCA(1984)}$ (kPa/mm)	22	68.1	27.5	40
TS2 Subgrade				
Subgrade γ_d (kN/m^3)	79	19.84	0.38	2
Subgrade w (%)	79	7.5	1.0	13
DCP-CBR$_{Subgrade}$ (%)	79	15.5	5.0	32
Subgrade $E_{LWD\text{-}Z3}$ (MPa)	80	30.7	5.3	17
Subgrade E_{V1} (MPa)	26	15.4	4.0	27
Subgrade E_{V2} (MPa)	26	47.3	7.6	16
k_{PLT*} (kPa/mm)	26	30.5	8.2	27
$k_{AASHTO(1993)}$ (kPa/mm)	26	179.0	38.8	22
$k_{PCA(1984)}$ (kPa/mm)	26	62.1	10.1	16
TS3 Subgrade				
$k_{FWD\text{-}Static\text{-}Corr}$(kPa/mm)	36	45.9	5.9	13
DCP-CBR$_{Subbase}$ (%)[2]	3	47.1	1.8	4
DCP-CBR$_{Subgrade}$ (%) [average of top 300 mm of subgrade]	3	15.3	1.1	7
H_{SB} (mm)	3	508	0	0
$k_{AASHTO(1993)}$ (kPa/mm)[3]		179.3		
$k_{PCA(1984)}$ (kPa/mm) [3]		63.3		
$k_{comp\text{-}AASHTO(1972)}$ (kPa/mm) [3]	N/A	168.3		N/A
$k_{comp\text{-}AASHTO(1993)}$ (kPa/mm) [3]		165.6		
$k_{comp\text{-}ACPA(2011)}$ (kPa/mm) [3]		189.8		

[1]Sand subbase layer with no confinement; [2]Subbase layers consisted of crushed aggregate placed over the sand layer; [3]Based on average values of DCP-CBRSubbase, DCP-CBRSubgrade, and H_{SB} values.

CHAPTER 6. SUMMARY AND CONCLUSIONS

This report presents results and analysis of field and laboratory tests from a field study conducted on US Highway 10 just north of Junction City, Wisconsin. This project involved new construction of 5.44 miles of 254 mm (10 in.) thick portland cement concrete (PCC) pavement with dowels; 152 mm (6 in.) thick dense aggregate base; 610 mm (24 in.) select borrow granular fill subbase; and clay subgrade. Field testing was conducted by the Iowa State University research team on three test sections (TS). TS1 involved testing the sand subbase and subgrade layers, TS2 involved testing the subgrade layer, and TS3 involved testing an existing PCC layer paved in 2009.

The modulus of subgrade reaction *k* values were determined from FWD, PLT, and DCP tests to compare with the design *k* values. CBR in a thawed state and M_r tests were conducted in the laboratory to estimate *k* values and compare with the design *k* values. Some key findings from these comparisons are as follows:

- The average *k* value determined from the FWD ($k_{FWD\text{-}Static\text{-}Corr}$) was close to the design *k* value, while the static PLT (k_{PLT^*}) was about 1.3 times lower than the design value. On the other hand, the estimated *k* values following empirical relationships from AASHTO (1993) and PCA (1984) based on in situ DCP-CBR measurements, were about 4.1 and 1.6 times higher than the design *k* value, respectively.
- The *k* values calculated from laboratory-determined subgrade M_r values were also about 4 times higher than the design *k* value.
- The composite *k* values (accounting for the subbase layer modulus and thickness) determined following AASHTO (1972), AASHTO (1993), and ACPA (2012) procedures based on in situ DCP-CBR measurements were also about 4 to 4.6 times higher than the design *k* value. The composite *k* values that were determined based on thawed subgrade CBR measurements following AASHTO (1993) procedures were about 3 times higher than the design *k* value.

These findings indicate that estimated *k* values vary significantly depending on the test method and the procedure followed. The *k* values determined from FWD and PLT tests are somewhat direct measurements although some empirical corrections are made. On the other hand, all other methods (i.e., from laboratory tests and in situ DCP tests) are indirect and rely solely on empirical relationships to determine *k* values. The difference in *k* values from direct versus indirect measurements is significant as noted above and calls into question the various methods listed in the new mechanistic-empirical pavement design guide (MEPDG) that are solely based on empirical relationships between soil classifications, CBR, etc.

LWD, NG, and DCP tests were conducted on subbase and subgrade layers by spacing the test locations about 3 m apart to capture the variability along the road alignment and also in a dense grid pattern (spaced at about 1 to 3 m) to capture spatial variability over a small area. Geostatistical semivariogram analysis was performed to analyze the point test data from the dense grid pattern testing to characterize and quantify spatial non-uniformity properties of the foundation layers. Some key findings from field test results and analysis are as follows:

- The coefficient of variation in NG dry unit weight measurements of subbase and subgrade layers varied about 2%, while the DCP-CBR, LWD modulus, and *k* values were in the range of 17 to 74%. The high variability in the stiffness/strength properties is attributed to variations in the moisture content and the influence of underlying layer properties, which are not reflected in the surface layer dry unit weight measurements.
- Geostatistical analysis of data obtained in the dense grid pattern on a subgrade test section showed that a spherical semivariogram model fits well for all the measurements. DCP-CBR and LWD modulus kriged contour maps showed similar spatial variation of soft and stiff areas, but they did not match with the spatial variability observed with dry unit weight measurements.

Laboratory testing was conducted on foundation layer materials obtained from the field to determine index properties, moisture-dry unit weight relationships from compaction tests, and M_r, and frost-heave and thaw-weakening susceptibility ratings. The M_r tests were conducted on homogeneous samples as well as layered composite samples (i.e., subbase over subgrade) to assess its influence on the M_r values. Frost-heave tests were conducted on subgrade samples by exposing the samples to two F/T cycles. Thaw-weakening susceptibility rating was determined by conducting CBR tests on compacted samples before and after two thawing cycles. Some key findings from laboratory M_r and frost-heave/thaw-weakening susceptibility rating tests are as follows:

- Comparisons of homogeneous sample versus layered composite sample (with subbase over subgrade) M_r values indicated that on average, the layered composite sample has about 1.4 times lower M_r than the single layer subbase sample at a similar density. The reason for this reduction in M_r in the layered composite sample is attributed to the weaker subgrade layer. This is an important finding and must be further studied with adequate testing in various combinations of layered composite sample configurations. Efforts are underway in this research study to further investigate the influence of composite soil layer configurations on M_r properties.
- Frost-heave test results on subgrade samples indicated that the heave rate was greater for the second freezing cycle than for the first freezing cycle, which indicates that the material is susceptible to increased heave with greater F/T cycles. Based on the frost-heave rate measurements, the subgrade soil is classified to have medium potential to frost-heave susceptibility.
- After completing the two F/T cycles, a moisture content profile in the sample was obtained by taking samples at different depths. Results showed that the moisture content was higher at all depths in the samples compared to the initial moisture content, as expected. The moisture content at the top of the sample was closer to the initial moisture content and increased with depth.
- The CBR values for the four thawed samples decreased to an average CBR = 7 from about 26 on a sample in unthawed state. Based on the thawed CBR values, the subgrade soil is classified to have medium potential to thaw-weakening.

REFERENCES

AASHTO T-307. (1999). *Standard method of test for determining the resilient modulus of soils and aggregate materials.* American Association of State Highway and Transportation Officials (AASHTO), Washington, D.C.

AASHTO. (1993). *AASHTO design guide for design of pavement structures*. American Association of State Highway and Transportation Officials, Washington D.C.

ACPA. (2012). *k-value Calculator,* American Concrete Paving Association (ACPA), <http://apps.acpa.org/apps/kValue.aspx> Date Accessed December 18, 2012.

Andrei, D., Witczak, M. W., Schwartz, C. W., and Uzan, J. (2004). "Harmonized resilient modulus test method for unbound pavement materials." *Transportation Research Record No. 1874*, Transportation Research Board, Washington, D. C., 29-37.

ASTM C136-06. (2010). "Standard test method for sieve analysis of fine and coarse aggregates." American Standards for Testing Methods (ASTM), West Conshohocken, PA.

ASTM D422-63. (2010). "Standard test method for particle-size analysis of soils." American Standards for Testing Methods (ASTM), West Conshohocken, PA.

ASTM D698-07e1. (2010). "Standard test method for laboratory compaction characteristics of soil using standard effort (12,400 ft-lbf/ft^3 (600 kN-m/m^3))." American Standards for Testing Methods (ASTM), West Conshohocken, PA.

ASTM D1557-07. (2010). "Standard test method for laboratory compaction characteristics of soil using modified effort (56,000 ft-lbf/ft^3 (2,700 kN-m/m^3))." American Standards for Testing Methods (ASTM), West Conshohocken, PA.

ASTM D2487-10 (2010). "Standard test method for classification of soil for engineering purposes (unified soil classification system)." American Standards for Testing Methods (ASTM), West Conshohocken, PA.

ASTM D3282-09 (2010). "Standard test method for classification of soils and soil-aggregate mixtures for highway construction purposes." American Standards for Testing Methods (ASTM), West Conshohocken, PA.

ASTM D4253-00. (2010). "Standard test methods for maximum index density and unit weight of soils using a vibratory table." American Standards for Testing Methods (ASTM), West Conshohocken, PA.

ASTM D4254-00. (2010). "Standard test methods for minimum index density and unit weight of soils and calculation of relative density." American Standards for Testing Methods (ASTM), West Conshohocken, PA.

ASTM D4318-10. (2010). "Standard test methods for liquid limit, plastic limit, and plasticity index of soils." American Standards for Testing Methods (ASTM), West Conshohocken, PA.

ASTM D5918-06 (2010). "Standard test methods for frost heave and thaw weakening susceptibility of soils." American Standards for Testing Methods (ASTM), West Conshohocken, PA.

ASTM D6951-03 (2010). "Standard test method for use of the dynamic cone penetrometer in shallow pavement applications." American Standards for Testing Methods (ASTM), West Conshohocken, PA.

ASTM D6938-08a. "Standard test method for in-place density and water content of soil and soil-aggregate by nuclear methods (shallow depth)." American Standards for Testing Methods (ASTM), West Conshohocken, PA.

Barbenberg, E. J., and Petros, K. A. (1991). *Evaluation of Concrete Pavements Using NDT Results,* Illinois Highway Research Project IHR-512, University of Illinois and Illinois Department of Transportation, Report No. UILU-ENG-91-2006, IL.

Clark, I., and Harper, W. (2002). *Practical geostatistics 2000*. 3rd reprint, Ecosse North America LLC, Columbus, Ohio.

Crovetti, J. A. and Dempsey, B. (1991). *Pavement Subbases*. Project IHR-525, Illinois Cooperative Highway Research Program, University of Illinois at Urbana-Champaign, IL.

Crovetti, J. A. (1994). "Design and evaluation of jointed concrete pavement systems incorporating open-graded bases." Ph.D. Dissertation, University of Illinois at Urbana-Champaign, IL.

Darter, M. I., Hall, K. T., and Kuo, C-M. (1995). *Support under Portland Cement Concrete Pavements,* NCHRP Report 372, Transportation Research Board, Washington, D.C.

ERES Consultants, Inc. (1982). *Nondestructive Structural Evaluation of Airfield Pavements,* Prepared for U.S. Army Corps of Engineering Waterways Experiment Station, Vicksburg, MS.

Foxworthy, P.T. (1985). "Concepts for the Development of a Nondestructive Testing and Evaluation System for Rigid Airfield Pavements." Ph.D. Thesis, University of Illinois at Urbana-Champaign, IL.

Hoffman, M.S., and Thompson, M.R. (1981). *Mechanistic Interpretation of Nondestructive Pavement Testing Deflections.* Transportation Engineering Series No. 32, Illinois cooperative Highway and Transportation Research Series No. 190, University of Illinois at Urbana-Champaign, Champaign, IL.

Ioannides, A. M. (1990). "Dimensional analysis in NDT rigid pavement evaluation", *Transportation Engineering Journal,* ASCE, Vol. 116, No. TE1.

Isaaks, E. H., and Srivastava, R. M. (1989). *An introduction to applied geostatistics*. Oxford University Press, New York.

Jannsen, D., and Snyder, M. (2000). Temperature-Moment Concept for Evaluating Pavement Temperature Data. *Journal of Infrastructure Systems, 6*(2), 81-83

MDOT (2005). *Pavement design and selection manual.* Prepared by Pavement Management Unit and Construction & Technology Division, Michigan Department of Transportation. <http://www.michigan.gov/documents/mdot/MDOT_Pavement_Design_and_Selection_Manual_257723_7.pdf> (Accessed, February 2011).

NCHRP 1-28A. (2002). *Recommended standard method for routine resilient modulus testing of unbound granular base/subgrade materials and subgrade soils – NCHRP protocol 1-28A,* National Cooperative Highway Research Program.

Mohammad, L. N., Herath, A., Gudishala, R., Abu-Farsakh, M. Y., and Alshibli, K. (2008). Development of Models to Estimate the Subgrade and Subbase Layers' Resilient Modulus from In Situ Devices Test Results for Construction Control. Final report submitted to Louisiana Department of Transportation and Development, Louisiana Transportation Research Center, Baton Rouge, LA.

Powell, W. D. Potter, J. F. Mayhew, H. C, and Nunn, M. E. (1984). "The structural design of bituminous roads." Report LR1132. Transport and Road Research Laboratory, UK.

Priddy, L. P., Jersey, S. R., and Reese, C. M. (2010). "Full-Scale Field Testing for Injected Foam Stabilization of Portland Cement Concrete. *Research Record: Journal of the Transportation Research Board, 2155,* 24-33.

Schmalzer, P. (2006). *LTPP Manual for Falling Weight Deflectometer Measurements–Version 4.1* (Report No. FHWA-HRT-06-132). Washington, D.C.: Federal Highway Administration.

Smith, K. D., Wade, M. J., Bruinsma, J. E., Chatti, K., Vandenbossche, J. M., Yu, H. T., Hoerner, T. E., Tayabji, S. D. (2007). *Using Falling Weight Deflectometer Data with Mechanistic-Empirical Design and Analysis*, Draft Interim Report, DTFH61-06-C-0046, Federal Highway Administration, Washington, D.C.

Substad, R. N., Jiang, Y. J., and Lukanen, E. O. (2006). *Guidelines for Review and Evaluation of Backcalculation Results*, FHWA-RD-05-152, Federal Highway Administration, Washington, D.C.

Vandenbossche, J. (2005). Effects of Slab Temperature Profiles on the Use of Falling Weight Deflectometer Data to Monitor Joint Performance and Detect Voids. *Transportation Research Record: Journal of the Transportation Research Board, 2005*, 75-85.

van Til, C. J., McCullough, B. F., Vallerga, B. A., and Hicks, R. G. (1972). Evaluation of AASHO Interim Guides for Design of Pavement Structures. NCHRP 128, Highway Research Board.

Vennapusa, P. (2004). *Determination of the Optimum Base Characteristics for Pavements*. Master's Thesis, Department of Civil Construction and Environmental Engineering, Iowa State University, Ames, Iowa.

Vennapusa, P., and White, D. J. (2009). "Comparison of light weight deflectometer measurements for pavement foundation materials." *Geotechnical Testing Journal*, ASTM, 32(3), 239-251.

Vennapusa, P., White, D. J. and Morris, M. (2010). Geostatistical analysis of spatial referenced roller-integrated compaction measurements. *Journal of Geotechnical and Geoenvironmental Engineering*, ASCE, 136(6), 813–822.

White, D. J., Vennapusa, P., and Jahren, C. T (2004). *Determination of the Optimum Base Characteristics for Pavements*. Final Report, Iowa DOT Project TR–482, Center for Transportation Research and Education Project 02-119, Iowa State University, Ames, IA.

White, D. J., Jaselskis, E., Schaefer, V., and Cackler, T. (2005). "Real-time compaction monitoring in cohesive soils from machine response." *Transportation Research Record, 1936*, Journal of the Transportation Research Board, Washington D.C., 173–180.

White, D. J., Vennapusa, P., Suleiman. M. T., and Jahren, C. T. (2007). "An in situ device for rapid determination of permeability for granular bases." *Geotechnical Testing Journal*, 30(4), 282–291.

White, D. J., Vennapusa, P., Eichner, D., Gieselman, H., Zhao, L., and Jahren, C. T. (2010). *Rapid, self-contained in situ permeameter for field QA/QC of pavement base/subbase materials.* NCHRP 1-130 IDEA Project, Transportation Research Board, Washington, D.C.

Witczak, M. W., and Uzan, J. (1988). "The universal airport design system – Report I of IV: Granular material characterization." Department of Civil Engineering, University of Maryland, College Park, MD.

Zorn, G. (2003). *Operating manual: Light drop-weight tester ZFG2000*, Zorn Stendal, Germany.

APPENDIX A: AASHTO 1972, AASHTO (1993), AND PCA (1984) DESIGN CHARTS

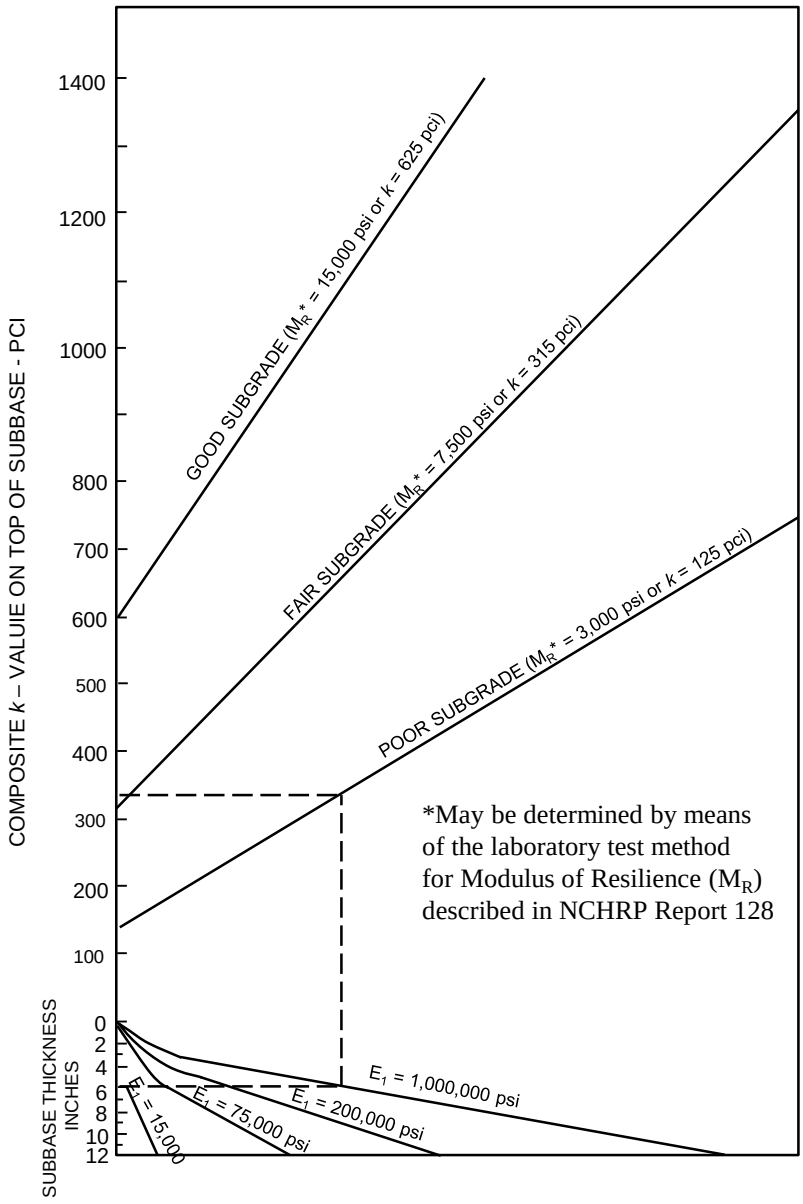

Figure 55. Chart for estimating $k_{comp\text{-}AASHTO(1972)}$ (reproduced from AASHTO 1972)

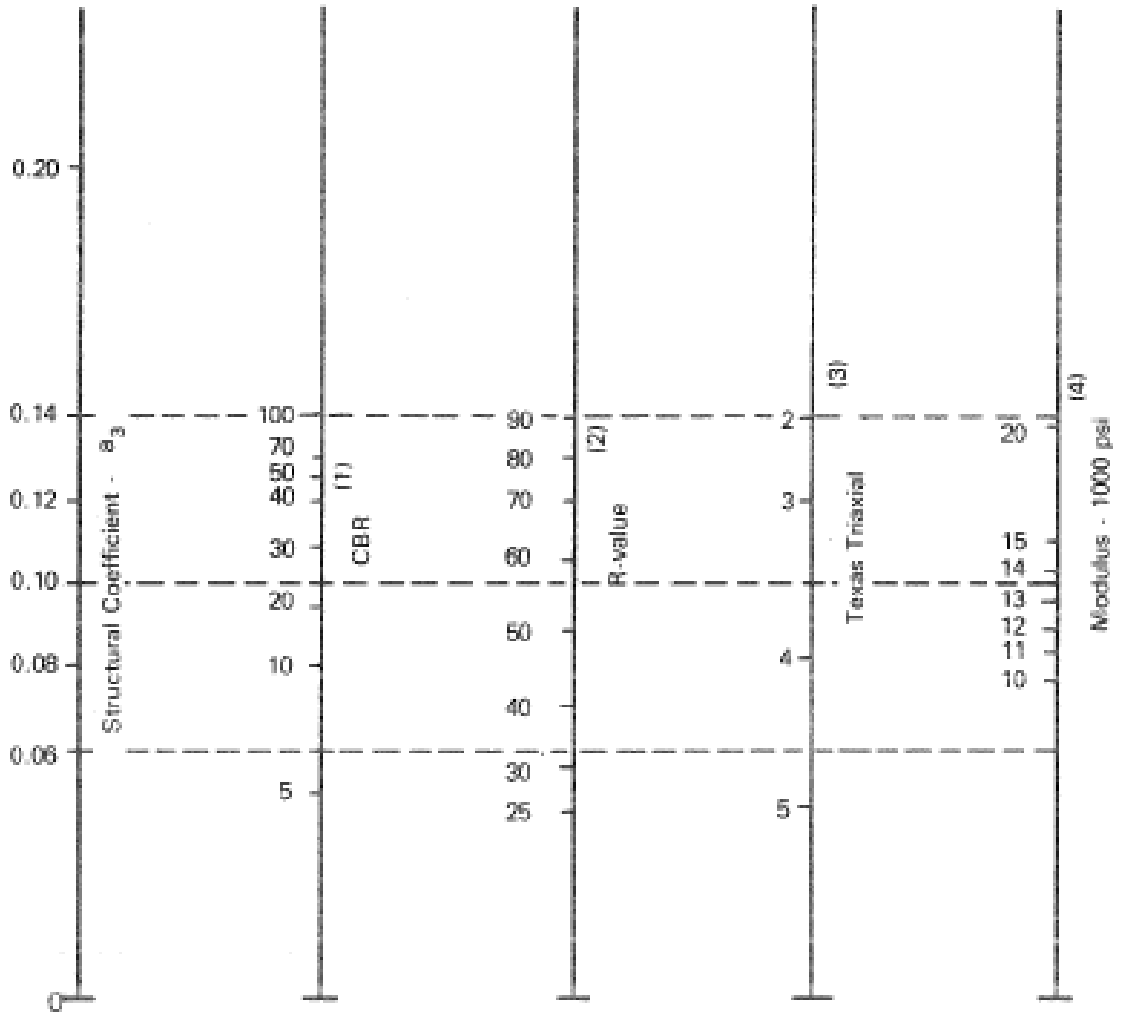

(1) Scale derived from correlations from Illinois.

(2) Scale derived from correlations obtained from The Asphalt Institute, California, New Mexico and Wyoming.

(3) Scale derived from correlations obtained from Texas.

(4) Scale derived on NCHRP project *(3)*.

Figure 56. Chart to estimate modulus of subbase layer (E_{SB}) from CBR (from AASHTO 1993 based on results from van Til et al. 1972)

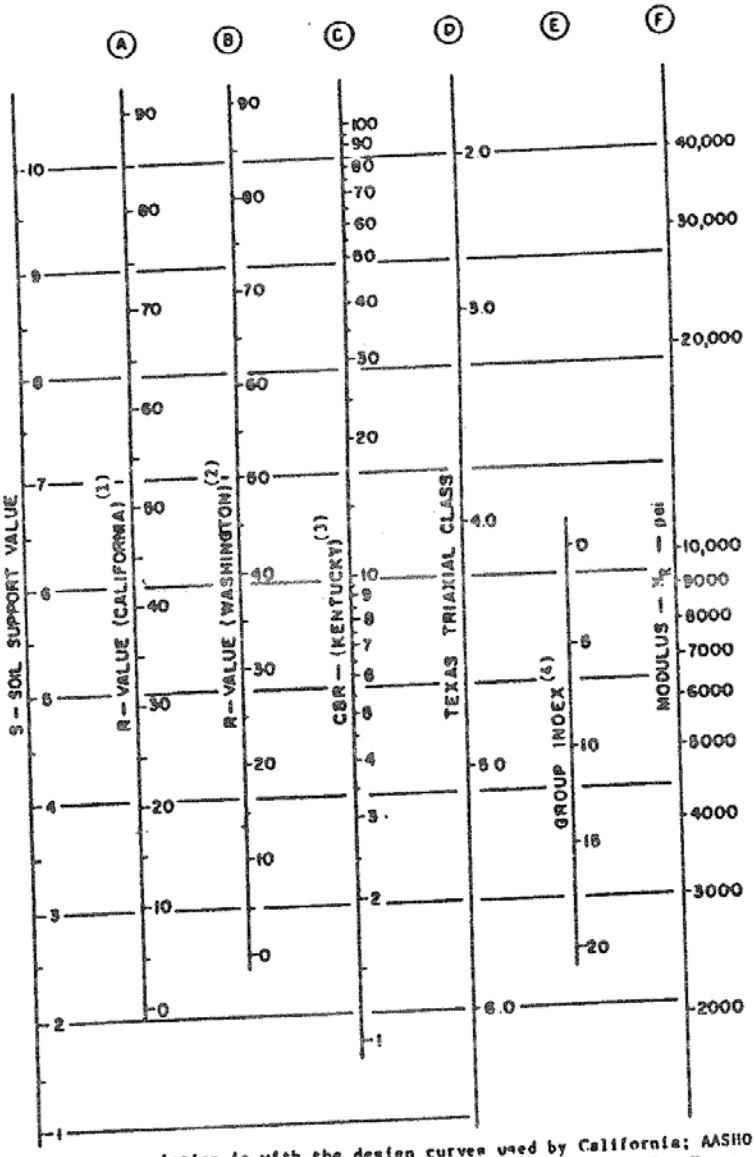

(1) The correlation is with the design curves used by California; AASHO designation is T-173-60, and exudation pressure is 240 psi. See Hveem, F.N., and Carmany, R.M., "The Factors Underlying the Rational Design of Pavements." Proc. HRB, Vol. 28 (1948) pp. 101-136.
(2) The correlation is with the design curves used by Washington Dept. of Highways; exudation pressure is 300 psi. See "Flexible Pavement Design Correlation Study." HRB Bull. 133 (1956).
(3) The correlation is with the CBR design curves developed by Kentucky. See Drake, W.B., and Havens, J.H., "Re-Evaluation of Kentucky Flexible Pavement Design Criterion." HRB Bull. 233 (1959) pp. 33-56. The following conditions apply to the laboratory-modified CBR: specimen is to be molded at or near the optimum moisture content as determined by AASHO T-99; dynamic compaction is to be used with a hammer weight of 10 lb dropped from a height of 18 in.; specimen is to be compacted in five equal layers with each layer receiving 10 blows; specimen is to be soaked for 4 days.
(4) This scale has been developed by comparison between the California R-value and the Group Index determined by the procedure in Proc. HRB Vol. 25 (1945) pp. 376-392.

Figure 57. Chart to estimate M_r of subgrade from CBR (from AASHTO 1993 Appendix FF)

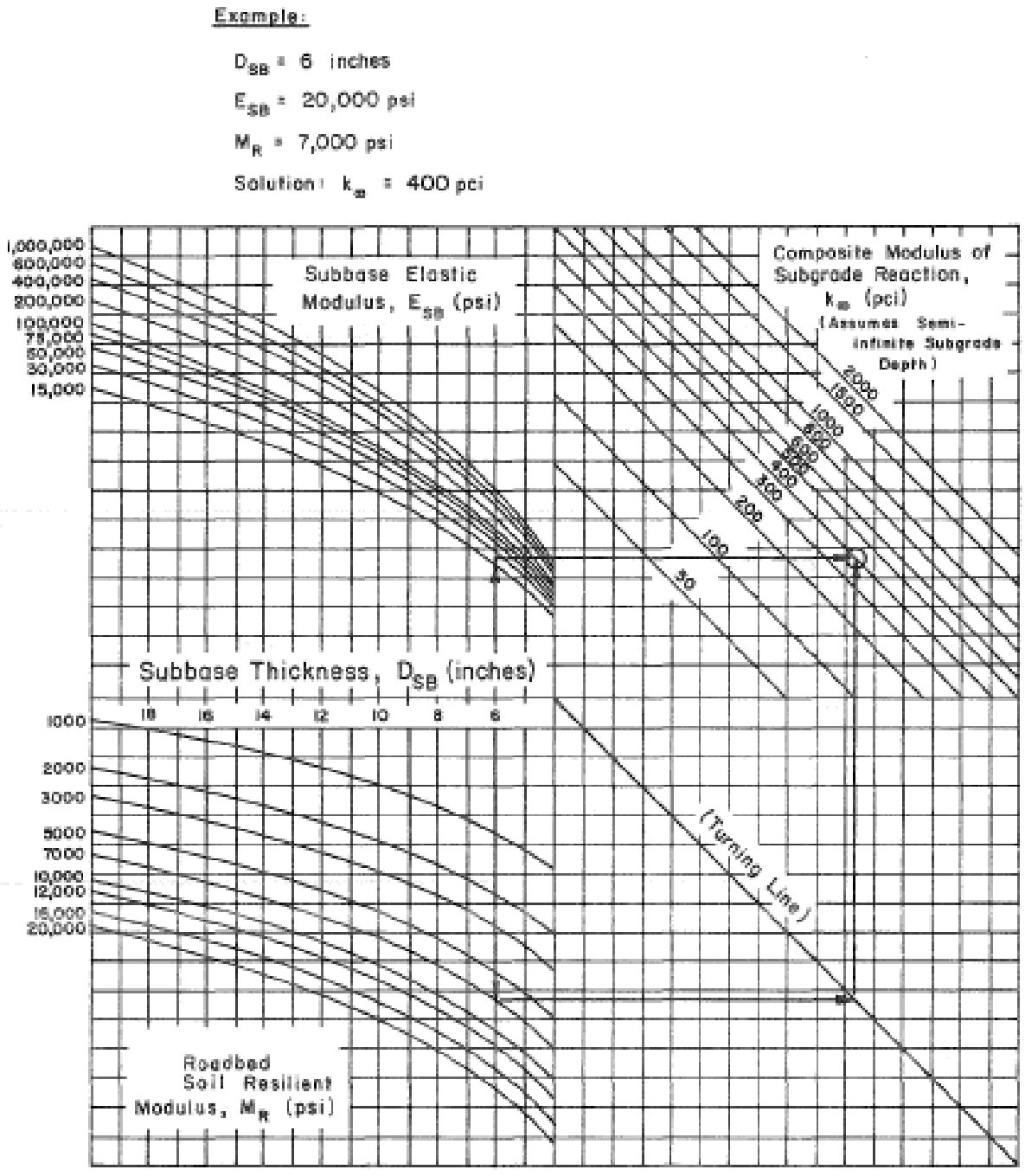

Figure 3.3. Chart for Estimating Composite Modulus of Subgrade Reaction, k_∞, Assuming a Semi-Infinite Subgrade Depth. (For practical purposes, a semi-infinite depth is considered to be greater than 10 feet below the surface of the subgrade.)

Figure 58. Chart for estimating composite modulus of subgrade reaction ($k_{comp\text{-}AASHTO(1993)}$) assuming a semi-infinite subgrade depth (from AASHTO 1993)

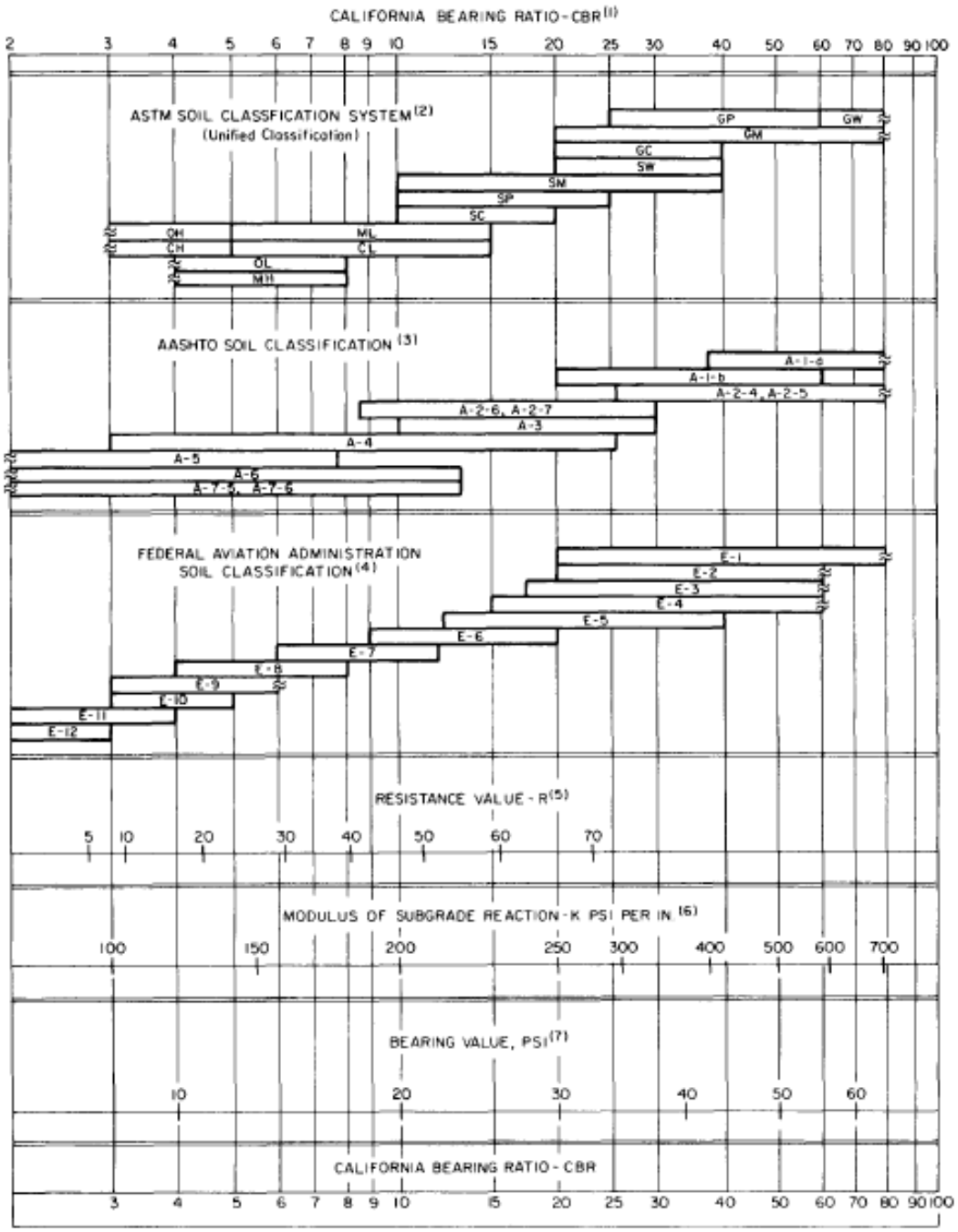

(1) For the basic idea, see O. J. Porter, "Foundations for Flexible Pavements," Highway Research Board *Proceedings of the Twenty-second Annual Meeting*, 1942, Vol. 22, pages 100-136.
(2) ASTM Designation D2487.
(3) "Classification of Highway Subgrade Materials," Highway Research Board *Proceedings of the Twenty-fifth Annual Meeting*, 1945, Vol. 25, pages 376-392.
(4) *Airport Paving*, U.S. Department of Commerce, Federal Aviation Agency, May 1948, pages 11-16. Estimated using values given in FAA *Design Manual for Airport Pavements*. (Formerly used FAA Classification; Unified Classification now used.)
(5) C. E. Warnes, "Correlation Between *R* Value and *k* Value," unpublished report, Portland Cement Association, Rocky Mountain-Northwest Region, October 1971 (best-fit correlation with correction for saturation).
(6) See T. A. Middlebrooks and G. E. Bertram, "Soil Tests for Design of Runway Pavements," Highway Research Board Proceedings *of the Twenty-second Annual Meeting*, 1942, Vol. 22, page 152.
(7) See item (6), page 184.

Figure 59. Chart for estimating modulus of subgrade reaction (*k*) from CBR (from PCA 1984)

APPENDIX B: STRESS-STRAIN CURVES FROM RESILIENT MODULUS TESTS

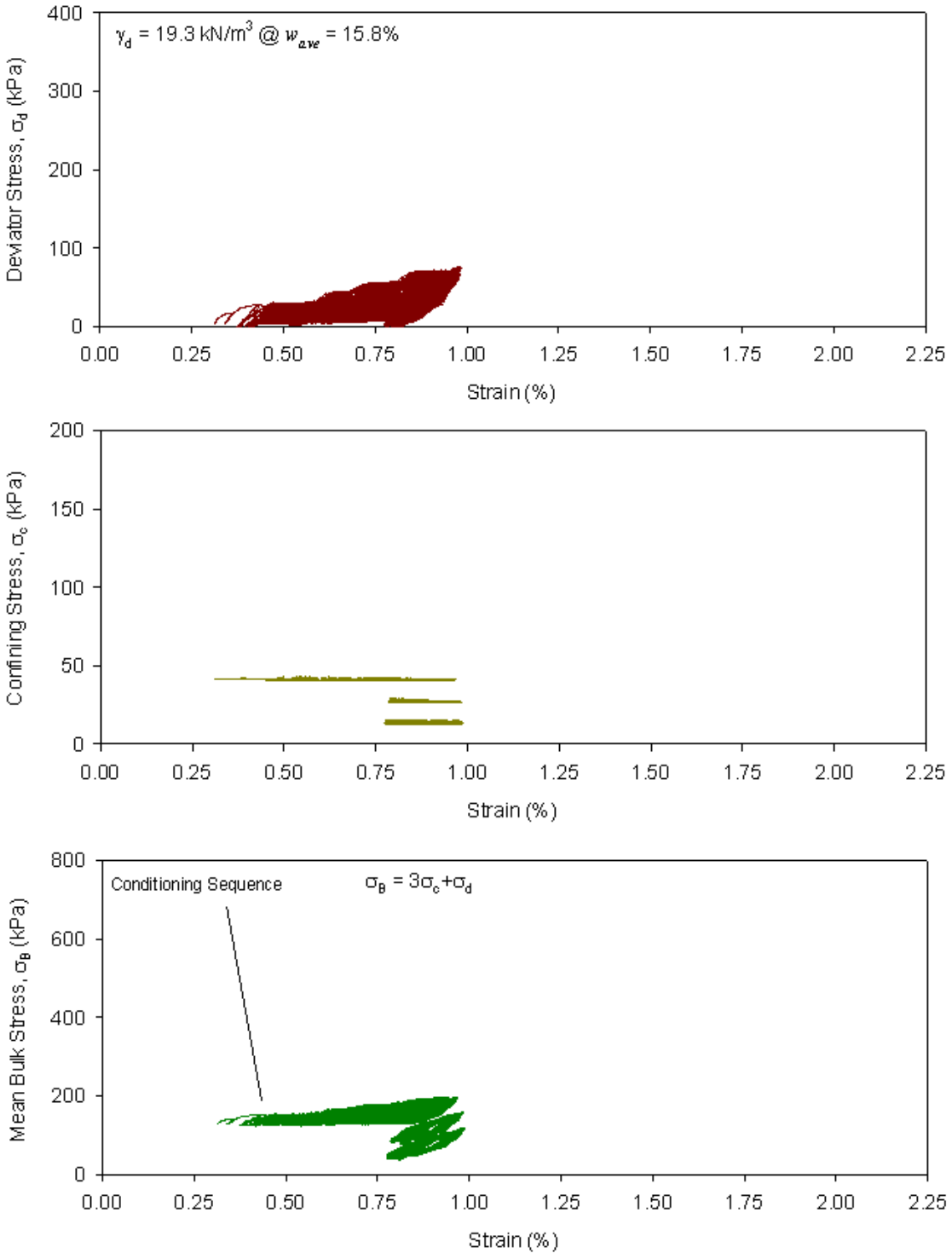

Figure 60. Cyclic stress-strain curves for subgrade sample # 1

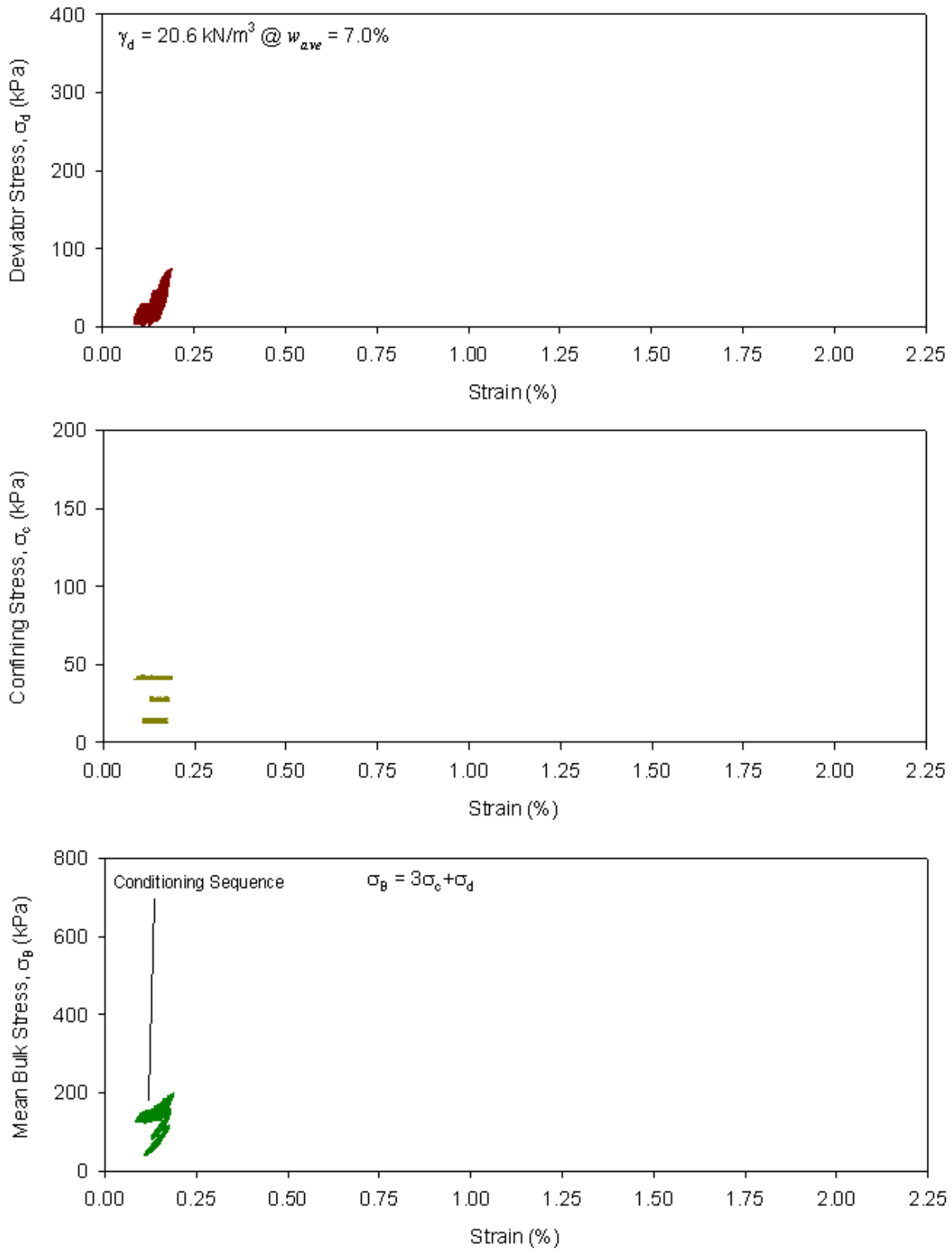

Figure 61. Cyclic stress-strain curves for subgrade sample # 2

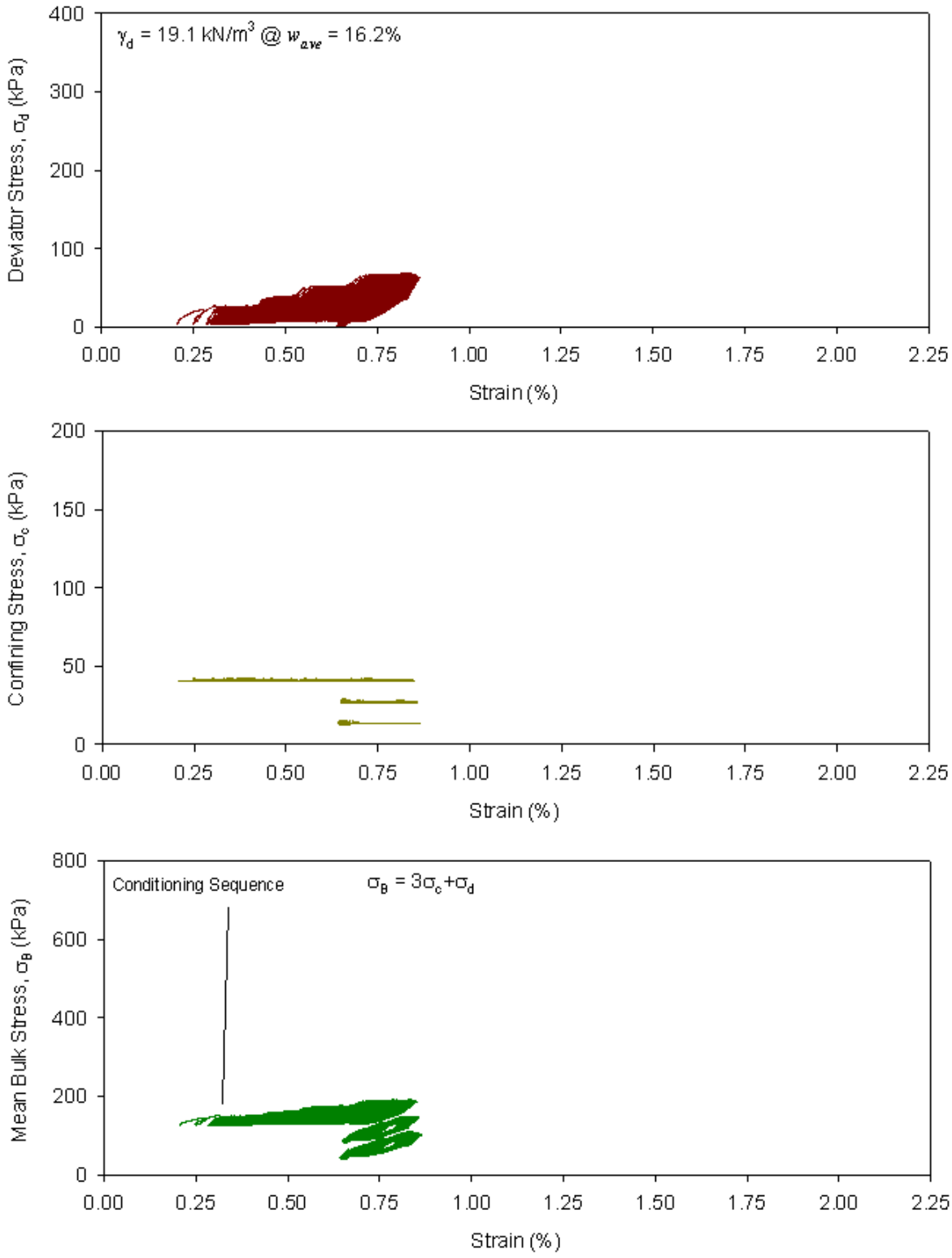

Figure 62. Cyclic stress-strain curves for subgrade sample # 3

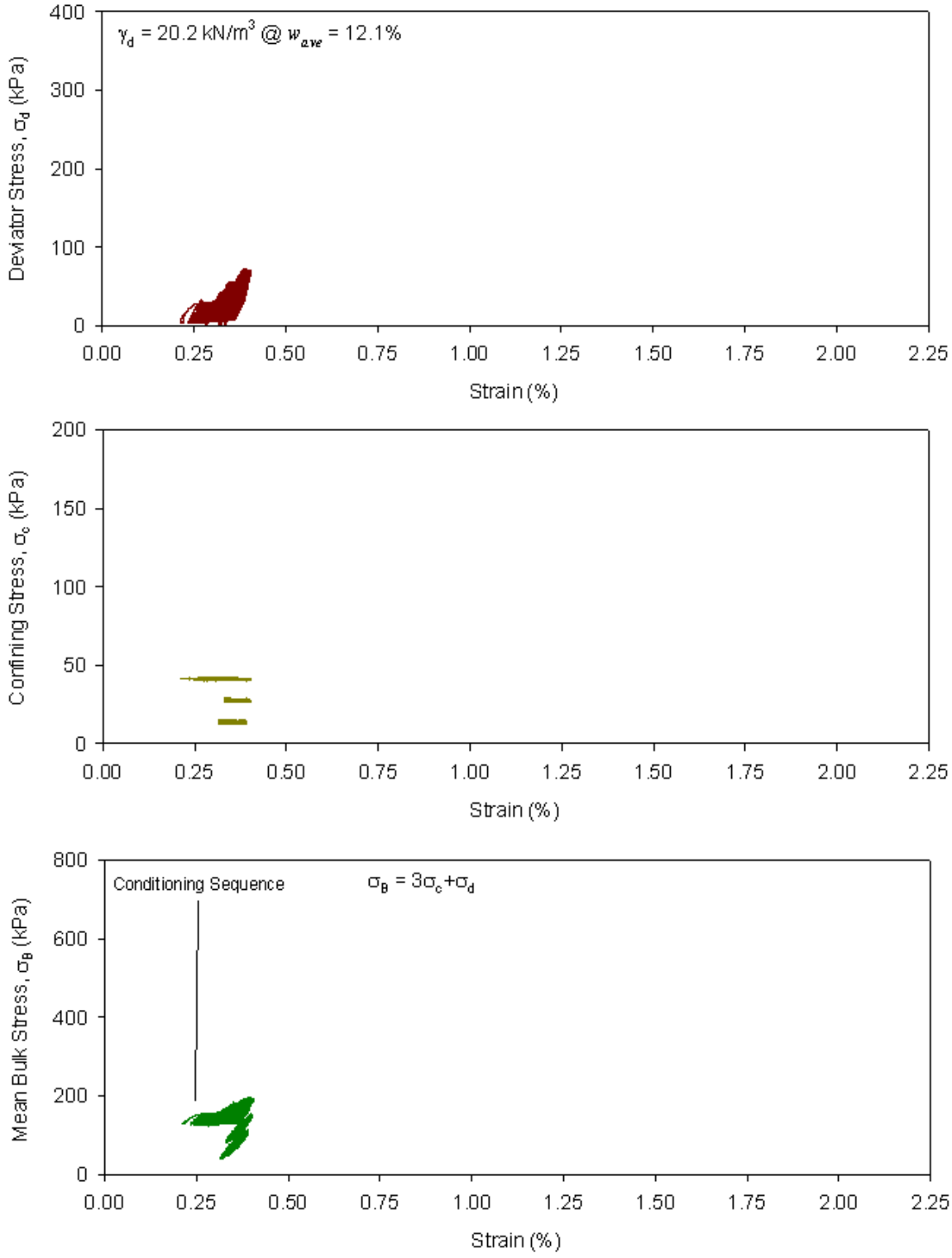

Figure 63. Cyclic stress-strain curves for subgrade sample # 4

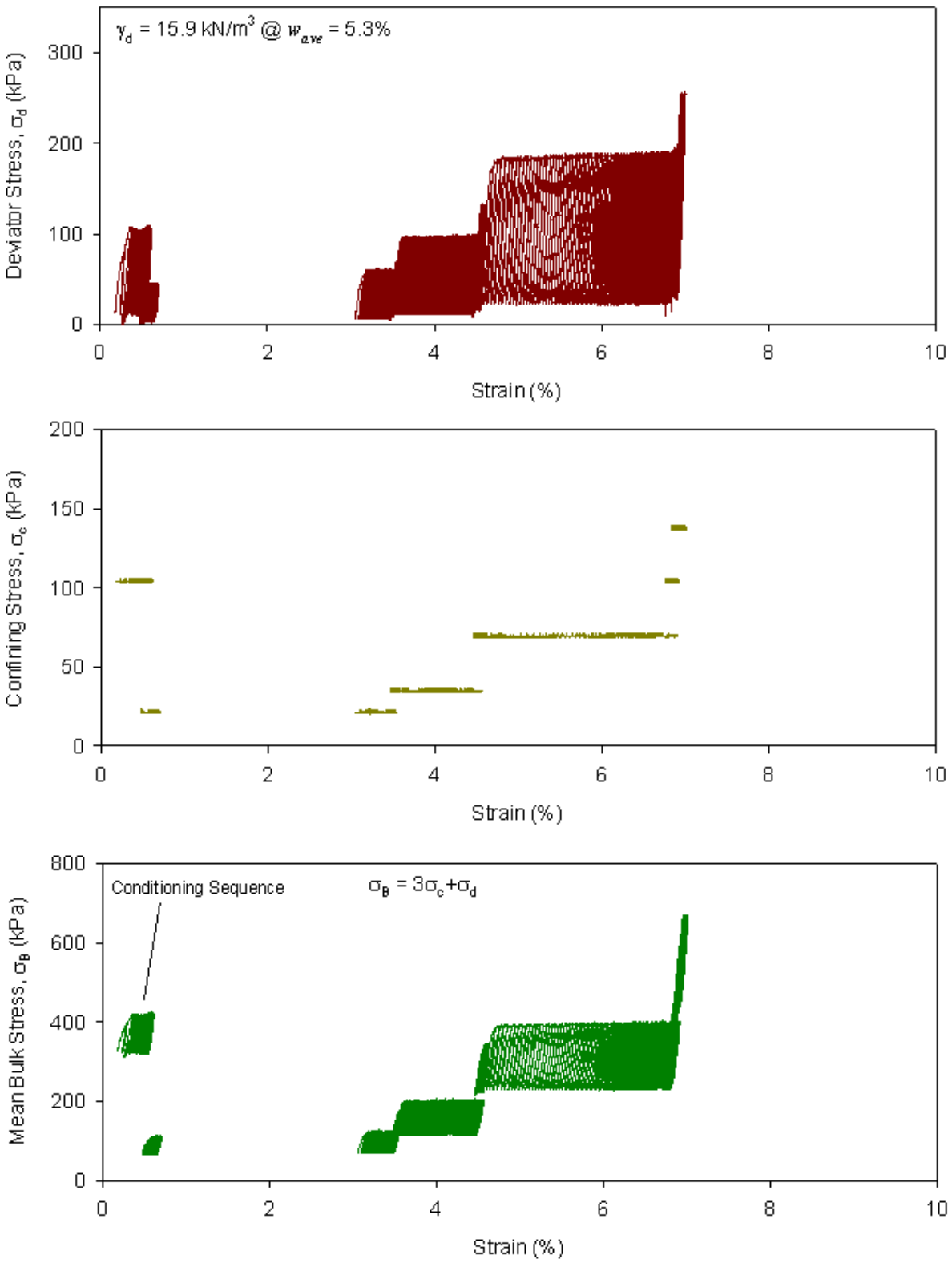

Figure 64. Cyclic stress-strain curves for subbase sample # 1

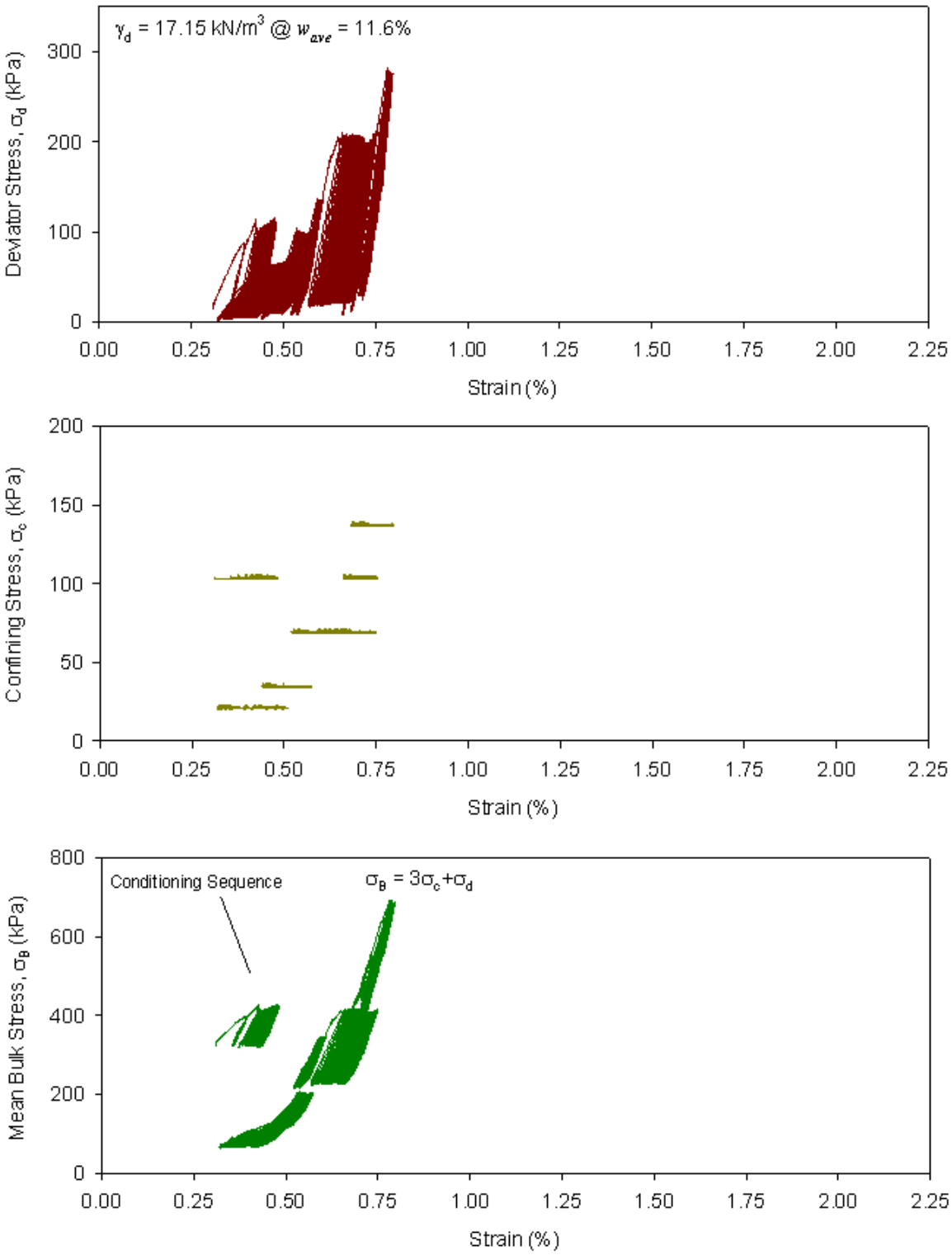

Figure 65. Cyclic stress-strain curves for subbase sample # 2

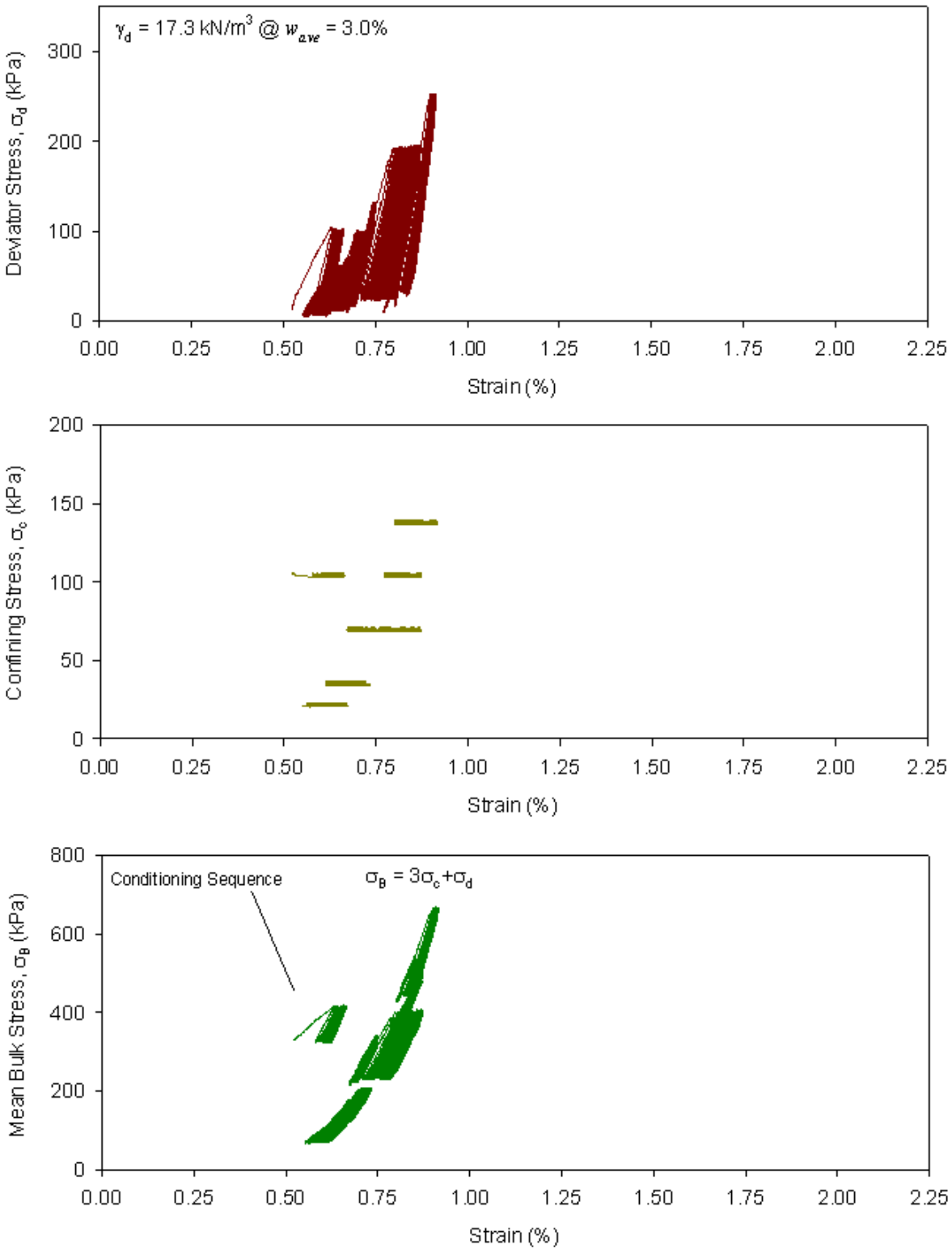

Figure 66. Cyclic stress-strain curves for subbase sample # 3

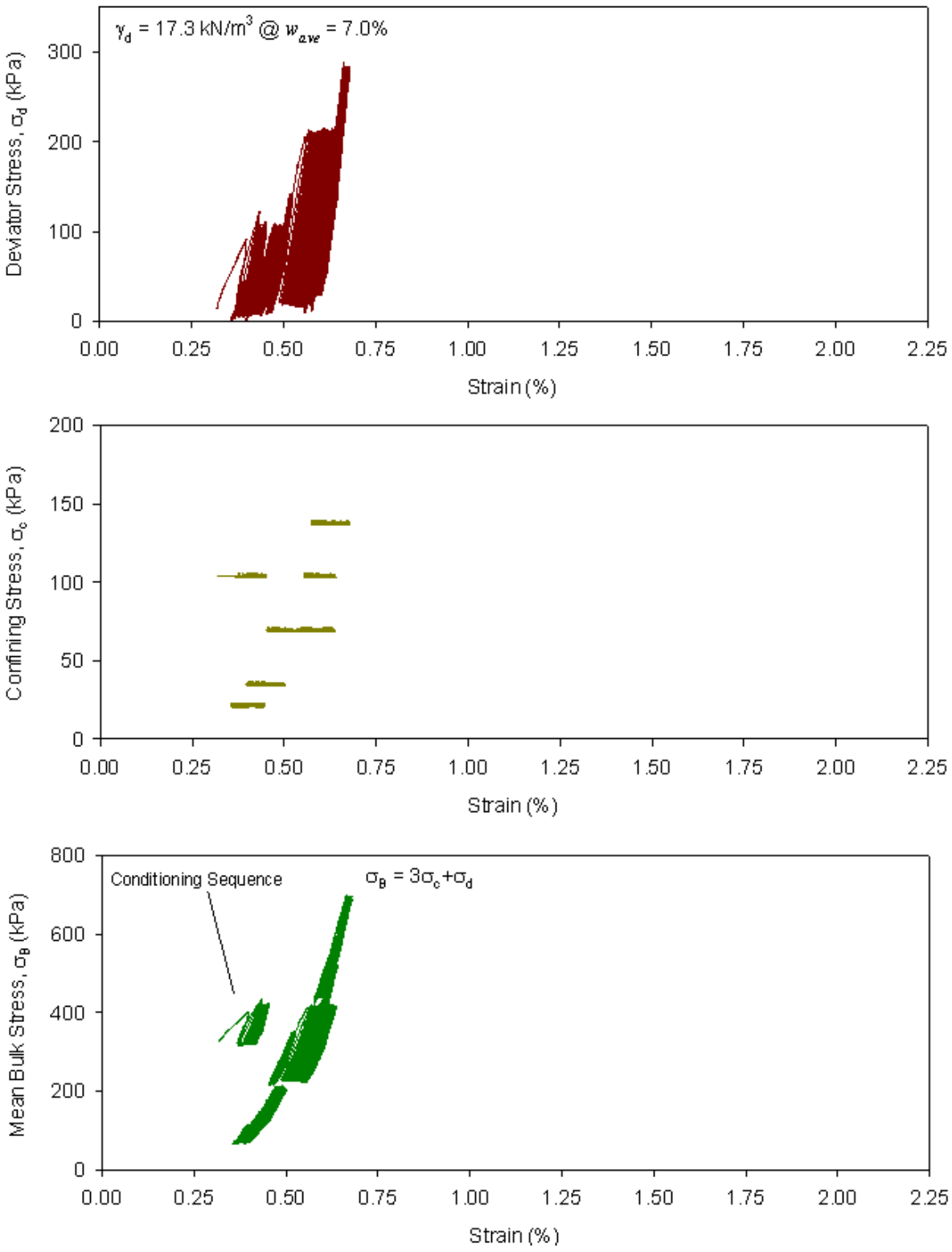

Figure 67. Cyclic stress-strain curves for subbase sample # 4

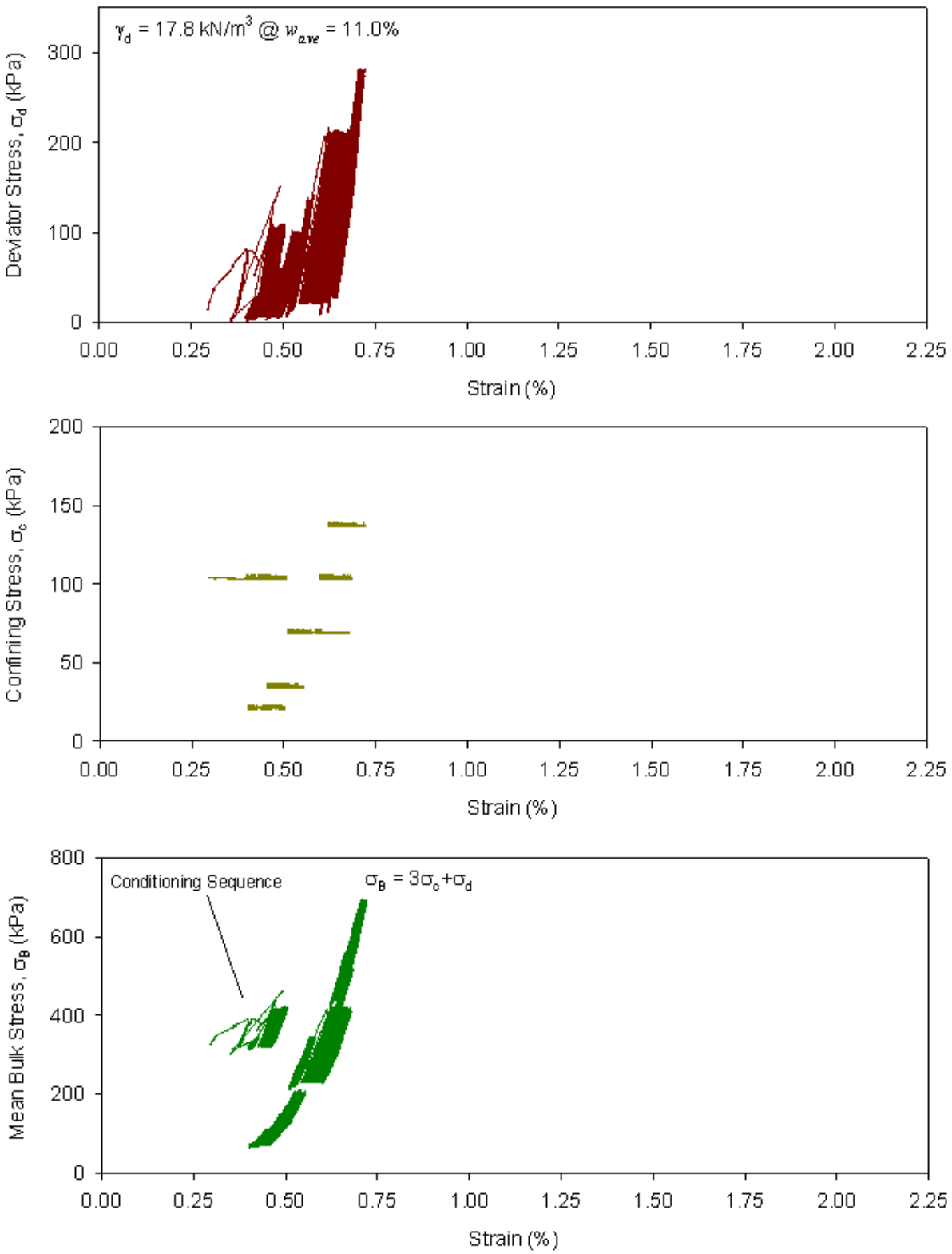

Figure 68. Cyclic stress-strain curves for subbase sample # 5

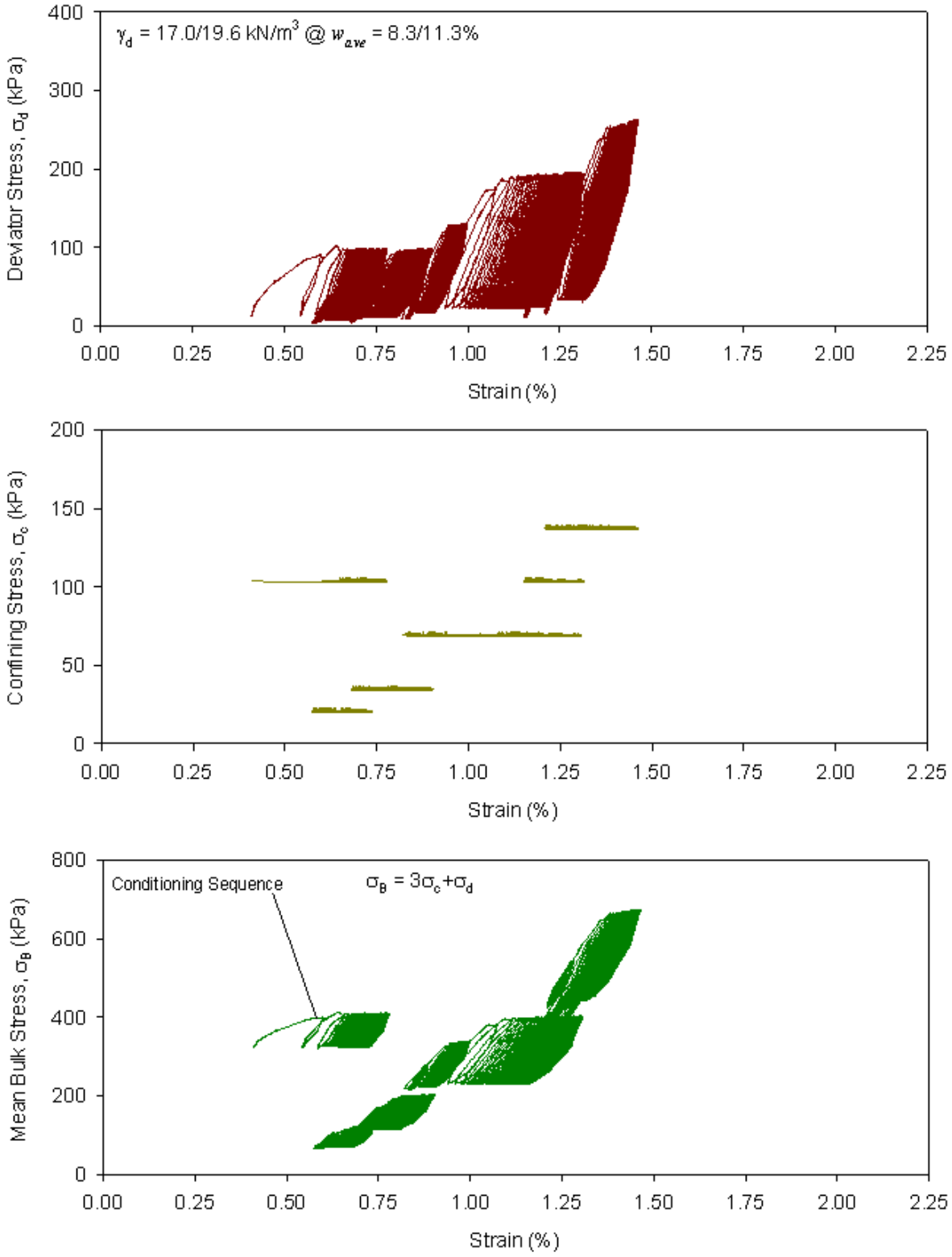

Figure 69. Cyclic stress-strain curves for subbase + subgrade composite sample